

# **Structural Characterization of Pro-inflammatory and Anti-inflammatory Immunoglobulin G Fc Proteins**

Thesis by  
Alysia Ashley Ahmed

In Partial Fulfillment of the Requirements for the  
degree of  
Doctor of Philosophy in Biology



CALIFORNIA INSTITUTE OF TECHNOLOGY

Pasadena, California

2015

(Defended May 21<sup>st</sup>, 2015)

© 2015  
Alysia Ahmed  
All Rights Reserved

## ACKNOWLEDGEMENTS

There are so many people I want to thank for helping me get to this point in my life. First and foremost I want to thank Professor Pamela Bjorkman for giving me the opportunity to conduct research in her lab. She has been an excellent mentor throughout this journey and has helped me grow as a scientist over the past five years. Although I faced many challenges in graduate school, Pamela always supported me. Despite having so many students, postdocs, and technicians in the lab Pamela always found time for me – this is why I feel that joining her lab was the best decision I've made. Pamela treats her postdocs, students, and technicians equally and takes time to make sure we understand every goal of the projects in the lab. This definitely is key to the success of our group.

Thanks to my committee – Raymond Deshaies, Douglas Rees, Judith Campbell and Ellen Rothenberg. The excellent discussions and continued guidance my committee has provided helped me excel in grad school.

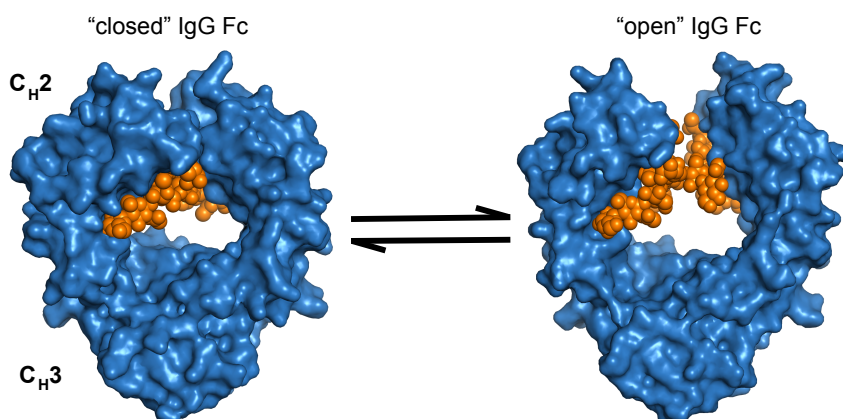
I would also like to thank members of the Bjorkman lab. They welcomed me with open arms and made me feel like a true Bjorklab member since day one. Priyanthi Gnanapragasm approached me on the first day of my rotation and went over the background for my project. She is such a great, warm, welcoming person and I'm certain I have made a lifelong friend in her. Marta Murphy is the glue that holds this lab together. Marta, aka my

“lab mom” takes care of us and ensures that we are all mentally and physically healthy, in addition to keeping our lab very organized. Marta, your kind words and motivation on a daily basis has been a true blessing and I am eternally grateful for that. Beth S. and Blaise, thank you for being such great mentors. Your advice over the years has been so valuable and it too has helped me grow as a scientist. “Original” Beth, Han, and Lyn, thanks for making this a great working environment. Fellow grad students, thank you for making this an exciting and interesting experience. I now have memories that will stay with me forever.

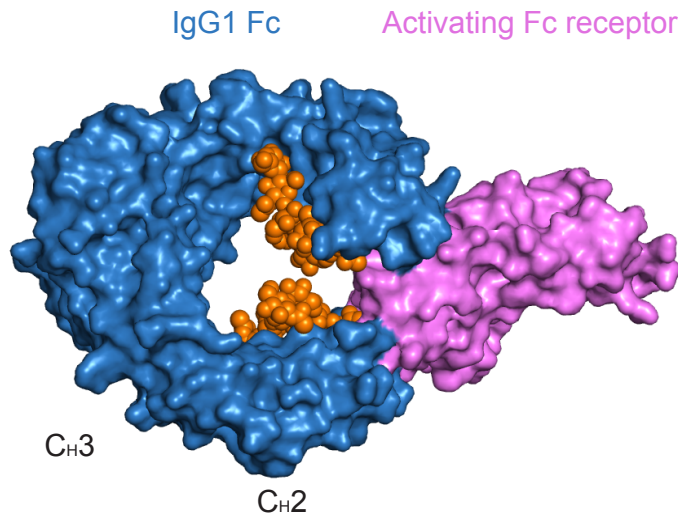
Last but most importantly I want to thank my family and friends. Thank you Mom and Dad for your constant love, encouragement, and support my whole life. I couldn’t ask for better parents and feel honored that I am your child. I would like to dedicate this to my Grandparents who I have lost. I know that they would have enjoyed sharing this moment with me.

## ABSTRACT

Immunoglobulin G (IgG) is central in mediating host defense due to its ability to target and eliminate invading pathogens. The fragment antigen binding (Fab) regions are responsible for antigen recognition; however the effector responses are encoded on the Fc region of IgG. IgG Fc displays considerable glycan heterogeneity, accounting for its complex effector functions of inflammation, modulation and immune suppression. Intravenous immunoglobulin G (IVIg) is pooled serum IgG from multiple donors and is used to treat individuals with autoimmune and inflammatory disorders such as rheumatoid arthritis and Kawasaki's disease, respectively. It contains all the subtypes of IgG (IgG1-4) and over 120 glycovariants due to variation of an Asparagine 297-linked glycan on the Fc. The species identified as the activating component of IVIg is sialylated IgG Fc. Comparisons of wild type Fc and sialylated Fc X-ray crystal structures suggests that sialylation causes an increase in conformational flexibility, which may be important for its anti-inflammatory properties.



Although glycan modifications can promote the anti-inflammatory properties of the Fc, there are amino acid substitutions that cause Fcs to initiate an enhanced immune response. Mutations in the Fc can cause up to a 100-fold increase in binding affinity to activating Fc gamma receptors located on immune cells, and have been shown to enhance antibody dependent cell-mediated cytotoxicity. This is important in developing therapeutic antibodies against cancer and infectious diseases. Structural studies of mutant Fcs in complex with activating receptors gave insight into new protein-protein interactions that lead to an enhanced binding affinity.



Together these studies show how dynamic and diverse the Fc region is and how both protein and carbohydrate modifications can alter structure, leading to IgG Fc's switch from a pro-inflammatory to an anti-inflammatory protein.

## TABLE OF CONTENTS

<b>ACKNOWLEDGEMENTS</b> .....	ii
<b>ABSTRACT</b> .....	iv
<b>TABLE OF CONTENTS</b> .....	vi
<b>CHAPTER 1: Review of Immunoglobulin G Fc Function</b>	
Introduction.....	1
<b>CHAPTER 2: Structural Characterization of Anti-Inflammatory Immunoglobulin G Fc Proteins</b>	
Published as Ahmed, A.A., Giddens, J., Pincetic, A., Lomino J.V., Ravetch, J.V., Wang, L-X., Bjorkman, P.J. (2014) Structural characterization of anti-inflammatory Immunoglobulin G Fc proteins. <i>J Mol Biol</i> 426:3166-3179	
Abstract.....	17
Introduction.....	18
Results.....	21
Discussion.....	30
Figure Legends.....	32
Methods.....	37
Acknowledgements.....	43
Figures and Tables.....	45

**CHAPTER 3: Structural Characterization of GASDALIE Fc Bound to Activating Fc Gamma Receptor Fc $\gamma$ R11a**

Abstract.....	59
Introduction.....	60
Results.....	63
Discussion.....	70
Figure Legends.....	73
Methods.....	76
Acknowledgements.....	79
Figures and Tables.....	81

**CHAPTER 4: Investigation of the Proposed Interaction of DC-SIGN with Sialylated Fc**

Introduction.....	91
Methods/Results.....	94
Conclusion.....	96

**CHAPTER 5: Conclusion of thesis**

Conclusion.....	98
Bibliography.....	105



## **Chapter 1: Review of Immunoglobulin G Fc Function**

## INTRODUCTION

### *Immunoglobulin G Review*

The Immunoglobulin G (IgG) is a glycoprotein consisting of two heavy and two light chains that are covalently linked through a series of disulfide bonds [1]. This protein is further divided into two major components: the fragment antigen-binding regions (Fab) and the fragment crystallizable region (Fc). The Fab is a heterodimer consisting of a portion of the heavy chain ( $V_H$ ,  $C_{H1}$ ) and light chain ( $V_L$ ,  $C_L$ ) that are covalently associated via a disulfide bond between the residues Cys220 in IgG1 and Cys131 in IgG2-IgG4 in the  $C_{H1}$  domain with a carboxy-terminal cysteine of the light chain [2]. The variable regions ( $V_H$  and  $V_L$ ) are involved in direct binding to a specific antigen, whereas the Fc region interacts with several receptors on innate immune cells. The Fc is a homodimer connected to the Fab region through a flexible hinge (residues Glu216-Pro230 for IgG1), which is stabilized by two disulfide bonds (Cys229 and Cys 226) [3] (Fig. 1A). The light chain is further classified into  $\kappa$  and  $\lambda$  chains based on their  $C_{H1}$  domain sequence [4]. Each chain of the Fc contains constant  $C_{H2}$  and  $C_{H3}$  domains. The  $C_{H2}$  domain contains a single *N*-linked glycosylation site at Asparagine 297 (Asn297). This glycan contributes to the overall “openness” of this protein giving it a horseshoe shape (Figure 1A,B) [5]. Each domain of IgG has a characteristic immunoglobulin fold (Ig) in both the Fab and Fc domains (Fig. 1C, 1D). They consist of two  $\beta$ -sheets comprised of anti-parallel  $\beta$ -strands sandwiched and stabilized by inter-chain

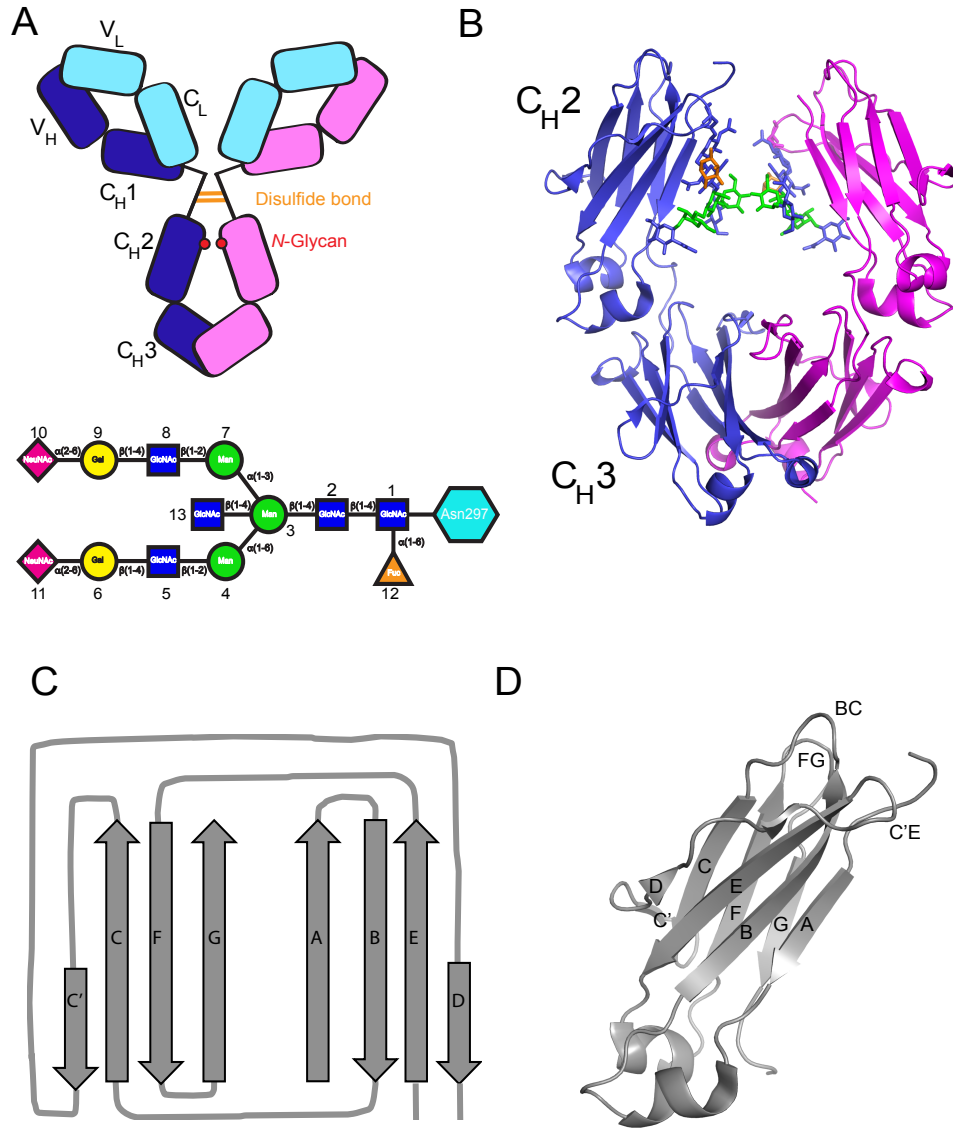


**Figure 1.** (A) Schematic structure of IgG1 and of an Asn297-linked N-glycan. The biantennary glycan consists of a mannose (Man) and N-acetylglucosamine (GlcNAc) core that is usually fucosylated (Fuc), and can be further modified by addition of a bisecting GlcNAc, terminal galactose (Gal), or sialic acid (NeuNAc). (B) Ribbon diagram of wild type Fc (PDB ID: 3AVE) with glycans shown as sticks. (C) Topology diagram and ribbon diagram (D) of Ig fold of immunoglobulin constant region.

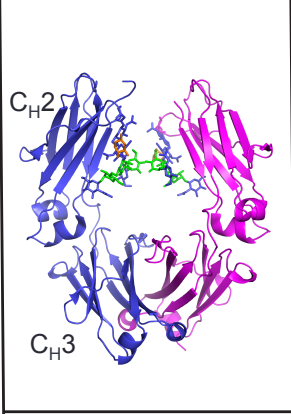
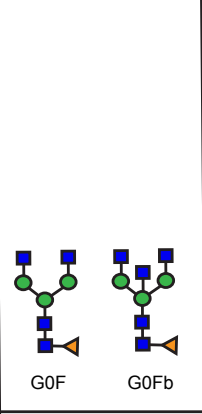
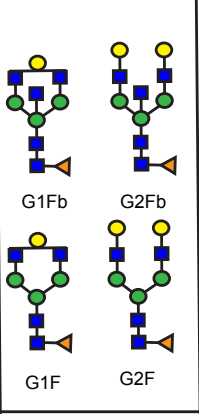
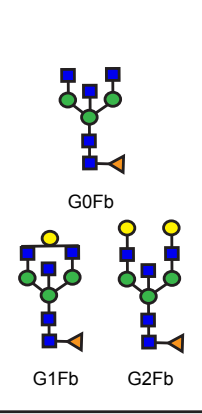
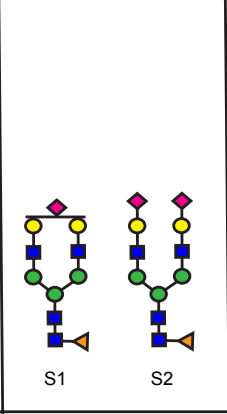
disulfide bonds [2, 4]. This folding creates loops BC, FG, and C'E in the C<sub>H</sub>2 domain of the Fc that are known binding sites of Fc gamma receptors (Fc $\gamma$ Rs), whereas the complementarity determining region (CDR) loops are known binding sites for specific antigens and are therefore variable. The constant domains of the Fc are conserved across each IgG subtype (IgG1-IgG4), however variability increases when it comes to the glycan chain[6, 7].

### ***N-linked Glycan of IgG***

The Asn297-linked glycan is a complex carbohydrate, made out of a mannose (Man) and *N*-acetylglucosamine (GlcNAc) core that is usually fucosylated. This glycan can be additionally modified with a bisecting GlcNAc, terminal galactose, and/or sialic acid [8] (Fig. 1A). This glycan contributes about 2-3% (4kDa) of the overall molecular weight of the IgG [7]. Due to glycan modifications and IgG subtypes there are over 120 glycovariants of IgG found circulating in human serum [9]. IgG1 is the most common of all subtypes with a circulating concentration of 10-15 mg/ml [7]. With respect to glycosylation, fucosylation is the most common, with about 70% of IgGs containing this modification. 50% are terminally galactosylated, with 35% containing agalactosylated (G0) species, 35% containing mono-galactosylated (G1), and 16% of the human pool containing digalactosylated (G2). 15% contains some form of sialylation; 11% mono-sialylated (S1) and 4% disialylated (S2) [10] (Table. 1). Removing the *N*-linked glycan leads to a dramatic change in Fc conformation and

abrogation of binding to any  $\text{Fc}\gamma\text{R}$ ; however, aglycosylated Fc can bind the  $\text{Fc}\gamma\text{Rn}$  protection receptor [11], which recognizes the interface between the  $\text{C}_{\text{H}2}$  and  $\text{C}_{\text{H}3}$  domains of each Fc chain [12], a site distant from the Asn297-linked *N*-linked glycan. Modification of this glycan is known to alter binding of Fc to  $\text{Fc}\gamma\text{Rs}$  reflecting its importance when it comes to Fc function.

**Table 1.** *N*-glycan composition of serum IgG

				
IgG Asn297 linked glycan	terminal GlcNAc	terminal galactose	bisecting GlcNAc	terminal sialic acid
abundance in human serum (%)	35	50	32	11 (S1), 4 (S2)

(■ GlcNAc; ● Man; ● Gal; ◄ Fuc; ◆ Sia)

### ***Antibody-Dependent Cell-Mediated Cytotoxicity***

Antibody-dependent cell-mediated cytotoxicity (ADCC) is an intricate process involving antibodies connecting the innate and adaptive immunity to attack and destroy invading pathogens and/or tumor cells. Effector cells are activated when antigen/antibody immune complexes (IC) bind activating Fc gamma receptors ( $\text{Fc}\gamma\text{Rs}$ ) expressed on the surface, thereby initiating a cascade leading to cell activation and ultimately destruction of target cells [13]. Three main activating

receptors involved in ADCC are Fc $\gamma$ RI/CD64, Fc $\gamma$ RIIa/CD32 (H131/R131), and Fc $\gamma$ RIIIa/CD16 (F158/V158). Fc $\gamma$ RI and Fc $\gamma$ RIIa are found predominantly on the surface of macrophages, and Fc $\gamma$ RIIIa on natural killer (NK) cells [13-15] (Fig. 3). Fc $\gamma$ RIIIa and Fc $\gamma$ RI are type I transmembrane proteins containing two or three extracellular C2-type immunoglobulin-like domains, respectively, and immunoreceptor tyrosine based activation motifs (ITAMs) on the cytoplasmic domain of a receptor-associated  $\gamma$ -chain. Fc $\gamma$ RIIa has two extracellular domains and an ITAM motif on a single chain [15-17].

There are multiple pathways activated in response to engagement of Fc $\gamma$ RIIIa with ICs. ITAMs become phosphorylated by Src kinases creating a docking site for spleen tyrosine kinases (Syk). Activated Syk then goes on to phosphorylate phospholipase C-gamma (PLC- $\gamma$ ) which translocates to the membrane to cleave phosphatidylinositol 4,5-bisphosphate (PIP<sub>2</sub>) to make diacylglycerol (DAG) and inositol-1,4,5-triphosphate (IP<sub>3</sub>). IP<sub>3</sub> goes on to cause an increase in intracellular calcium resulting in activation and mobilization of cells [18, 19]. Activation of Src kinases also results in phosphorylation of phosphoinositol 3-kinase (PI-3K) that goes on to phosphorylate PIP<sub>2</sub>, which becomes PIP<sub>3</sub>. PIP<sub>3</sub> then recruits PLC- $\gamma$  [2]. Syk

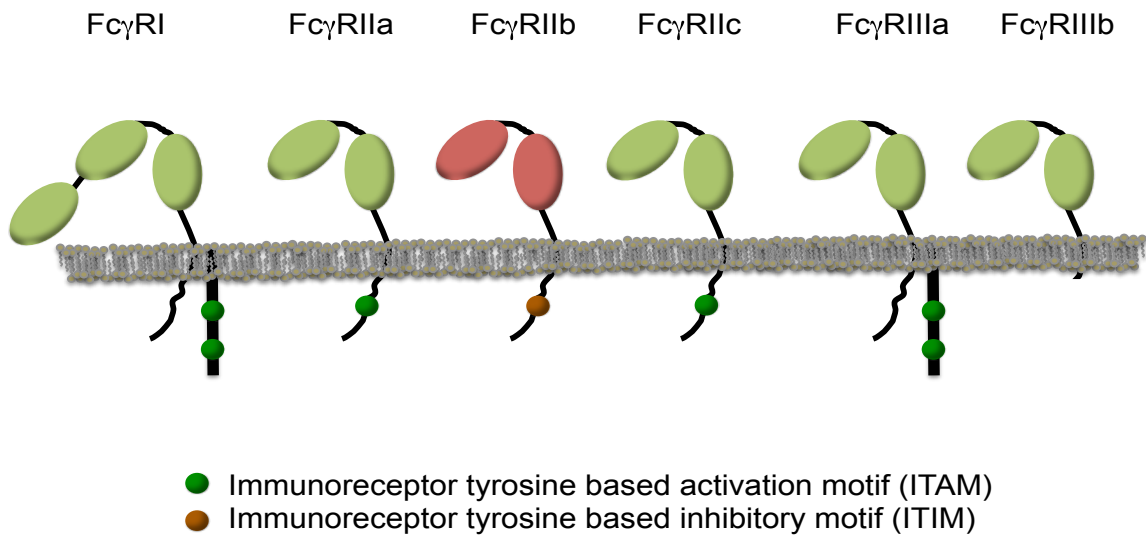


**Figure 2.** Cartoon representation of Fc gamma receptors (Fc $\gamma$ Rs). Activating Fc $\gamma$ Rs with immunoreceptor tyrosine based activation motifs (ITAMs; green) or the inhibitory receptor with an immunoreceptor tyrosine based inhibitory motif (ITIM; red).

also activates Vav/Rho proteins involved in ADCC, however, the exact mechanism remains unclear [20, 21]. The signaling cascades described above are specific for Fc $\gamma$ RIIIa – these mechanisms have not been confirmed for Fc $\gamma$ RIa, Fc $\gamma$ RIIa, or Fc $\gamma$ RIIIb. Similar to Fc $\gamma$ RIIa, Fc $\gamma$ RIIb is a type I transmembrane protein with two C2-type Ig domains expressed on B cells, macrophages, neutrophils, and mast cells [15, 18, 22]. This receptor inhibits calcium influx, cell activation, and mobilization due to its immunoreceptor tyrosine-based inhibitory motif (ITIM). Crosslinking of cell surface receptors leads to recruitment of SH2 containing

inositide phosphatase (SHIP), which hydrolyzes proteins involved in the PLC- $\gamma$ , PI-3K, and Vav/Rho pathways [18, 23].

Several killing pathways in response to the crosslinking of Fc $\gamma$ RIIIa on NK cells have been characterized. The most widely known and accepted is the perforin/granzyme pathway that results in apoptosis of the target cell. The activated effector NK cell releases a perforin:granzyme complex which interacts with Mannose-6 phosphate receptor (MPR), a surface protein on target cells. This interaction leads to endocytosis of the perforin:granzyme complex in the target cell. Granzyme B, a serine protease, is then released into the cytosol, from endosomes containing both granzyme and perforin, by a perforin pore, leading to activation of caspases and apoptosis. Perforin activation can independently cause lysis and cell death [24]. Crosslinking of Fc $\gamma$ RIIIA resulting from binding of antibody/target cell ICs on the surface of natural killer cells causes a transcriptional upregulation of Fas ligand (FASL). NK cells expressing FASL then go to kill target cells expressing the FAS receptor (CD95/ APO-1), inducing apoptosis [24, 25].

### ***Mutations/Modifications to Enhance ADCC***

A glycovariant known to greatly enhance ADCC is afucosylated Fc ( $\alpha$ 1,6 linked fucose removed). Afucosylated Fc is a non-common form of IgG Fc that is produced in Lec13 cells that have decreased GDP-Man-4,6-dehydratase activity. IgGs expressed in these cells are shown to have decreased fucosylation by 80% compared to 98% fucosylated product when expressed in Chinese hamster ovary



(CHO) cells with normal GDP-Man-4,6-dehydratase activity [26-28]. The afucosylated product was found to have 100-fold higher binding to Fc $\gamma$ R11a by both enzyme-linked immunosorbent assays (ELISA) and surface plasmon resonance (SPR) experiments when compared to fucosylated Fc [27-31]. Subsequently, this increase in binding affinity to one of the main activating receptors involved in ADCC also caused an increase in cytotoxicity of target cells [27, 32]. A key study by Shields *et al.* characterized the cytotoxic effects of afucosylated vs. fucosylated Fc. Anti-HER2 antibody hu4D5-8 expressed in Lec13 cells was used in an ADCC assay against human breast cancer cells SK-BR-3 expressing HER2. Effector peripheral blood mononuclear cells (PBMCs) from six donors expressing either Fc $\gamma$ R11a (Val158/Phe158) or Fc $\gamma$ R11a (Phe158/Phe158) were used at a 30:1 ratio (pBMC:SK-BR-3). A 53-fold increase in cytotoxic effects was observed when afucosylated Fc was used, in comparison to fucosylated Fc which directly correlated to the increase in binding affinity to Fc $\gamma$ R11a [27]. In addition to these *in vitro* studies, *in vivo* studies also demonstrated that afucosylated Fc increased ADCC in mouse models. These studies also showed increased ADCC has a direct correlation to increased binding to activating Fc $\gamma$ Rs.

Murine IgG2 has the highest binding affinity to Fc $\gamma$ Rs in comparison to human subtypes, of which IgG1 has the highest affinity [33]. When fucose is removed, the binding affinity of murine IgG2 to the inhibitory receptor (Fc $\gamma$ R11b) and activating receptor (Fc $\gamma$ R1V) increased when compared to fucosylated IgG2. Post induction of melanoma lung metastasis, mice were treated with either fucosylated IgG2 or

afucosylated IgG2. The authors found that afucosylated Fc significantly decreased the number of tumor cells compared to its fucosylated counterpart which showed little to no effect [32].

A study by Ferrara *et al.* also demonstrated the importance of fucosylation in relation to binding to Fc $\gamma$ Rs. Afucosylated Fc showed an increased binding to Fc $\gamma$ R111a by surface plasmon resonance (SPR) [29, 30, 34]. In addition to showing increased binding, the authors solved high-resolution crystal structures of afucosylated Fc and fucosylated Fc in complex with Fc $\gamma$ R111a. There were new carbohydrate-carbohydrate and protein-carbohydrate interactions observed in the afucosylated complex structure that were not seen in the fucosylated one. Specifically, GlcNAc1 on the Fc forms new hydrogen bonds with GlcNAc1 and GlcNAc2 of the N-linked glycan at site 162 of the receptor. Man3 of Asn162 on Fc $\gamma$ R111a also forms hydrogen bonds with Gln295 (afucosylated Fc) and Lys128 (Fc $\gamma$ R111a), respectively, further stabilizing the complex. There was also a displacement of the Asn162 glycan in the fucosylated complex where there is an increase in distance of the carbohydrate interactions between that glycan and the Asn297 glycan of the Fc. This complex was key in understanding how removal of the core fucose allows better binding to the receptor.

Although afucosylation is widely known to enhance ADCC both *in vitro* and *in vivo*, efforts have been made to increase Fc $\gamma$ R111a binding through modification of the polypeptide, as opposed to glycan modification. Lazar *et al.* conducted a screen of

different combinations of mutants in the C<sub>H</sub>2 domain of known Fc<sub>γ</sub>R binding regions [35, 36]. A G236A/S239D/I332E (GASDIE) mutant Fc was shown to have 70-fold enhanced binding to activating receptor Fc<sub>γ</sub>R1a and enhanced phagocytosis *in vitro*. Mutants S239D/I332E (SDIE) and S239D/A330L/I332E (SDALIE) demonstrated enhanced ADCC and increased binding to activating receptor Fc<sub>γ</sub>R11A. The difference between these two Fcs is the A330L mutation. Addition of this mutation destroys complement-dependent cytotoxicity (CDC), which might result from A330 being in close to the C1q binding site, selecting for an ADCC response [37]. The published unbound structure of the SDALIE mutant did not show any significant changes in the known Fc<sub>γ</sub>R binding region although it was in an overall more open conformation when compared to wtFcs [38].

### ***Anti-Inflammatory Properties of IgG Fc***

In addition to eliciting inflammation, IgG Fcs plays a certain role in suppressing immune response. Throughout the years efforts have been made to treat autoimmune and inflammatory disorders such as rheumatoid arthritis and Kawasaki's disease, respectively. One widely known treatment is intravenous immunoglobulin G (IVIG) therapy. Patients are administered 1g/kg of pooled IgG from the serum of various donors every few weeks to treat their disease and to suppress inflammation. Although this therapy is successful, it only works at high doses because sialylated Fc is the activating component in IVIG. Sialylation is not a common modification of IgGs, with only 11% mono-sialylated and 4% disialylated in the human serum. Additionally those who suffer from rheumatoid

arthritis have an even smaller amount of sialylated antibodies and a higher amount of agalactosylated species [39, 40]. Several *in vivo* experiments have shown that disialylated Fc is important and lead to various models proposed for its activation.

### ***K/BxN Mouse Model***

The K/BxN arthritis mouse model was a valuable tool used to study antibody therapies for autoimmune and inflammatory disorders. K/Bxn mice were produced to have the arthritogenic T Cell receptor (TCR), KRN, and MHC class II allele  $A^{g7}$  (I-A<sup>g7</sup>), which results in joint inflammation reflective of human arthritis [41]. The KRN TCR recognized anti-glucose-6-phosphate isomerase (GPI) antibodies presented by MHC class II I-A<sup>g7</sup> on B cells. This lead to B cell expansion and secretion of GPI autoantibodies [41, 42]. Serum from these transgenic mice, or the injection of GPI autoantibodies into naive mice, is sufficient to induce inflammation [42].

This model was of central importance in characterizing IVIG. When inflammation is induced intravenously in mice, using K/Bxn serum, followed by administration of a high dose of IVIG (1g/kg), protection from inflammation is observed along with a visible decrease in joint inflammation [43, 44]. These results prompted the question: Why is such a high dose required for protection against inflammation? When IVIG was administered at a lower dose (0.33g/kg) protection was not observed, which suggested that only a small fraction of a specific species was responsible for anti-inflammatory protection [43, 44]. Additionally, when IVIG was

treated with neuraminidase (NA), an enzyme that removes sialic acid, and administered to mice after post-induction of inflammation, protection was not observed [43]. The same result was observed when the glycan was removed by peptide-*N*-glycosidase (*PNGase*) F [43].

IVIG IgG and IVIG Fc (papain digested) were enriched for sialylation using *Sambucus Nigra* (SNA) lectin, a lectin that binds preferentially to  $\alpha$ 2,6 linked sialic acids [45]. A smaller amount (.033g/kg) of SNA-enriched IgG and Fc was needed to initiate the same protective effect as unmodified IVIG IgG and Fc administered at 1g/kg [43, 44]. Fcs enzymatically sialylated with  $\alpha$ 2,6 sialyltransferase (ST6Gal1) also produced the same affect as SNA-enriched Fcs [46]. Although these experiments showed that Fcs that are mono-sialylated and disialylated were the active component in IVIG, the exact pathway is poorly understood.

### ***Role of DC-SIGN in the Anti-Inflammatory Pathway***

Dendritic cell-specific intercellular adhesion molecule-3-grabbing non-integrin (DC-SIGN) is a type II transmembrane protein that is calcium dependent and exists as a tetramer in the membrane of both macrophage and dendritic cells. It contains a carbohydrate recognition domain (CRD) that is the main binding site of sugars for this C-type lectin, and a neck region responsible for tetramerization, a transmembrane region, and cytoplasmic domain [47-49]. The mouse orthologue of DC-SIGN is specific intercellular adhesion molecule-3-grabbing nonintegrin-related 1 (SIGN-R1)[50]. DC-SIGN is known to bind gp120 on the HIV viral spike, thereby

facilitating infection; however, only recently it was found to be involved in the anti-inflammatory pathway and essential for IVIG function [46, 48].

A study published in 2011 identified DC-SIGN and Fc $\gamma$ RIIB as key receptors of the anti-inflammatory pathway mediated by sialylated Fcs [46]. Using the K/BxN model, inflammation was induced in wild type mice (SIGN-R1<sup>+</sup>), mice lacking the SIGN-RI receptor (SIGN-R1<sup>-/-</sup>), and mice expressing hDC-SIGN (hDC-SIGN<sup>+</sup>/SIGN-R1<sup>-/-</sup>), followed by treatment with a low dose of sialylated Fc (.03 g/kg). The wild type mice showed a decrease in inflammation after five days of being treated with sialylated Fcs. No protective effect was observed upon administration of sFc to the SIGN-R1<sup>-/-</sup> knockout mice; however, if hDC-SIGN was introduced in the SIGN-R1<sup>-/-</sup> knockout, sFc was effective in decreasing inflammation. This led to the conclusion that DC-SIGN/SIGN-R1 is involved in the anti-inflammatory pathway. In addition to DC-SIGN, cytokines IL-4 and IL-33 were found to be a crucial part of this pathway. When IL-4<sup>-/-</sup> mice were administered sFc post treatment with K/BxN, inflammation was not suppressed. This was also the case when the IL-4 receptor (IL-4R $\alpha$ ), expressed predominantly on effector macrophages, or the receptor associated signaling adaptor proteins (Stat6) were knocked out. Depletion of basophils known to release IL-4 was also able to abrogate the protective effect of IVIG and sFc. Additionally if IL-33 or its associated receptors (expressed on Fc $\epsilon$ R1<sup>+</sup> leukocytes) were knocked out, protection was not observed. IL-4 upregulates Fc $\gamma$ RIIB on the surface of monocytes, therefore this receptor was also considered a potential candidate for the anti-inflammatory

pathway [51]. In Fc $\gamma$ R1IB  $-/-$  mice, IVIG-mediated protection from inflammation is not observed. Even though the key players involved in this pathway have been identified, the question remains to be asked if DC-SIGN is in fact the binding partner of sialylated Fc.

### ***NMR Analysis of Sialylated Fc***

Nuclear magnetic resonance (NMR) is a key tool used to understand dynamics of glycoproteins and polysaccharides. Specifically, NMR was used to study motions of IgG Fc glycans ( $\alpha$ 1,3 branch and  $\alpha$ 1,6 branch) and also to observe changes in the branch resulting from sialylation [52]. The galactose residue of the  $\alpha$ 1,6 branch was shown to experience slightly less motion when compared to the  $\alpha$ 1,3 branch for both mono- and disialylated Fc; however the sialic acids were highly dynamic and did not interact strongly with the polypeptide backbone. This data supports hypersialylated and disialylated crystal structures where the terminal sialic acid modeled on the  $\alpha$ 1,6 arm projects away from the protein backbone [53, 54].

## **Chapter 2: Structural Characterization of Anti-Inflammatory Immunoglobulin G Fc Proteins**

Published as Ahmed, A.A., Giddens, J., Pincetic, A., Lomino J.V., Ravetch, J.V., Wang, L-X., Bjorkman, P.J. (2014) Structural characterization of anti-inflammatory Immunoglobulin G Fc proteins. *J Mol Biol* 426:3166-3179



## ABSTRACT

Immunoglobulin G (IgG) is a central mediator of host defense due to its ability to recognize and eliminate pathogens. The recognition and effector responses are encoded on distinct regions of IgGs. The diversity of the antigen recognition Fab domains accounts for IgG's ability to bind with high specificity to essentially any antigen. Recent studies have indicated that the Fc effector domain also displays considerable heterogeneity, accounting for its complex effector functions of inflammation, modulation and immune suppression. Therapeutic anti-tumor antibodies, for example, require the pro-inflammatory properties of the IgG Fc to eliminate tumor cells, while the anti-inflammatory activity of intravenous immunoglobulin G (IVIg) requires specific Fc glycans for activity. In particular, the anti-inflammatory activity of IVIg is ascribed to a small population of IgGs in which the Asn297-linked complex *N*-glycans attached to each Fc C<sub>H</sub>2 domain include terminal α2,6-linked sialic acids. We used chemoenzymatic glycoengineering to prepare fully di-sialylated IgG Fc and solved its crystal structure. Comparison of the structures of asialylated Fc, sialylated Fc, and F241A Fc, a mutant that displays increased glycan sialylation, suggests that increased conformational flexibility of the C<sub>H</sub>2 domain is associated with the switch from pro- to anti-inflammatory activity of the Fc.

## KEYWORDS

sialylated IgG Fc, inflammation, IVIg, *N*-linked glycan, X-ray crystallography

## INTRODUCTION

IVIG is used worldwide as an antibody replacement therapy and as a treatment for a variety of inflammatory disorders [55]. IVIG is pooled IgG from the serum of healthy donors. It contains the four different subtypes of human IgG (IgG1, IgG2, IgG3, and IgG4) and over 30 glycovariants [9]. Although the beneficial effects of IVIG as an anti-inflammatory preparation are apparent, the mechanism of action has only recently begun to be understood as being correlated with the relatively constant portion, or Fc region, of IgGs [56]. The Fc region of IgG interacts with a variety of receptors, determined by the amino acid and glycan composition of the Fc. Among these receptors are the canonical Fc $\gamma$ Rs: four are activating (Fc $\gamma$ RI, Fc $\gamma$ RIIA, Fc $\gamma$ RIIIA, Fc $\gamma$ RIIIB) and one is an inhibitory receptor (Fc $\gamma$ RIIB) [56]. The simultaneous expression of these receptors on effector cells sets a threshold for inflammatory responses [57]. IVIG causes an up-regulation of the inhibitory receptor Fc $\gamma$ RIIB, initiating anti-inflammatory responses [58].

A downside of IVIG therapy is that it is only effective when administered at high doses (1-3 g/kg) when treating inflammatory diseases [59]. Rationalizing the high dose requirements, the anti-inflammatory activity of IVIG has been attributed to a small population of IgGs with  $\alpha$ 2,6-sialylated *N*-linked glycans attached to a conserved asparagine (Asn297) in the Fc C<sub>H</sub>2 domain [44]. The Asn297-linked carbohydrate is a complex, usually core-fucosylated, biantennary glycan containing a pentasaccharide Man<sub>3</sub>GlcNAc<sub>2</sub> core (Man, mannose; GlcNAc, N-acetylglucosamine), which can be modified by addition of terminal galactose or

sialic acid [8] (Fig. 1). Approximately 10% of the Fc regions in IVIG terminate in sialic acid, of which 1-3% are disialylated [7, 43]. *In vivo* studies have shown that Fc sialylation is the main determinant in IVIG anti-inflammatory activity [43, 60]. For example, IVIG that was enriched in terminally-sialylated Fc glycans showed a 10-fold increase in anti-inflammatory activity [44, 46], and if IVIG was treated with neuraminidase to remove terminal sialic acids or with PNGase F to remove the entire N-linked glycan, the anti-inflammatory activity of IVIG was abrogated [43]. Similar results were found for recombinant, 2,6 sialylated IgG1 [44]. In mouse models, including a serum-induced arthritis model in mice, sialylated Fc (sFc; defined here as referring to a mixture of sialylated glycoforms) decreased inflammation of ankle joints [43], and IVIG activity was shown to be dependent upon terminally-sialylated Fc regions in four independent *in vivo* model systems of autoimmune disease mediated by auto-antibodies [60].

The anti-inflammatory properties of sFc have been attributed to the effect of sialylation switching the specificity of Fc binding to its receptors. *In vivo* experiments showed that the anti-inflammatory effects of sFc required expression of the C-type lectin-like receptor-specific intracellular adhesion molecule-grabbing non-integrin R1 (SIGN-RI) (the mouse homolog of human dendritic cell-specific intercellular adhesion molecule-3-grabbing nonintegrin; DC-SIGN), leading to a model in which conformational changes in Fc resulting from sialylation of the Asn297-attached glycan allowed interactions with members of the SIGN receptor family [61]. Indeed, previous structural studies demonstrated that modification of

the Asp297-linked glycan could affect Fc structure. For example, it was shown that the glycan contributed to an “open” conformation of IgG Fcs, in which the C<sub>H</sub>2 domains were separated by a larger distance than in deglycosylated Fc structures [5]. If the IgG Fc glycan was enzymatically removed, the C<sub>H</sub>2 region adopted a “closed” state [62]. Conformational changes have also been observed when individual sugar residues on the Fc-linked glycan were modified. When fucose was removed, a subtle change involving Tyr296 was observed in X-ray crystallographic and NMR structures [29, 31]. This modification resulted in an increased affinity for the activating receptor FcγRIIIa, leading to enhanced antibody-dependent cellular cytotoxicity (ADCC) activity [27, 32]. Solution NMR studies have reported increased mobility of the glycan arms upon sialylation, further supporting the contention that alterations in the glycan composition can influence the structure of the Fc [52].

Here we solved the crystal structure of a chemically-homogeneous disialylated Fc (di-sFc) and compared it to new structures of a partially sialylated Fc (F241A Fc) and wtFc, as well as to wtFc and glycomutant Fc structures available in the protein data bank (PDB). We found that di-sFc and F241A Fc show increased conformational heterogeneity in crystals compared to wtFc, a characteristic that may relate to sialylation and anti-inflammatory properties.

## RESULTS

### ***Glycan Analysis of Purified Fc Proteins***

Proteins were produced by transient transfection in HEK 293-6E cells as IgG1 Fc fragments (wtFc, F241A Fc and F243A Fc) or in a stably-transfected Chinese hamster ovary (CHO) cell line (wtFc) [63]. Disialylated sFc (di-sFc) was prepared by chemoenzymatic glycoengineering [64] of an Fc fragment isolated after papain cleavage of Rituximab, a human IgG1.

Carbohydrate analyses of *N*-glycans released from the Fc proteins revealed that the *N*-glycans attached to Asn297 of wtFc expressed in either HEK293 or CHO cells consisted of only three glycoforms: G0F, G1F, and G2F (Fig. 2a,b,). This result was consistent with previous studies investigating glycoforms of IgGs expressed in HEK cells [65]. Neither mono- nor disialylated *N*-glycans on either form of wtFc were detected. By contrast, the glycans attached to the F241A and F243A Fc mutants contained more diverse glycoforms: in addition to the G0F, G1F, and G2F glycoforms, significant portions of the *N*-glycans carried a bisecting GlcNAc moiety and contained terminal sialic acids (Fig. 2c,d,). The sialylated forms included about 20% of terminally monosialylated *N*-glycans (S1G2F and other monosialylated glycoforms) and about 4% of disialylated *N*-glycans (S2G2F and other disialylated glycoforms). These results were consistent with a recent study of the F241A and F243A Fc mutants [65], suggesting that these substitutions promote further processing of Fc glycans resulting in generation of sialylated and bisecting GlcNAc-containing glycoforms. The chemoenzymatically remodeled Fc

(di-sFc) was almost homogeneous: >95% of the *N*-glycans were the disialylated glycoform (Fig. 2e, Fig. S1).

We also compared the Fc proteins in a Western blot using *Sambucus Nigra* (SNA), a lectin that binds preferentially to  $\alpha$ 2,6-linked sialic acid attached to a terminal galactose [45]. As expected, SNA blots of wtFc, F241A, F243A and di-sFc proteins demonstrated sialylation of di-sFc, F241A Fc and F243A Fc, but not wtFc (Fig. 3). These results were consistent with previous reports of partial sialylation of the *N*-glycans of F241A and F243A Fc [66].

Liquid chromatography/electrospray ionization mass spectrometry (LC-ESI-MS) was used to analyze wtFc that was expressed as an Fc fragment in HEK cells before and after complete removal of the *N*-glycans by PNGase F treatment. The analysis revealed two major species that were 950 and 1315 Da larger than the calculated molecular mass of the polypeptide backbone following PNGase F treatment, suggesting the existence of additional posttranslational modifications (Fig. S2a). A similar analysis of wtFc expressed in CHO cells revealed three major species that were 269, 922, and 1218 Da larger than the calculated molecular mass of the polypeptide backbone (Fig. S2b). The results for the F241A Fc and F243A Fc proteins that were expressed in HEK cells were the same as the HEK-expressed wtFc (Fig. S2c,d). In contrast, an Fc fragment prepared from papain cleavage of an intact IgG1 (Rituximab) did not contain posttranslational modifications other than the *N*-glycans (Fig. S2e). A monosaccharide composition

analysis of the recombinant Fcs after removal of the *N*-glycans with PNGase F revealed the presence of GalNAc, GlcNAc, Gal, and Neu5Ac (Fig. S3b,c), suggesting the existence of O-linked glycans. In contrast, the Fc fragment prepared from papain cleavage of Rituximab did not contain any monosaccharides after PNGase F cleavage (Fig. S3d). On the basis of the additional molecular mass (950 Da) in comparison with the polypeptide backbone, the major O-glycan on the HEK-expressed Fcs appeared to be a core 1 structure carrying two sialic acid residues [calculated mass for (Neu5Ac)<sub>2</sub>-Gal-GalNAc-H<sub>2</sub>O = 947.86 Da]. In the CHO-expressed wtFc, an additional mass of 1218 Da on the polypeptide backbone was observed. However, this additional mass does not correspond to typical O-glycan structures, implicating potential additional modifications to the core structures; e.g., acetylation on the sialic acid moieties. The detailed structures of the O-glycans remain to be determined. However, the lack of reactivity of HEK-expressed wtFc in the SNA blot (Fig. 3) demonstrated that there were no  $\alpha$ 2,6-linked sialic acids on the putative O-glycans. Since the hinge region of IgG where the O-glycans would likely be located is usually disordered in Fc crystal structures, these glycans (if present) would not be visible in published structures of recombinantly-expressed Fc fragments [38, 65, 67, 68]. Nor are there apparent differences in the structural properties of Fcs that correlate with whether they were expressed as Fc fragments versus prepared by cleavage of intact IgG (Table 1).

The finding of putative O-glycans on proteins expressed as Fc fragments, but not on an Fc fragment derived by cleavage of intact IgG, could be explained if expression of Fc as a fragment allows access during biosynthesis by O-glycan-

adding enzymes in the Golgi apparatus to a region of the IgG hinge that is inaccessible when intact IgG is trafficking through the Golgi. Although there were no apparent structural differences in Fcs as a function of whether or not they were produced in a form predicted to contain the putative O-glycan, these results suggest that functional studies employing Fcs expressed directly as fragments should compare results with Fcs derived by enzymatic cleavage of intact IgGs to rule out potential effects of unnatural O-glycosylation.

### ***wtFc Structures Are Relatively Similar***

In order to assess potential conformational differences in Fc structures, we first compared wtFc structures available in the Protein Data Bank (PDB) and a 2.4 Å resolution wtFc structure solved in this study (space group P2<sub>1</sub>2<sub>1</sub>2<sub>1</sub>; one molecule per asymmetric unit) (Supplementary Table 1). We defined “wild type” as those Fc structures that were derived from IgGs or Fc fragments containing the naturally-occurring mixture of *N*-glycans attached to Asn297 when the protein was produced in mammalian cells, which included our new wtFc structure and PDB entries 1H3X, 3AVE, 2DTS, 3DO3, 1FC1, and 1HZH. Fc fragments are homodimers in which the N-terminal C<sub>H</sub>2 domains contact each other through their Asn297-linked *N*-glycans, and the C-terminal C<sub>H</sub>3 domains form a stable interface that is relatively constant between structures (Fig. 1b and 4a). Although the C<sub>H</sub>2 domain *N*-glycans are generally heterogeneous in wtFc proteins (Fig. 2), ordered electron density is usually observed for eight or nine carbohydrate residues of the biantennary



complex glycan attached to the Asn297 of each C<sub>H</sub>2 domain (PDB codes: 1H3X, 3AVE, 2DTS, 3DO3, 1FC1, and 1HZH).

In order to evaluate potential differences in wtFc and sialylated Fc structures (Fig. 4), the C<sub>H</sub>3 domains of the wtFc structures were aligned, and we monitored the separation of the C<sub>H</sub>2 domains as previously described [69] by measuring distances between the Ca atoms at C<sub>H</sub>2 positions 238, 241, 301, and 329. The differences in C<sub>H</sub>2 domain separation (Table 1) relative to a published wtFc structure (3AVE) were plotted for each set of paired Ca positions (Fig. 5). Despite differences in crystal packing, the wtFc structures exhibited only small deviations in C<sub>H</sub>2 domain separation distances, demonstrating relatively little structural variability. By contrast, a low-resolution wtFc structure solved from crystals grown under high salt conditions [5] (PDB: 1H3Y) showed deviations from other wtFc structures that were crystallized in lower salt concentrations (Fig. 5, Table 1). Structures of Fc proteins with different defined glycoforms showed a larger degree of variability in C<sub>H</sub>2 domain separation than wtFc structures, as was also true for Fc structures with mutations introduced to enhance effector functions, and Fc structures solved as complexes with other proteins (Fig. 5). There were no systematic differences in C<sub>H</sub>2 domain separation or structure based on whether or not the Fc fragment was predicted to contain an O-glycan in its hinge region (Table 1; Fig. 5).

### ***Structures of Two Forms of di-sFc***

A 3.0 Å resolution of di-sFc was solved in space group  $P2_1$  with two di-sFc molecules per asymmetric unit. The structure was compared with wtFc structures and a previously described structure of sFc that included a mixture of di- and monosialylated Fc (PDB: 4BYH) [53]. In the di-sFc structure, electron density for biantennary *N*-linked glycans was visible for all four di-sFc chains in the two di-sFc dimers, but although the di-sFc protein was fully disialylated (Fig. 2e), electron density for a terminal sialic acid was found only on the 6-arm of chains B and C, with the 6-arm of chains A and D showing ordered glycan residues up to a GlcNAc or galactose, respectively, and the 3-arm showing electron density for glycan moieties up to the GlcNAc (chains A, B, C and D) (Fig. 6). Similarly, sialic acid was visible only on the 6-arm of chain A in the 4BYH sFc structure [53]. In all three sFc structures (in 4BYH as well as in the two copies of di-sFc in the new sFc structure), the 6- and 3-arms of the biantennary glycans projected away from the protein surface and were solvent exposed; thus the ordered sialic acid on the glycan 6-arm was not positioned into a pocket formed by Glu258 and Lys290, as previously proposed [61].

Interestingly, the two di-sFc dimers in the asymmetric unit of the  $P2_1$  crystals exhibited differences in the arrangement of their  $C_H2$  domains. One di-sFc (chains A and B) exhibited a relatively “closed” conformation, as defined by the separation between the two  $C_H2$  domains, whereas the second di-sFc (chains C and D) exhibited a relatively “open” conformation (Table 1 and Fig. 4b). As compared with a representative wtFc structure (3AVE), the open di-sFc exhibited a

6.8 Å root mean square deviation (RMSD) (calculated for the 103 C $\alpha$  atoms of one C<sub>H2</sub> domain after alignment of the partner C<sub>H2</sub> domain in each structure), as compared to a 15.0 Å RMSD between the wtFc and closed di-sFc C<sub>H2</sub> domains, a 7.9 Å RMSD between the open di-sFc and the 4BYH sFc, and a 8.8 Å RMSD between the closed di-sFc and the 4BYH sFc. To quantitatively evaluate C<sub>H2</sub>-C<sub>H2</sub> domain separation distances, which cannot be easily defined by a single number reflecting an average separation, we used a previously-defined metric in which the distance between four partner C $\alpha$  atoms on each C<sub>H2</sub> domain are measured (Pro238, Pro329, Phe241 and Arg301) and compared between structures [69]. In addition to determining C<sub>H2</sub>-C<sub>H2</sub> separation distances for these C $\alpha$  residues (Table 1), we calculated the differences relative to a reference wtFc structure (3AVE) to determine how greatly the various structures deviated from wtFc and other Fc structures. As defined by the distances between these C $\alpha$  atoms, the closed di-sFc exhibited a greater difference in C<sub>H2</sub> domain separation when compared to wtFc structures than 4BHY sFc, whereas the open di-sFc C $\alpha$  exhibited a difference within the range observed for other wtFc structures (Fig. 5).

We next aligned individual C<sub>H2</sub> domains of the closed di-sFc, open di-sFc, wtFc (3AVE), and 4BYH sFc structures to compare the orientations of hydrophobic side chains (Phe241 and Phe243) adjacent to the *N*-linked glycan attached to Asn297 (Fig. 7a). No major changes were observed in the overall fold of the C<sub>H2</sub> domains, and only minor changes were found in the Phe243 side chain orientation. However, larger changes were observed in the Phe241 side chain, which was rotated ~90° compared to Phe241 in other Fc structures (Fig. 7b). Typically the

aromatic rings of the Phe241 and Phe243 side chains were stacked with respect to each other; however in both C<sub>H</sub>2 domains of the closed and open di-sFc structures, Phe241 adopted a different conformation such that it was no longer stacked with Phe243 (Fig. 7b,c and Fig. S4). The Phe241 side chain was not involved in crystal contacts in any of the structures (data not shown); thus these differences were not related to crystal packing. Although the Asn297-linked *N*-glycan is adjacent to Phe241 and Phe243, no major differences were observed in the glycan conformation (Fig. 7a), thus the Phe241 side chain orientation did not affect the glycan conformation.

### ***Structure of F241A Fc***

We also solved a 2.2 Å resolution crystal structure of F241A Fc (space group P2<sub>1</sub>2<sub>1</sub>2<sub>1</sub>; one molecule per asymmetric unit) and compared it to wtFc and sFc structures and to PDB code 4BM7, a previous F241A Fc structure [65] (Fig. 8a, b). On chain A of the new F241A Fc structure, there was ordered electron density for residues Pro230 to Leu443, which included part of the hinge region (Glu216 to Pro230 for human IgG1 proteins) that normally links the Fab to the N-terminus of the Fc region (Fig. 8c). By contrast, the first ordered residue on both chains of wtFc structures was usually Leu234, Leu235, Gly236, Gly237, or Pro238 (PDB codes: 1H3X, 3AVE, 2DTS, 3DO3, 1FC1 and 1HZH), and the first ordered residue of the F241A B chain was Gly237. The hinge region was also disordered in the 4BM7 F241A Fc structure (the first ordered residues were Gly237 on chain A and Pro238 on chain B). At Asn297, six ordered glycan residues were modeled on

chain A and nine residues on chain B of the new F241A structure (Fig. 6), but sialic acids were not visible in the new F241A or the 4BM7 F241A structures although the F241A glycans included both mono- and disialylated species [65] (Fig. 2 and Fig. 8b). Because *N*-glycans were not completely resolved even in the di-sFc structure, which was solved from crystals containing Fc protein with completely homogeneous *N*-glycans, we cannot use the F241A Fc structures to determine the compositions of *N*-glycans in the F241A Fc crystals. Therefore it is not possible to determine whether a defined glycan species crystallized from the heterogeneous protein preparations used to produce both of the F241A Fc structures and all of the wtFc structures.

Comparison of the C<sub>H</sub>2 domain separations of the F241A Fc structure with other Fc structures showed that the new F241A Fc structure was similar to wtFc structures and the open di-sFc structure, but substantially more closed than the 4BM7 F241A Fc (Fig. 5, Table 1). (Because portions of the chain B C<sub>H</sub>2 domain of the 4BM7 F241A Fc structure were disordered, including the Asn297-linked glycan and residues 264-274 (BC loop), 296-300 (C'E loop), and 324-332 (FG loop), we could not measure all of the inter-chain distances in the 4BM7 F241A Fc structure.) This large degree of difference in F241A Fc conformations is similar to that observed for di-sFc conformations but distinct from wtFc conformations. Since both of the F241A Fc structures (the structure reported here and the 4BM7 structure) were derived from proteins that were partially sialylated, this observation is consistent with the suggestion that a greater degree of conformational heterogeneity is available to sialylated Fc proteins than to wtFc with conventional

glycosylation species. Alternatively, or perhaps in addition, the F241A substitution itself could result in greater conformational heterogeneity.

## DISCUSSION

The Fc regions of IgGs can function to either promote or suppress the inflammatory response. Previous studies have shown that the Asn297-linked *N*-glycan composition is a determining factor in function [46, 70]. Both biochemical and *in vivo* studies have shown that sialylation of the Fc glycan is essential for the anti-inflammatory activity of IVIG [9, 43, 46]. Here we compared structures of wtFc, which carries mostly asialylated *N*-glycans, to sialylated forms of Fc, both a fully disialylated form produced by chemoenzymatic glycoengineering, and an F241A mutant form of Fc. Compared with wtFc, the Asn297-linked *N*-glycan of F241A and F243A Fc showed increased mono- and disialylated products when the protein was expressed in mammalian cells. This suggests that IgGs with an F241A mutation may be effective anti-inflammatory molecules due to increased sialylation.

Our analyses of the wtFc proteins produced in two different mammalian cell lines demonstrated that the Asn297-linked *N*-glycans were mainly G0F, G1F and G2F glycoforms, consistent with previous studies [65], thus we assume a similar composition for the *N*-glycans on the relatively structurally-invariant wtFc structures in the pdb. Not only are these glycans mostly asialylated, they also contain only a small percentage of digalactosylated forms. In a systematic comparison of wtFc structures reported here and previously, we found only small

deviations in the “openness” of the Fc, evaluated by the distance between the partner C<sub>H</sub>2 domains in the Fc dimer, despite different crystal packing environments: however, we noted that certain glycan species cause increased variation in crystal structures. For example, the F241A Fc structure reported here and one described previously [65] showed a larger degree of variation in C<sub>H</sub>2 domain orientations than seen in a survey of seven wtFc structures. Other glycovariants of Fc, including a recent structure of a digalactosylated form of wtFc [71], also showed a larger degree of conformational variability as assessed by differential C<sub>H</sub>2 domain separations.

Similar to the partially sialylated F241A Fc structures, crystal structures of sialylated wtFc (sFc) have been found in several conformations. In our crystal structure of fully disialylated Fc, we found both open and closed C<sub>H</sub>2 domain conformations in the same crystal, and a previously published sFc structure [53] revealed a conformation similar to the canonical wtFc structures, again suggesting a large degree of inter-domain flexibility of sialylated forms of Fc compared to the relatively invariant structures of asialylated wtFc.

Recent molecular dynamics simulations showed a wide range of conformations that Fc can adopt [71]. Here we have documented a greater flexibility of glycovariant forms of Fc that may be key to the ability of the Fc region of IgG to modulate inflammatory and anti-inflammatory activities mediated by glycan differences. Further structural investigations of how glycan composition and conformational flexibility affect binding to Fc receptors that mediate differential activities will be critical to understanding the significance of these results.

## FIGURE LEGENDS

Fig. 1. IgG, Fc and glycan structures. (a) Schematic structure of IgG1. (b) Ribbon diagram of wtFc (PDB: 3AVE) with Asn297-linked *N*-glycans shown as sticks. Glycan residues are colored as in panel c. (c) Schematic of an Asn297-linked *N*-glycan. The biantennary glycan consists of a mannose (Man) and *N*-acetylglucosamine (GlcNAc) core that can be modified by addition of core fucosylation (Fuc), a bisecting GlcNAc, terminal galactose (Gal) and sialic acid (NeuNAc).

Fig. 2. HPAEC-PAD analysis of PNGase F-released *N*-glycans of IgG Fc proteins. (a) wtFc expressed in HEK cells. (b) wtFc expressed in CHO cells. (c) F241A Fc expressed in HEK cells. (d) F243A expressed in HEK cells. (e) di-sFc prepared by chemoenzymatic glycoengineering of an Fc fragment isolated after papain cleavage of Rituximab. The amounts of mono- and disialylated *N*-glycans are shown. \* indicates a mixture of heterogeneous monosialylated glycoforms. † indicates a mixture of heterogeneous disialylated glycoforms. ‡ indicates a satellite peak due to epimerization of reducing end GlcNAc to ManNAc.

Fig. 3. SDS-PAGE (left) and SNA blot (right) of Fc proteins expressed in HEK cells. wtFc, F241A Fc and F243A Fc were expressed as Fc fragments; di-sFc was prepared by papain cleavage from Rituximab IgG.



Fig. 4. Comparison of wtFc and sFc structures. Fc structures were aligned by superimposing the C<sub>H</sub>3 domains. (a) Alignment of wtFc structures (the wtFc structure solved in this study plus PDB entries 1HZH, 1FC1, 2DTS, 3AVE, 1H3X, and 3DO3). (b) Alignment of closed and open structures of di-sFc (this study), sFc (PDB 4BYH), and wtFc (PDB 3AVE).

Fig. 5. Comparison of C<sub>H</sub>2 domain separation in Fc structures. Left: location of C<sub>α</sub> atoms of Phe241, Arg301, and Pro329 (red spheres) and Asn297 (blue spheres) indicated on the C<sub>H</sub>2 domains of wtFc (PDB: 3AVE). C<sub>H</sub>2 domain separation in individual Fc structures was evaluated by measuring distances (dotted lines) between the corresponding red spheres on each chain. Right: Differences in C<sub>H</sub>2 domain separation relative to a reference wtFc structure (3AVE) plotted for each set of paired C<sub>α</sub> positions in the indicated category of Fc structure. When a structure category had more than one member, the mean and standard deviation are superimposed upon the values. Fc structure categories are as follows: wtFc (structure solved in this study plus PDB entries 1H3X, 3AVE, 2DTS, 3DO3, 1FC1, 1HZH), wtFc high salt (1H3Y), glycovariant (GV) Fcs (1H3W, 1H3U, 1H3V, 2WAH, 4ACP, 3DNK, 4KU1, and 3S7G), mutant (mut) Fcs (2QL1, 3FJT, and 3C2S), Fcs complexed with other proteins (com Fc) (3D6G, 1L6X, 1OQO, 1OQX, 1DN2, 1FCC, 1FC2, 1E4K, 1T83, 1T89, 3AY4, 3RY6, 3SGK, and 3SGJ), di-sFc closed, di-sFc open, sFc (4BYH), F241A Fc (this study), and F241A Fc (4BM7).

Fig. 6. Comparison of ordered glycans on Fc structures. 2Fo-Fc electron density (contoured at  $0.7\sigma$ ) from an annealed omit map in the region of the Asn297-linked *N*-glycan is shown for both chains of di-sFc closed, di-sFc open, F241A Fc, and wtFc (this study). Ordered glycan residues are shown schematically below each map using the colors and shapes defined in Fig. 1c.

Fig. 7. Comparison of glycan and protein residue conformations in sFc and wtFc structures. (a) Alignment of Asn297-linked *N*-glycans of di-sFc closed (blue), di-sFc open (green), F241A Fc (magenta), F241A Fc 4BM7 (yellow), sFc 4BYH (cyan), wtFc from this study and wtFc 3AVE (both gray). The side chains of Phe241 and Phe243 are shown in red on the C<sub>H</sub>2 domain of wtFc. (b) Alignment of Phe(Ala)241–Leu242–Phe243 region in the structures of di-sFc closed (blue), di-sFc open (green), F241A Fc (magenta), F241A Fc 4BM7 (yellow), sFc 4BYH (cyan), wtFc from this study and wtFc 3AVE (both gray). (c) 2Fo-Fc electron density (contoured at  $0.7\sigma$ ) from an annealed omit map in the region of the Phe241 and Phe243 side chains for the di-sFc structures. See also Fig. S5.

Fig. 8. Comparison of F241A Fc structures. (a) Superimposition of Ca traces of F241A Fc (this study) (magenta) and F241A Fc (PDB 4BM7) (cyan). Locations of Ca traces of F241A Fc (this study) (magenta) and F241A Fc (PDB 4BM7). (b) 2Fo-Fc electron density (contoured at  $0.7\sigma$ ) from annealed omit maps for F241A Fc (this study) and F241A Fc (PDB: 4BM7). Ordered glycan residues are shown schematically below each map using the colors and shapes defined in Fig.

1c. (c) 2Fo-Fc electron density (annealed omit map) of an ordered portion of the hinge region (blue) on chain A contoured at  $0.6\sigma$ . (d) 2Fo-Fc electron density (contoured at  $0.7\sigma$ ) from annealed omit maps in the region of the Phe243 and Ala241 side chains for the structures of F241A Fc (this study) (left) and F241A Fc (PDB: 4BM7) (right).

Fig. S1. LC-ESI-MS analysis of reduced Rituximab Fc. (a) Reduced Rituximab Fc treated with wild type EndoS (calculated MW = 25289 Da). (b) Reduced di-sFc produced from Rituximab Fc (transglycosylated product) treated with wild type EndoS (calculated MW = 27288 Da).

Fig. S2. LC-ESI-MS analysis of reduced recombinant Fc fragments before (left panels) and after (right panels) PNGase F treatment to completely remove *N*-glycans. ESI-MS spectra after deconvolution are shown for (a) wtFc (HEK cells) [calculated MW after PNGase F treatment = 25838 Da; experimentally found MW = 26788 and 27153 Da (+950 and +1315 Da, respectively)]; (b) wtFc (CHO cells) [calculated MW after PNGase F treatment = 25337 Da; experimentally found MW = 25606, 26259, and 26555 Da (+269, +922, and +1218 Da, respectively)]; (c) F241A Fc (HEK cells) [calculated MW after PNGase F treatment = 25762 Da; experimentally found MW = 26713 and 27077 Da (+951 and +1315 Da, respectively)]; (d) F243A Fc (HEK cells) [calculated MW after PNGase F treatment = 25762 Da; experimentally found MW = 26713 and 27077 Da (+951 and +1315 Da, respectively)]; (e) wtFc fragment prepared by papain digestion of Rituximab

IgG [calculated MW after PNGase F treatment = 24938 Da; experimentally found MW = 24938 Da].

Fig. S3. HPAEC-PAD neutral monosaccharide compositional analyses of putative O-glycans. Left panels: neutral monosaccharide compositional analyses. Right panels: sialic acid compositional analyses. (a) Monosaccharide standards. (b) Analytes from wtFc expressed in HEK cells after complete removal of *N*-glycans. (c) Analytes from wtFc expressed in CHO cells after complete removal of *N*-glycans. (d) Analytes from Fc fragment isolated after papain digest of Rituximab.

Fig. S4. Comparison of glycan and protein residue conformations in sFc and wtFc structures (see also Fig. 7). (a) Glycan conformation in the vicinity of the Phe241 and Phe243 residues (highlighted in red). Glycan residues are colored as in Fig. 1c. (b) Schematic structures of ordered glycan residues using the colors and shapes defined in Fig. 1c. (c) 2Fo-Fc electron density (contoured at  $0.7\sigma$ ) from annealed omit maps in the region of the Phe243 and Phe241 side chains for the indicated structures.

## METHODS

### *Protein Expression and Purification*

Fc proteins were expressed in transiently-transfected HEK 293-6E suspension cells (F241A Fc and F243A Fc) or stably-transfected Chinese hamster ovary cells (wtFc) as described [63, 72]. Fc proteins were isolated from harvested supernatants using protein A chromatography (GE Healthcare) followed by size exclusion chromatography in 25 mM Tris-Cl pH 7.5, 100 mM NaCl on a Superdex 16/60 gel-filtration column (GE Healthcare). Fractions corresponding to the Fc were pooled and used for crystallization and glycan analysis.

Fc protein for di-sFc production was prepared by papain cleavage of Rituximab (Rituxan®) (Genentech, Inc., California), a human IgG1 Fc. Rituximab (40 mg) was buffer exchanged into 10 mM Tris-HCl pH 7.5 overnight at 4°C. Dialyzed material was concentrated to 20 mg/ mL (~2 mL). Immobilized papain (Thermo Scientific) was prepared following the manufacturer's protocol. 1 mL of immobilized papain slurry (50% immobilized papain) was added to the Rituximab solution. The reaction was incubated at 37°C for 5 hours while continuously inverting the sample tube. The resin was removed using a spin column and the filtrate was loaded over a protein A column (2 x 5 mL) that was pre-equilibrated with 10 mM Tris-HCl, pH 7.5. The column was washed with 10 column volumes of 10 mM Tris-HCl, pH 7.5 until no protein was detected in the flow through. Bound Fc was eluted in 4 mL of a 100 mM citric acid solution pH 3.5. Eluted fractions were quickly neutralized using a 1.5 M solution of Tris-HCl pH 8.8. Purified Fc was combined, concentrated and injected over a 40 mL (4 x 10 mL) HiTrap desalting

column (GE Healthcare) pre-equilibrated in a phosphate buffered saline solution (pH 7.4) to give 10 mg of Fc. wtFc for crystallization was prepared similarly by papain digestion of the anti-HIV-1 IgG1 antibody 21c (expressed in HEK 293-6E cells as described [72]).

### ***Preparation of Disialylated Fc (di-sFc)***

Purified Fc (10 mg) prepared by papain cleavage of Rituximab IgG was treated with 30  $\mu$ g of recombinant *S. pyogenes* EndoS [64] for 1 hr at 37°C. Analysis by LC-MS showed complete cleavage of the glycan. The deglycosylated Fc was isolated using a Sephacryl S-200 HR size exclusion column (GE Healthcare) while monitoring UV absorbance and collecting peaks. The fractions containing deglycosylated Fc were pooled and concentrated to give 9 mg of the intermediate (Fuc $\alpha$ 1,6)GlcNAc-Fc. A solution of (Fuc $\alpha$ 1,6)GlcNAc-Fc (5 mg) and sialoglycan-oxazoline (5 mg) buffered with Tris-HCl (100 mM, pH 7.0, 0.5 mL) was incubated with EndoS-D233A (200  $\mu$ g) [64] at 30°C. Aliquots were taken at time intervals for LC-MS analysis of reaction progression. Quantitative conversion was achieved in 2 hours. The product was purified using size exclusion chromatography as described above. Product fractions were pooled and concentrated to give di-sFc (4.5 mg). LC-MS data: calculated for (Fuc $\alpha$ 1,6)GlcNAc-Fc monomer, MW = 25287.3 Da; found MW = 25289 Da (deconvolution data obtained from the original spectrum). Calculated for fully sialylated N-glycan-Fc monomer, MW = 27288.9 Da; found MW = 27289 Da (deconvolution data).

### ***N-glycan Analysis***

25 µg of each Fc fragment was treated with PNGase F (NEB) in a G7 buffer (0.5 M sodium phosphate, pH 7.5) following the manufacturer's instructions. Samples were purified over a CarboPac PGC column and analyzed using HPAEC-PAD on a Dionex ICS 5000 with a CarboPac PA200 column. The *N*-glycans were eluted in 100 mM NaOH with the following gradient conditions: 0-10 mM NaOAc in 20 min and then 10-100 mM NaOAc in 20 min. Peaks were assigned using *N*-glycan standards purified from PNGase F digestions of Rituximab, sheep IgG (Sigma), and sialylglycopeptide (SGP) from chicken egg yolk.

### ***Monosaccharide Compositional Analysis of Putative O-glycans***

PNGase *F*-treated Fc proteins lacking *N*-glycans were dissolved in 3M TFA in screw-cap vials. The tubes were sealed and incubated at 100 °C for 4 hours. Tubes were then cooled to 25 °C, and the reaction mixture was evaporated to dryness in a SpeedVac. The dried samples were dissolved in water and subjected to HPAEC-PAD analysis on a CarboPac PA10 column. Monosaccharides were eluted with 18 mM NaOH and detected with pulsed amperic detection with a gold electrode using a standard monosaccharide waveform. For analysis of sialic acids from putative *O*-glycans, the de-*N*-glycosylated Fc proteins were treated with neuraminidase (NEB) for 16 hours in the desialylation buffer provided by the manufacturer (NEB). The samples were then subjected to HPAEC-PAD analysis on a CarboPac PA10 column using a sialic acid standard (Sigma) for detection and quantification.

### ***LC-ESI-MS Analysis of Fc Fragments***

Fc fragments and PNGase F-treated Fc fragments were reduced with 50 mM TCEP at 37 °C for 15 minutes and subjected to LC-ESI-MS analysis on an Agilent C8 column eluted with a gradient of 0-60% acetonitrile in 10 min.

### ***Crystallization and Data Collection***

Crystals of di-sFc (space group  $P2_1$ ;  $a = 52.73 \text{ \AA}$ ,  $b = 154.22 \text{ \AA}$ ,  $c = 66.12 \text{ \AA}$ ,  $b = 110.78$ ; two Fc dimers per asymmetric unit) were grown in sitting drop vapor diffusion by mixing equal volumes of di-sFc (6.15 mg/ml) with a solution containing 0.2 M magnesium chloride, 0.1 M sodium acetate pH 5, and 20% (w/v) PEG 6000 at 20°C. Crystals were cryopreserved in well solution supplemented with 30% glycerol. Data were collected to 3.0 Å resolution at beamline 8.2.1 of the Advanced Light Source (ALS) at Lawrence Berkeley National Laboratory (LBNL).

Crystals of wtFc (space group  $P2_12_12_1$ ;  $a = 49.56 \text{ \AA}$ ,  $b = 79.69 \text{ \AA}$ ,  $c = 138.06 \text{ \AA}$ ; one Fc dimer per asymmetric unit) were grown in sitting drop vapor diffusion by mixing equal volumes of protein with a solution containing 0.1 M sodium cacodylate pH 6.5 and 18% (w/v) PEG 3350 at 20°C. The protein solution contained mainly 21c Fab produced by papain digestion of 21c IgG, but contaminating amounts of the Fc crystallized. The Fc crystals were cryopreserved in well solution containing 30% glycerol. F241A Fc crystals (space group  $P2_12_12_1$ ;  $a = 57.91 \text{ \AA}$ ,  $b = 74.70 \text{ \AA}$ ,  $c = 113.71 \text{ \AA}$ ; one Fc dimer per asymmetric unit) were grown in hanging drops by mixing F241A Fc (4.4 mg/ml) with 30% PEG 1500 at



20°C and cryopreserved in well solution containing 25% glycerol. Data were collected for both wtFc (2.4 Å resolution) and F241A Fc (2.2 Å resolution) at beamline 12-2 of the Stanford Synchrotron Radiation Lightsource (SSRL).

### ***Data Processing and Structure Determination***

Diffraction data were processed and indexed using iMosflm [73] and integrated and scaled using POINTLESS and SCALA [74, 75]. In addition to considering  $I/\sigma(I)$  and completeness of the highest resolution shell, we used the  $CC_{1/2}$  statistic [76] (correlation coefficient between two random halves of the data set where  $CC_{1/2} > 10\%$ ) to determine the high-resolution cutoff for our data. We used Phenix [77] to compute  $CC_{1/2}$  values. Structures were solved by molecular replacement using PHASER [78] and using published Fc structures as search models (PDB 1H3X for F241A Fc and wtFc; 3D03 for di-sFc). Modeling was done using COOT [79] using composite omit maps for building glycans and nearby protein residues in the  $C_H2$  domains. Crystallographic refinement was done using the Phenix crystallography package [77] by refining individual B factors for the higher resolution structures (F241A Fc and wtFc; 2.2 Å and 2.4 Å resolution, respectively). For the lower resolution di-sFc structure (3.0 Å resolution), we refined group B factors and used non-crystallographic symmetry (NCS) restraints during refinement. Because the  $C_H2$  domain orientations differed between the two di-sFc molecules in the asymmetric unit, the NCS restraints were applied to individual domains ( $C_H2$  domain residues Phe240 – Ile336, and residues  $C_H3$

domain Pro343 – Leu443 on each Fc chain). We used PyMol [80] for superposition calculations and molecular representations.

The F241A Fc model ( $R_{\text{free}} = 23.2\%$ ;  $R_{\text{work}} = 20.6\%$ ) included 421 protein residues in the F241A Fc dimer (Pro230 - Leu443 on chain A and Gly237- Leu443 on chain B), 16 glycan residues (GlcNAc1-Gal6, Fuc12 on chain A and GlcNAc1-GlcNAc8, Fuc12 on Chain B), and 351 water molecules. No electron density was observed for residues Thr225 and Cys226 of the Fc hinge or for Man7-NeuNAc10 or Gal9-NeuNAc11 in the *N*-linked glycan of chain A or B, respectively. The wtFc model ( $R_{\text{free}} = 26.4\%$ ;  $R_{\text{work}} = 21.1\%$ ) included 415 protein residues in the wtFc dimer (Pro238-Ser444 on chain A and Gly236-Pro443 on chain B), 13 glycan residues (GlcNAc1-GlcNAc5, Man7, GlcNAc8, Fuc12 on both chains A and B), and 165 water molecules. No electron density was observed for residues Cys226 to Pro230 of the Fc hinge or for Gal6, Gal9 or NeuNAc10 on the *N*-glycan. Side chains were disordered for residues 269 and 311 on chain A and 246, 269, 311, and 326 on chain B. The di-sFc structure ( $R_{\text{free}} = 28.0\%$ ;  $R_{\text{work}} = 26.0\%$ ) included two conformationally distinct Fc dimers (chains A and B in the closed dimer and chains C and D in the open dimer). The closed di-sFc dimer model included 414 protein residues (Gly236 - Ser444 and Pro238 - Ser444 on chains A and B, respectively) and 16 glycan residues (GlcNAc1- GlcNAc5, Man7, GlcNAc8 on chain A and GlcNAc1 - GlcNAc8, NeuNAc11 on chain B). No electron density was observed for residues Glu225 to Pro230 of the Fc hinge or for Gal6, Gal9 - NeuNAc10 (chain A) or Gal9, NeuNAc11 (chain B) in the *N*-linked glycan. Side chains were disordered for residues 246, 251, 258, 268, 269, 272, 274, 280, 288,

292, 294, 295, 296, 301, 307, 317, 326, 340, 355, 360, 365, 386, 410, 414, 416, 418, and 433 on chain A and 248, 269, 272, 274, 283, 298, 314, 326, 340, 355, 384, and 386 on chain B. The open di-sFc dimer model included 410 protein residues (residues Pro238 - Leu443 on each Fc chain) and 17 glycan residues (GlcNAc1-GlcNAc8, NeuNAc11 on chain C and, GlcNAc1-GlcNAc8 on chain D). No electron density was observed for residues Cys226 to Pro230 of the Fc hinge, Ala327-Ile332 (chain C), Val264-Asp270 (Chain D) or for Gal9, NeuNAc10 (chain C) or Gal9-NeuNAc11 (chain D) in the *N*-linked glycan. Side chains were disordered for residues 242, 246, 268, 269, 270, 272, 274, 285, 288, 290, 293, 295, 300, 301, 309, 311, 312, 320, 340, 342, 360, 380, 384, 386, 416, 418, 419, and 433 on chain C and 248, 263, 272, 276, 286, 288, 290, 295, 301, 302, 323, 332, 334, 360, 377, 384, 386, and 439 on chain D.

## **ACCESSION NUMBERS**

Atomic coordinates and structure factors have been deposited in the Protein Data Bank with accession codes 4Q7D (wtFc), 4Q6Y (di-sFc), and 4Q74 (F241A Fc).

## **ACKNOWLEDGEMENTS**

We thank Jost Vielmetter and the Caltech Protein Expression Center for protein production, Beth Stadtmueller and members of the Bjorkman, Ravetch, and Wang laboratories for critical reading of the manuscript, Marta Murphy for help making figures, and Jens Kaiser and members of the staff at the Stanford Synchrotron Radiation Lightsource (SSRL) and the Advanced Light Source (ALS) for help with

data collection and processing. Operations at SSRL are supported by the US Department of Energy and the National Institutes of Health. The Advanced Light Source is supported by the Director, Office of Science, Office of Basic Energy Sciences, of the U.S. Department of Energy under Contract No. DE-AC02-05CH11231. This research was supported by the National Institute Of Allergy And Infectious Diseases of the National Institutes of Health Grant HIVRAD P01 AI100148 (P.J.B. and J.V.R.); (the content is solely the responsibility of the authors and does not necessarily represent the official views of the National Institutes of Health), the National Institutes of Health (R01 AI041239 to P.J.B.), Award DP1OD006961 from the Office of The Director, National Institutes of Health (to P.J.B.), R01 GM096973 (to L.X.W.), R56 AI034662 (to J.V.R.), and the Molecular Observatory at Caltech supported by the Gordon and Betty Moore Foundation. P.J.B. is a Howard Hughes Medical Institute investigator.

## FIGURES

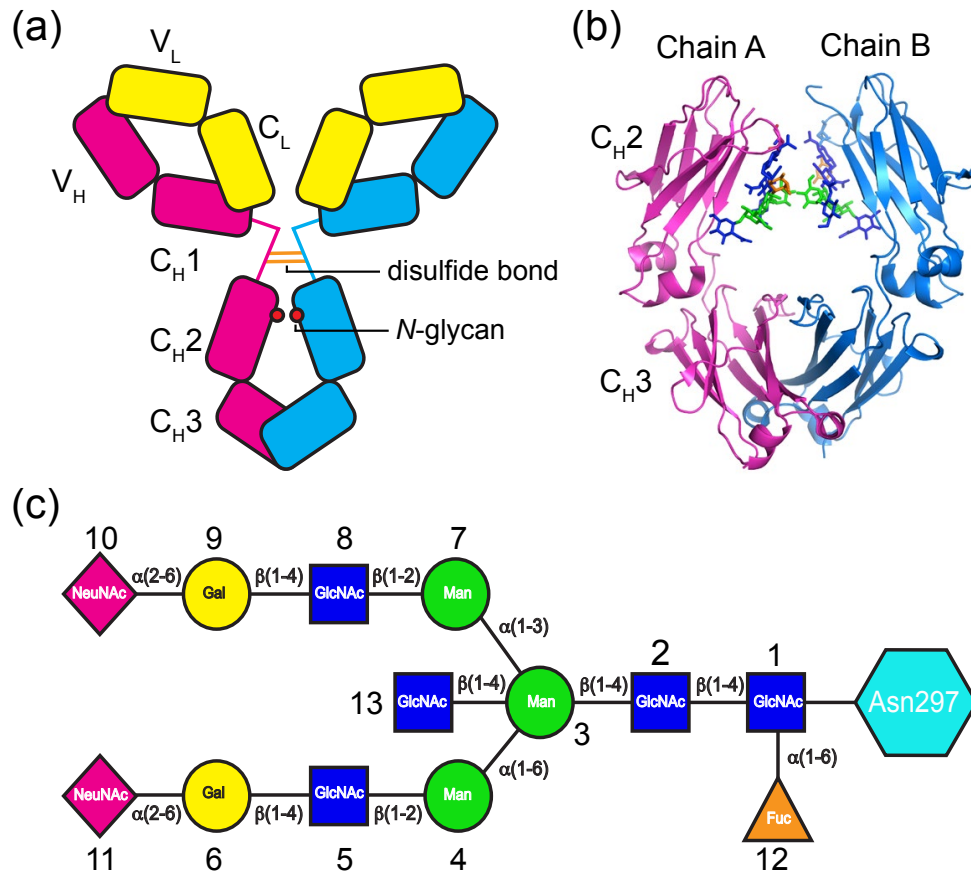


Figure 1. IgG, Fc and glycan structures.

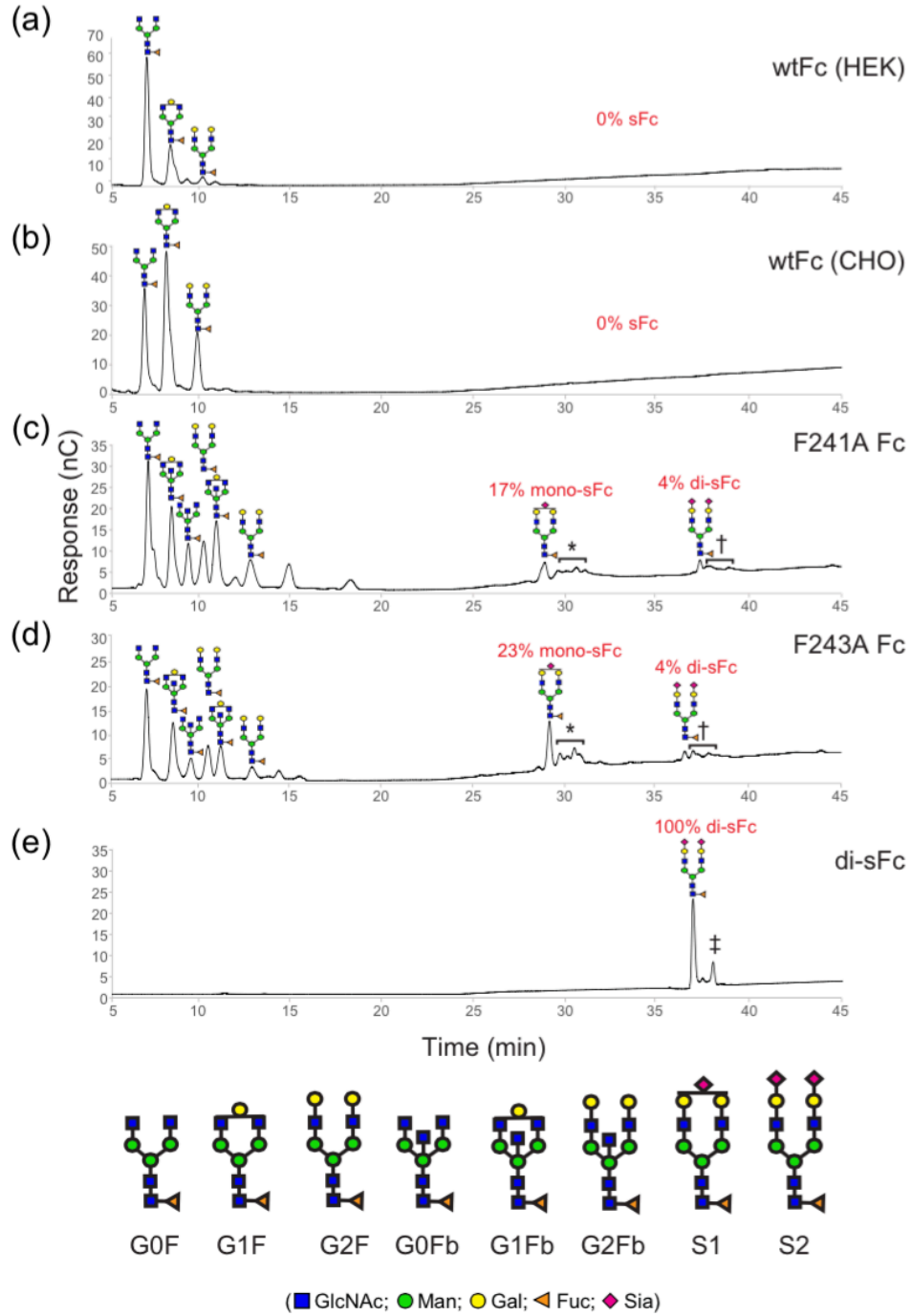


Figure 2. HPAEC-PAD analysis of PNGase F-released *N*-glycans of IgG Fc proteins.

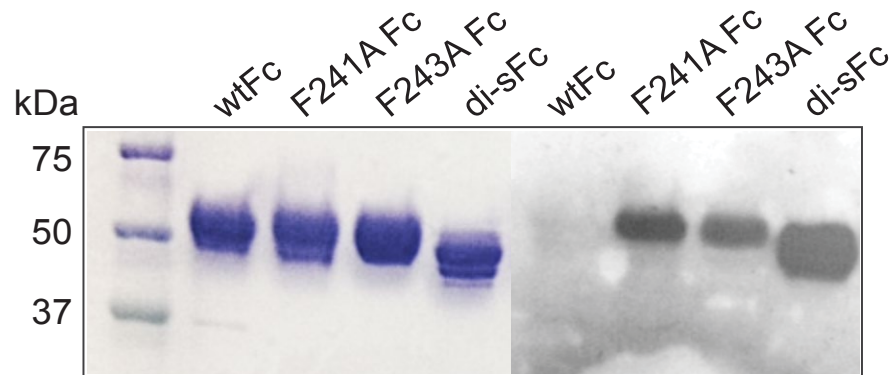


Figure 3. SDS-PAGE (left) and SNA blot (right) of Fc proteins expressed in HEK cells.

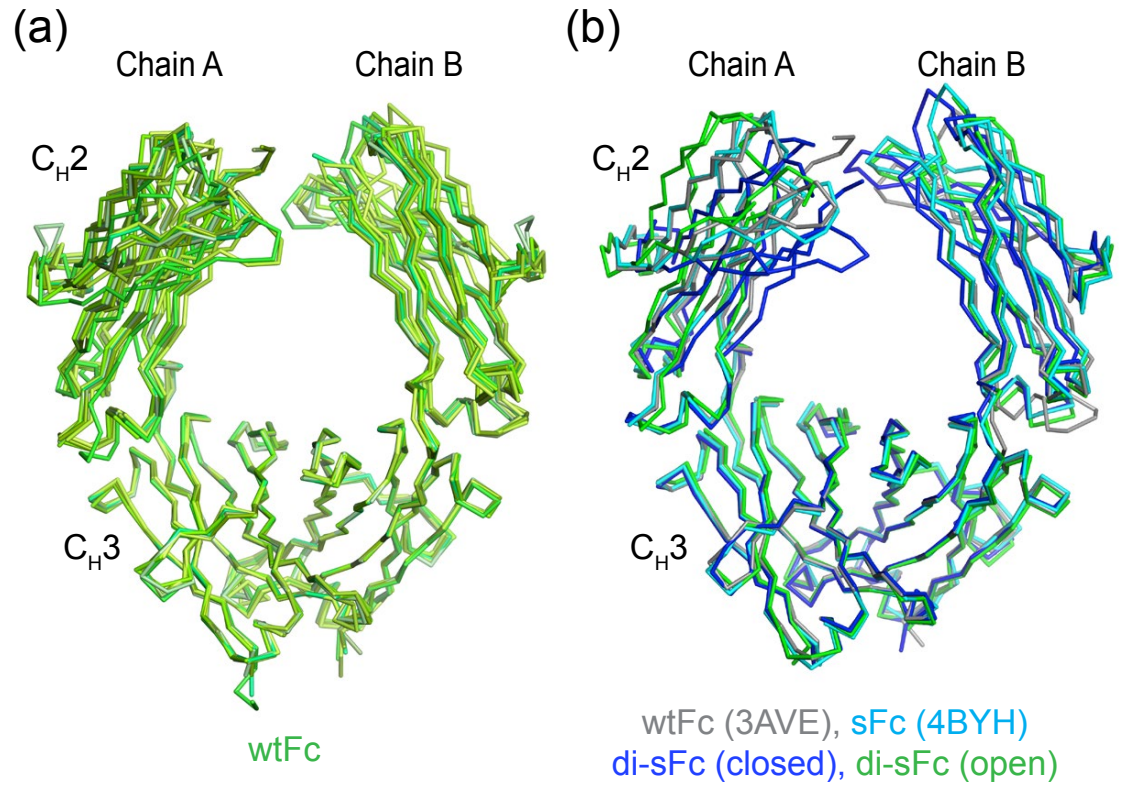


Figure 4. Comparison of wtFc and sFc structures. Fc structures were aligned by superimposing the CH3 domains.



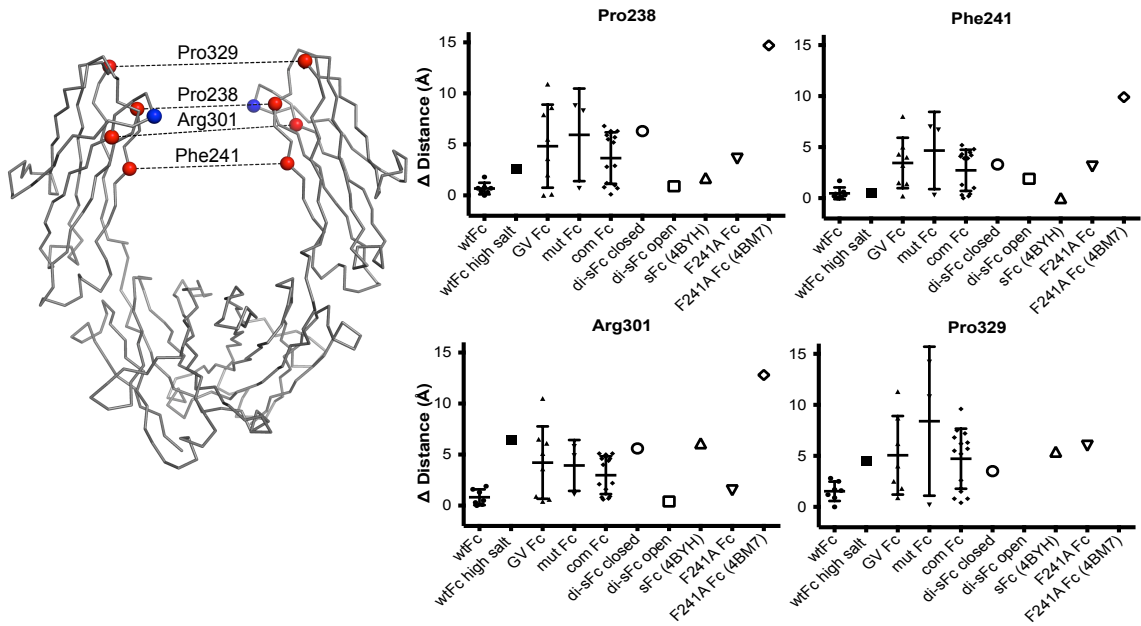


Figure 5. Comparison of CH2 domain separation in Fc structures.

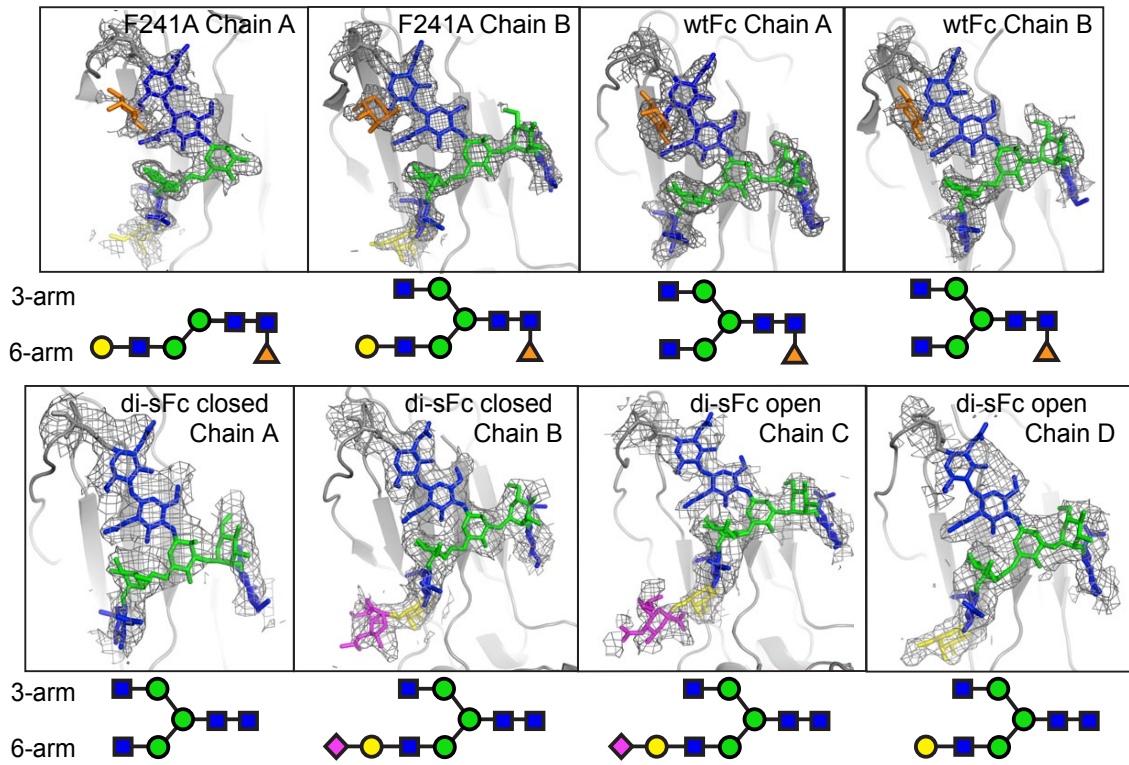


Figure 6. Comparison of ordered glycans on Fc structures.

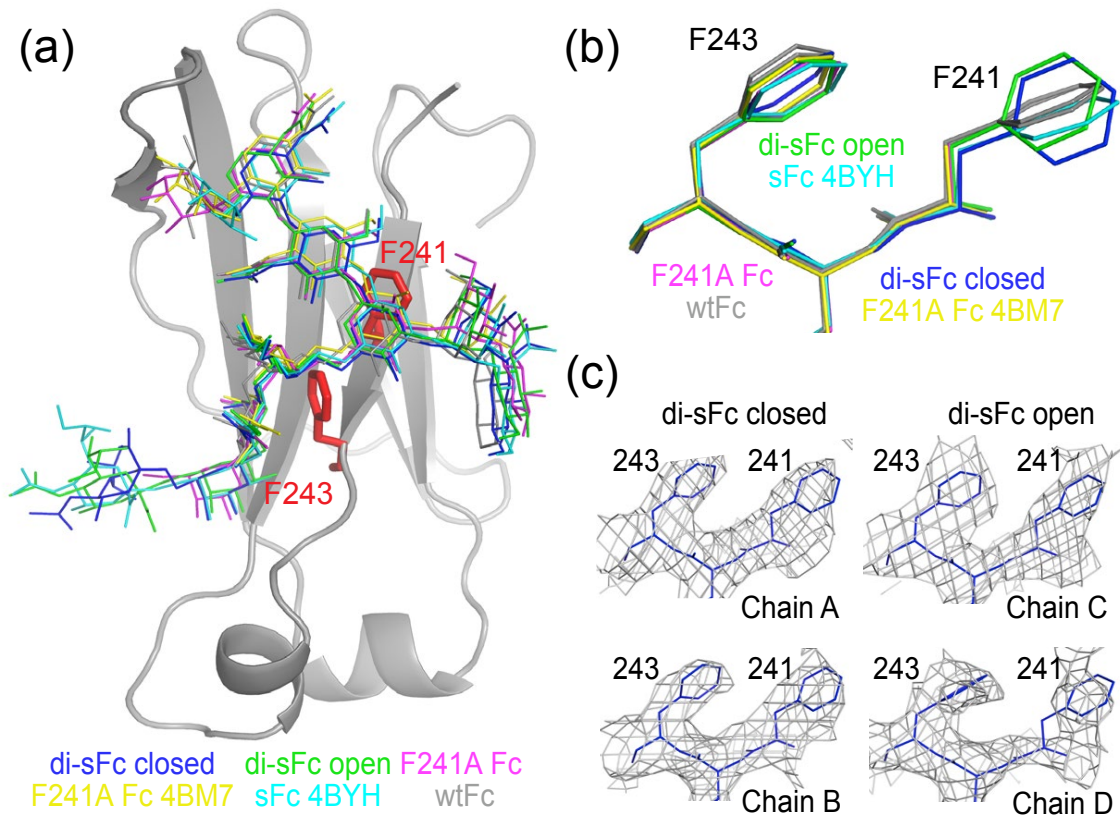


Figure 7. Comparison of glycan and protein residue conformations in sFc and wtFc structures.

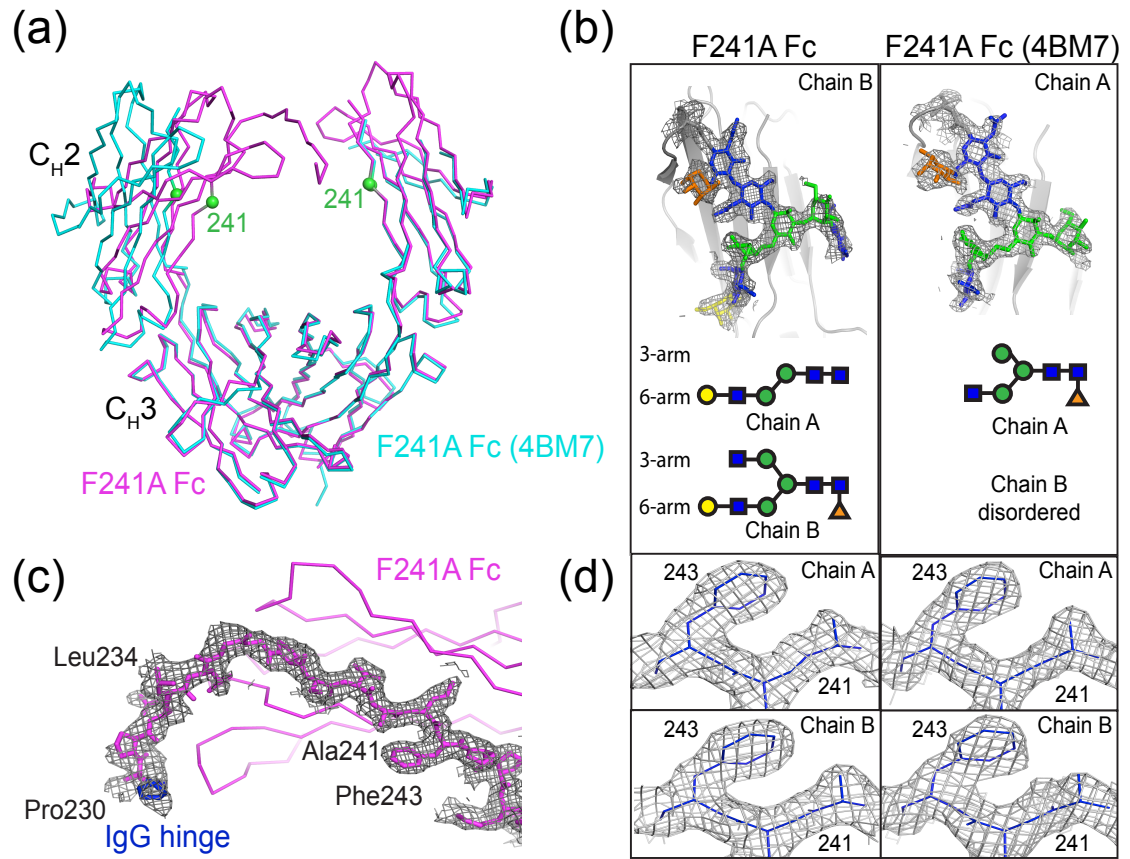


Figure 8. Comparison of F241A Fc structures.

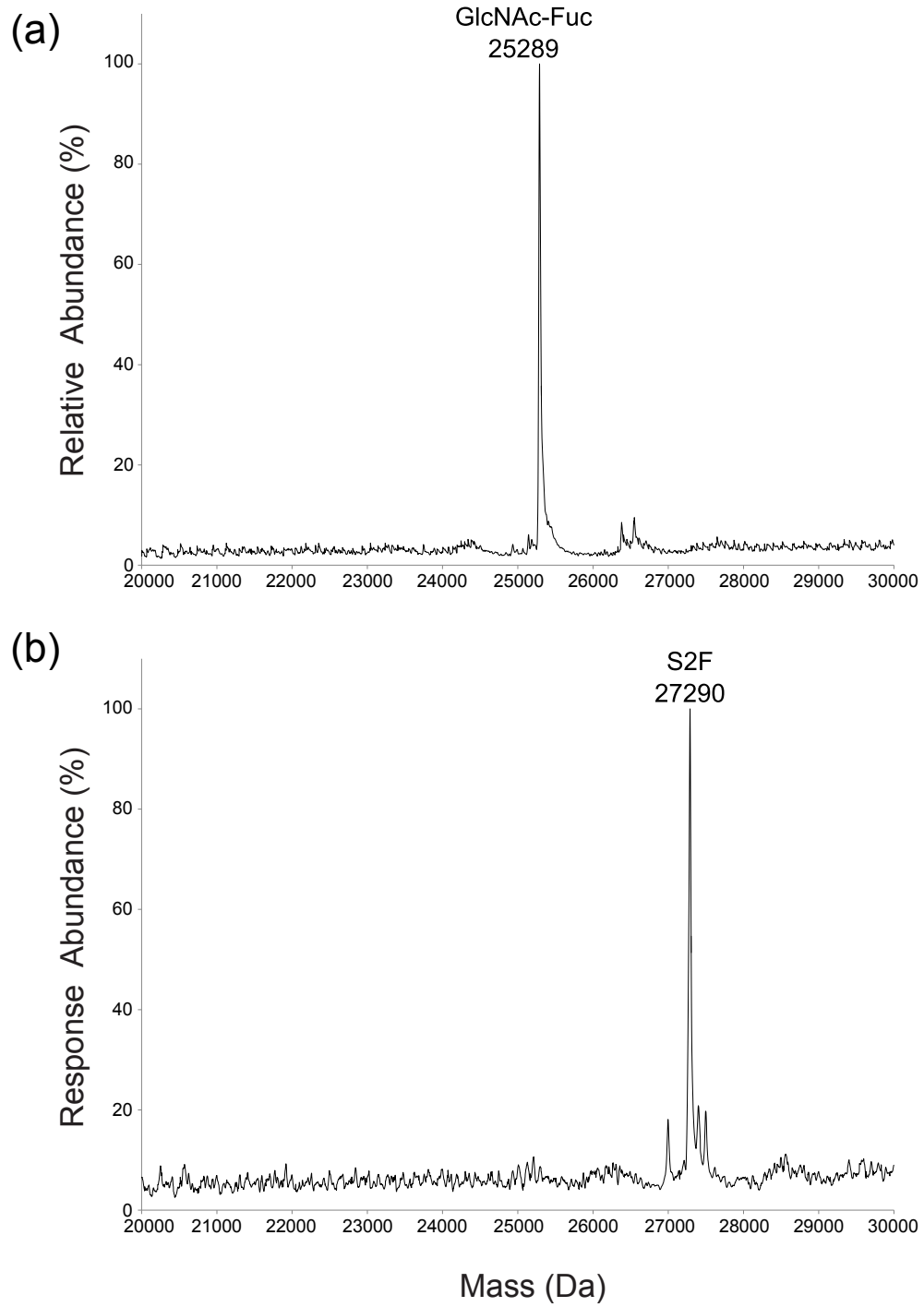


Figure S1. LC-ESI-MS analysis of reduced Rituximab Fc.

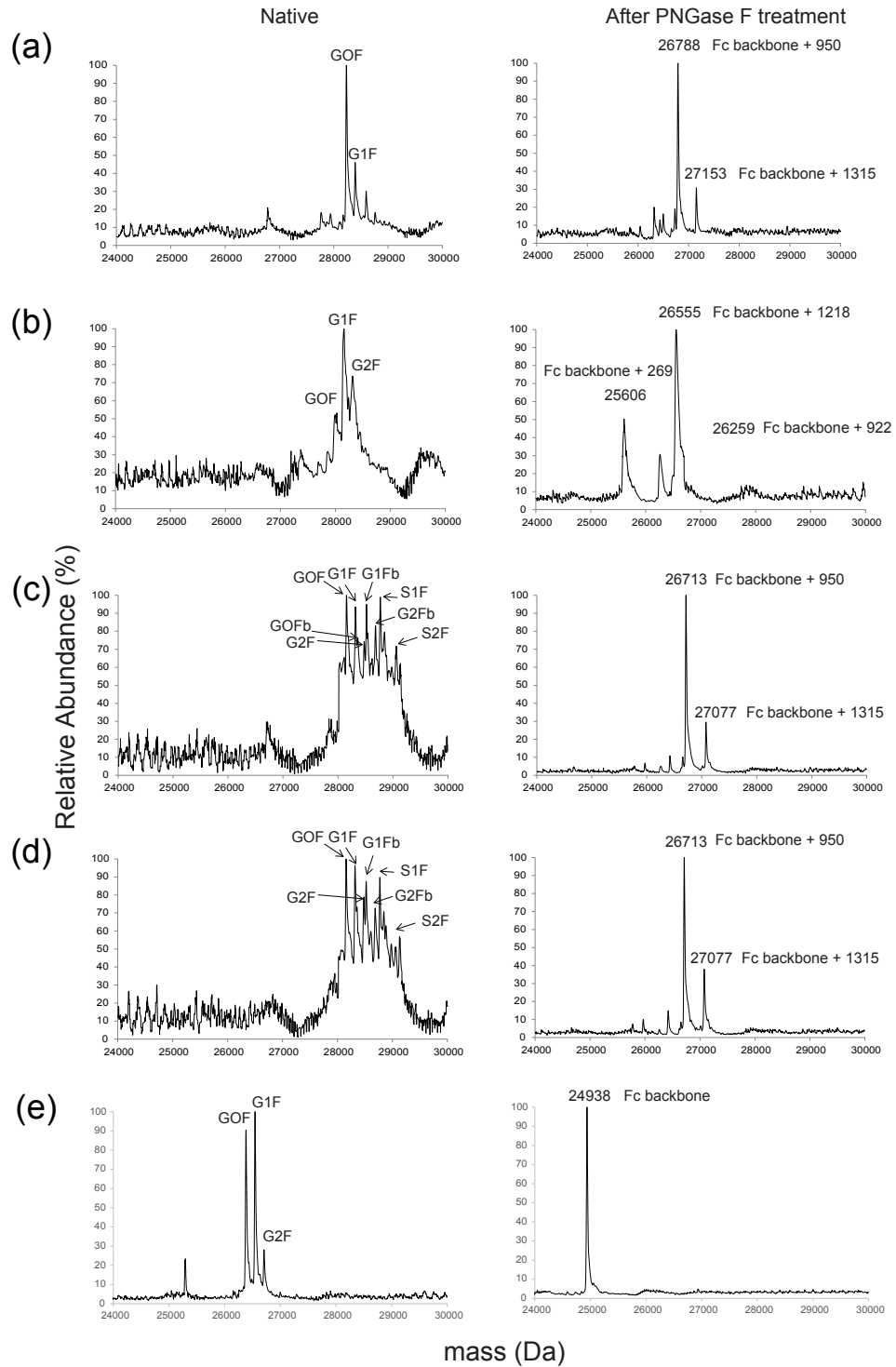


Figure S2. LC-ESI-MS analysis of reduced recombinant Fc fragments before (left panels) and after (right panels) PNGase F treatment to completely remove *N*-glycans.

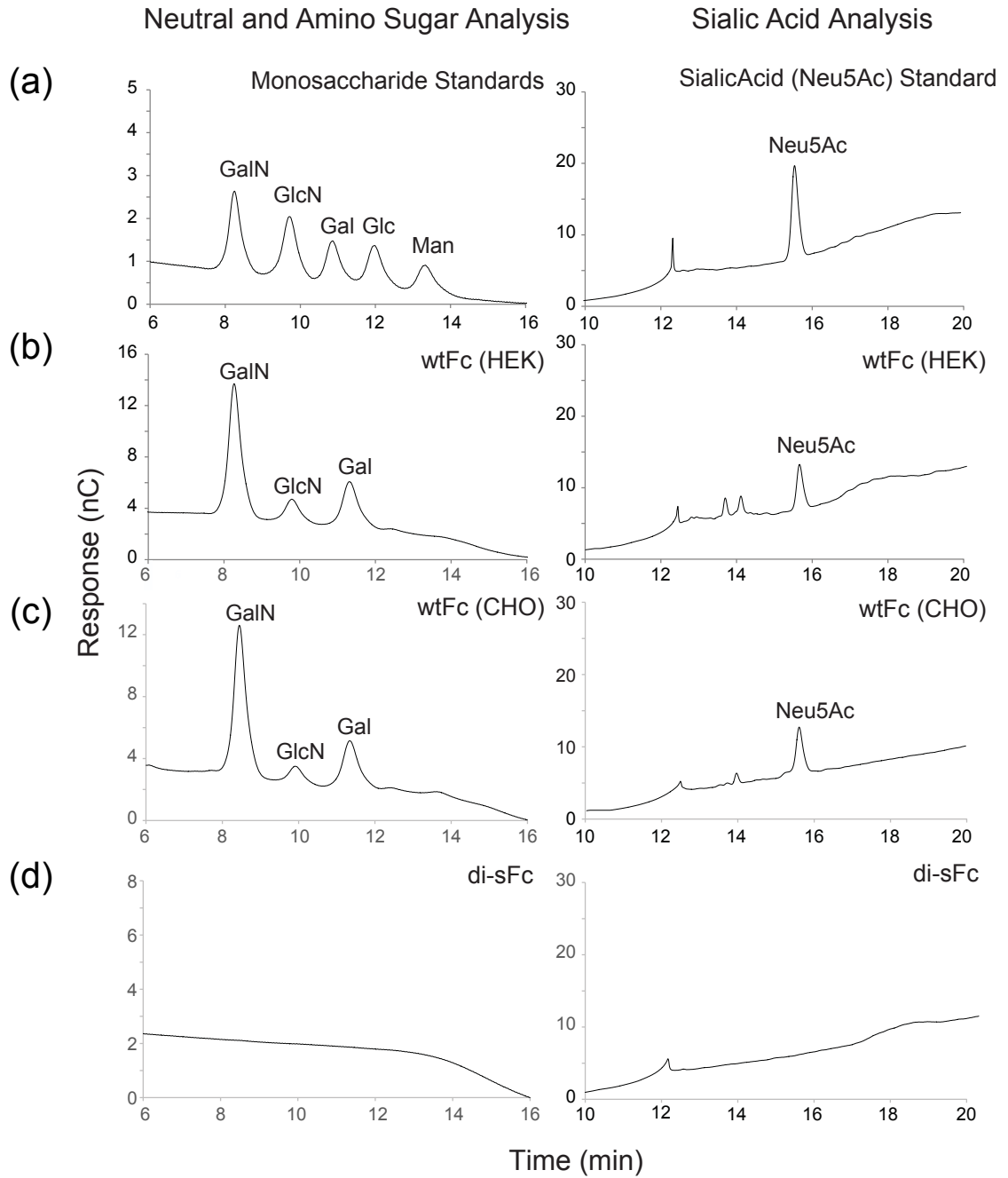


Figure S3. HPAEC-PAD neutral monosaccharide compositional analyses of putative O-glycans.

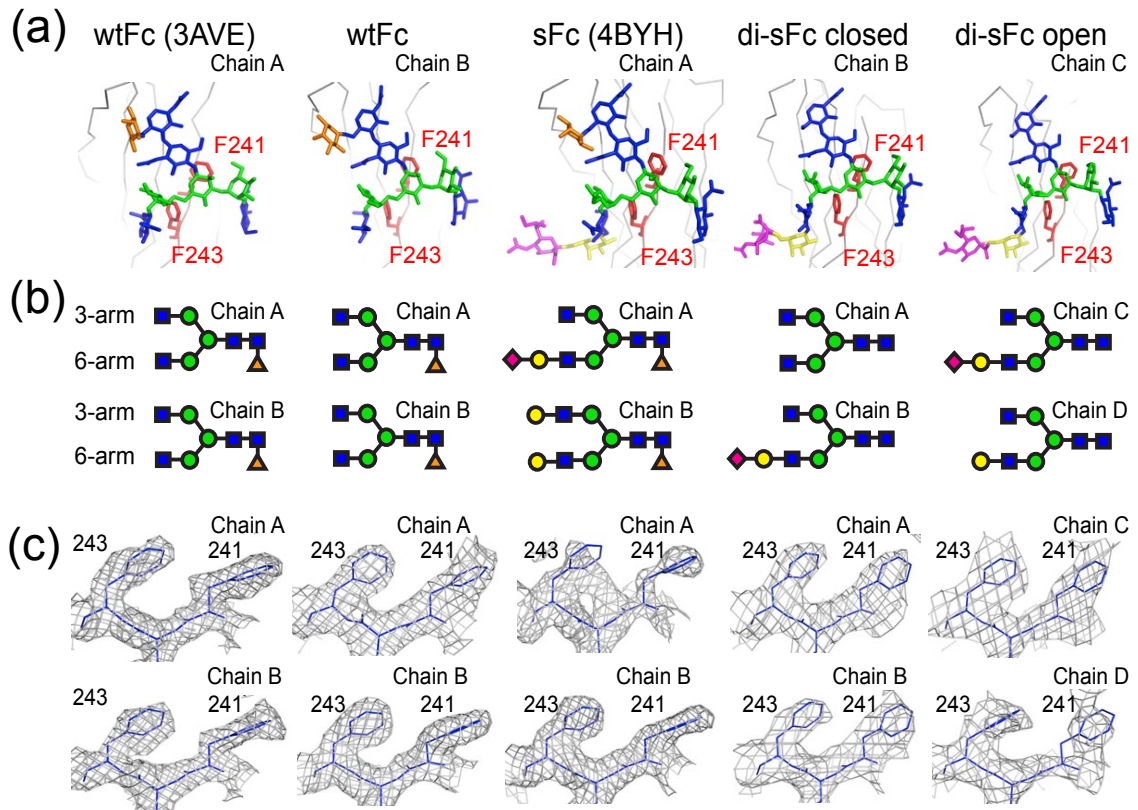


Figure S4. Comparison of glycan and protein residue conformations in sFc and wtFc structures.



**Supplementary Table 1. Data collection and refinement statistics**

	<b>wtFc</b>	<b>di-sFc</b>	<b>F241A Fc</b>
<b>Data Collection</b>			
Space group	P2 <sub>1</sub> , 2 <sub>1</sub>	P2 <sub>1</sub>	P2 <sub>1</sub> , 2 <sub>1</sub>
Cell dimensions			
<i>a</i> , <i>b</i> , <i>c</i> (Å)	49.52, 79.48, 137.94	52.73, 154.22, 66.12	57.91, 74.70, 113.71
$\alpha$ , $\beta$ , $\gamma$ (°)	90.0, 90.0, 90.0	90.0, 110.8, 90.0	90.0, 90.0, 90.0
Resolution (Å)	52.09 - 2.35 (2.43 - 2.35)	48.23 - 3.00 (3.11 - 3.00)	35.65 - 2.19 (2.27 - 2.19)
R <sub>merge</sub>	0.055 (0.479)	0.060 (0.536)	.053 (0.559)
Completeness (%)	99.9 (99.8)	97.8 (96.1)	93.6 (75.5)
Redundancy	2.0 (2.0)	1.9 (1.9)	1.8 (1.7)
I/ $\sigma$ I	9.07 (1.89)	11.07(1.75)	9.76 (1.38)
CC <sub>1/2</sub> (%)	99.9 (79.5)	99.2 (88.5)	99.9 (72.9)
<b>Refinement</b>			
Resolution (Å)	2.35	3.00	2.19
No. reflections	23368	19336	24276
R <sub>work</sub> /R <sub>free</sub>	.211/.264	.260/.280	.206/.232
No. atoms			
Protein	3322	6146	3328
Ligand/ion	198	429	195
Water	165	0	351
Average B factor	51.70	71.01	33.20
rmsd			
Bond lengths (Å)	.022	0.013	.007
Bond angles (°)	1.85	1.62	1.17

Statistics for the highest-resolution shell are shown in parentheses.

**Structural Characterization of GASDALIE Fc Bound to  
the Activating Fc receptor Fc $\gamma$ R11a**

## ABSTRACT

The Immunoglobulin G (IgG) Fc region initiates inflammatory responses such as antibody-dependent cell-mediated cytotoxicity (ADCC) through binding to activating Fc receptors (Fc $\gamma$ RI, Fc $\gamma$ RIIa, Fc $\gamma$ RIIIa, Fc $\gamma$ RIIIb). These receptors are expressed on the surface of immune cells including macrophages, dendritic cells, and natural killer (NK) cells together with an inhibitory receptor, Fc $\gamma$ RIIb, thereby setting a threshold for cell activation. The affinity of IgG Fc for binding activating Fc receptors depends on IgG subclass and the composition of *N*-linked glycans attached to a conserved asparagine in the Fc C<sub>H</sub>2 domain. For example, Fc regions with afucosylated glycans bind more tightly to activating receptors than fucosylated Fc, and afucosylated Fcs exhibit enhanced ADCC activity *in vivo* and *in vitro*. Enhanced pro-inflammatory responses have also been seen for Fc regions with amino acid mutations. GASDALIE Fc is an Fc mutant (G236A/S239D/A330L/I332E) with increased affinity for activating receptors Fc $\gamma$ RIIIa. We determined the crystal structure of GASDALIE Fc alone and in complex with the activating receptor Fc $\gamma$ RIIIa to gain insight on potential structural changes in Fc and/or enhanced receptor-Fc interactions between GASDALIE Fc and Fc $\gamma$ RIIIa. The structure of GASDALIE Fc alone was similar to wild-type Fc structures. However, we found increased electrostatic interactions in the GASDALIE Fc:Fc $\gamma$ RIIIa interface compared with other Fc:Fc $\gamma$ R structures that could contribute to the increased affinity of GASDALIE Fc for Fc $\gamma$ RIIIa.

## INTRODUCTION

Immunoglobulin G (IgG) plays critical roles in antibody-mediated immune responses through specific engagement of both antigens and immune effector cells. The fragment crystallizable (Fc) region specifically engages Fc gamma receptors (Fc $\gamma$ Rs), the initial step in effector functions such as antibody-dependent cell-mediated cytotoxicity (ADCC) and phagocytosis [7]. In humans there are two activating Fc $\gamma$ Rs that play a key role in ADCC: Fc $\gamma$ RIIa and Fc $\gamma$ RIIIa. Fc $\gamma$ RIIIa is expressed primarily on the surface of natural killer (NK) cells, while Fc $\gamma$ RIIa is commonly found on macrophages and granulocytes [13]. Both are low-affinity receptors, therefore activation of cells results only from crosslinking of these surface receptors upon engagement of clustered Fc regions in antibody-antigen immune complexes (ICs), although this is not the case for Fc $\gamma$ RI, a high affinity receptor that can activate cells by binding to monomeric IgG [81]. Activation is mediated by immunoreceptor tyrosine-based activating motifs (ITAMs) found on the receptor-associated  $\gamma$ -chain. Upon engagement of ICs with Fc $\gamma$ Rs, these motifs become phosphorylated leading to a cascade of events that activate the cell to destroy an invading pathogen or infected cell [55]. An inhibitory receptor, Fc $\gamma$ RIIb, is found on B cells, macrophages, neutrophils, and mast cells [15, 18, 22]. Immunoreceptor tyrosine-based inhibitory motifs (ITIMs) in the cytoplasmic tail of Fc $\gamma$ RIIb mediate suppression of Fc $\gamma$ R activation by activating phosphatases that reverse the effects of kinases in the ITAM signaling pathway [55]. Co-expression of activating and inhibitory receptors sets a threshold for activation of effector cells.

Fc regions are independently-folded, stable regions of IgGs comprising an N-terminal hinge (connected to each of two antigen-binding Fab arms) followed by two Ig constant domains, C<sub>H2</sub> and C<sub>H3</sub>, on each chain of the Fc homodimer. Fc<sub>γ</sub>R receptors bind asymmetrically to Fc homodimers with a 1:1 Fc<sub>γ</sub>R:Fc stoichiometry to a site involving the hinge region and N-terminal portions of the C<sub>H2</sub> domains [29]. The Fc region includes a heterogeneous *N*-linked glycan attached to a conserved residue, Asn297, in each Fc C<sub>H2</sub> domain. The Asn297-linked glycan is a complex carbohydrate composed of a mannose (Man) and N-acetylglucosamine (GlcNAc) core that is usually fucosylated. The glycan can be additionally modified with a terminal galactose or sialic acid. Typically, wild-type (wt) IgG is agalactosylated (G0; 35%), mono-galactosylated (G1; 35%), or digalactosylated (G2; 16%) and asialylated (S0; 85%), although mono- and disialylated IgG represent 11% and 4%, respectively, of IgG in human serum [10]. Modification of the *N*-linked glycan of IgG Fc can alter its function. For example, terminally sialylating the glycan switches the Fc from a pro-inflammatory to anti-inflammatory molecule [9, 43, 44, 46, 55, 57, 61, 70], which may correlate with increased conformational flexibility compared with wtFc regions [54]. Afucosylation of the normally core-fucosylated glycan leads to enhanced binding to the activating receptor Fc<sub>γ</sub>RIIIa, resulting in enhanced ADCC [28, 29, 31] due to increased protein-protein and protein-carbohydrate interactions between the Fc and receptor [29, 31]. Removing the *N*-linked glycan leads to a closed Fc conformation that exhibits no binding to any Fc<sub>γ</sub>R [11, 66]; however, aglycosylated Fc can bind the FcRn protection receptor [11], which recognizes the interface between the C<sub>H2</sub> and

C<sub>H</sub>3 domains of each Fc chain [12], a site distant from the Asn297-linked *N*-linked glycan.

Previous efforts have been made to alter the IgG Fc region to either enhance or suppress binding to Fc $\gamma$ Rs [11, 29, 31, 35, 36, 38, 55, 82, 83]. In a 2006 study, IgG Fc with mutations S239D/I332E (SDIE) or S239D/A330L/I332E (SDALIE) showed enhanced ADCC and 60-fold (SDIE Fc) and 170-fold (SDALIE Fc) increased affinity for binding to Fc $\gamma$ R11a, respectively [35]. SDIE and SDALIE Fc also showed increased binding to the inhibitory receptor, Fc $\gamma$ R11b, by 70-fold and 40-fold, respectively [35, 38, 84]. The crystal structure of unbound SDALIE Fc revealed a more open conformation compared with wtFc structures, but no major changes in the Fc $\gamma$ R recognition interface [38]. Related Fc mutants also showed increased activity and affinity for binding to Fc $\gamma$ Rs. A single G236A substitution in the Fc showed 7-fold enhanced binding to Fc $\gamma$ R11a and enhanced phagocytosis *in vitro* while Fcs with mutations G236A/S239D/I332E (GASDIE) demonstrated 70-fold enhancement [36]. The G236A substitution alone did not cause enhanced binding to Fc $\gamma$ R11b, whereas the GASDIE mutant showed 14-fold enhanced affinity for this receptor [36]. A variant of SDALIE Fc, GASDALIE (G236A/S239D/A330L/I332E) Fc, which combined the G236A substitution with the SDALIE substitutions, showed increased affinity for activating receptors Fc $\gamma$ R11a and Fc $\gamma$ R11a (13- to 20-fold, respectively). Although GASDALIE Fc bound to Fc $\gamma$ R11a with lower affinity than the SDALIE Fc:Fc $\gamma$ R11a interaction, GASDALIE Fc showed only a ~2-fold increase in affinity for the inhibitory receptor Fc $\gamma$ R11b [33, 85]. Thus unlike SDALIE Fc, GASDALIE Fc did not cause a great increase in

affinity to Fc $\gamma$ R11b (40-fold vs. 2-fold) but did produce an enhanced affinity for activating Fc $\gamma$ Rs.

In order to determine the mechanism by which the GASDALIE substitutions enhance binding to activating Fc $\gamma$ Rs, we solved crystal structures of GASDALIE Fc alone and in complex with Fc $\gamma$ R11a, comparing the bound and free GASDALIE Fc structures to the previously-solved unbound SDALIE Fc structure [38, 84] and other Fc structures. We find that the GASDALIE substitutions do not dramatically alter the overall Fc conformation; however, the GASDALIE Fc:Fc $\gamma$ R11a structure revealed increased electrostatic interactions at the binding interface that may account for its increased affinity for Fc $\gamma$ R11a. Our solved GASDALIE Fc:Fc $\gamma$ R11a crystal structure and homology model of GASDALIE Fc:Fc $\gamma$ R11b suggested that the G236A substitution that distinguishes GASDALIE Fc from SDALIE Fc is localized to the Fc $\gamma$ R11a/Fc $\gamma$ R11b binding site, thereby counteracting the normally enhanced binding of the SDALIE mutations for Fc $\gamma$ Rs, leading to decreased binding affinity to activating Fc $\gamma$ Rs and little to no change in affinity of GASDALIE Fc compared with wtFc for the inhibitory receptor.

## **RESULTS**

### ***Structure of GASDALIE Fc Bound to Fc $\gamma$ R11a***

GASDALIE Fc and the Fc $\gamma$ R11a ectodomain were expressed and purified in transiently-transfected mammalian cells as previously described [63, 72]. In the

case of Fc $\gamma$ R11a expression, three of five potential *N*-linked glycosylation sites were removed by site directed mutagenesis (N38Q, N74Q, N169Q), and *N*-linked glycans at asparagines 45 and 162 were retained due to their effects on protein expression and binding affinity, respectively [29, 30] (Fig. 1). The complex structure was solved by molecular replacement using an afucosylated Fc:Fc $\gamma$ R11a complex structure (PDB 3SGK) as a search model and refined to 3.1 Å ( $R_{\text{cryst}} = 0.27$ ;  $R_{\text{free}} = 0.29$ ) (Fig. 2A). The overall quality of the electron density map allowed building of *N*-linked glycans up to a terminal galactose on the 6-arm and up to a terminal GlcNAc on the 3-arm of the *N*-linked glycans of chains A and B of the Fc (Fig. 3A). On Fc $\gamma$ R11a, ordered electron density was observed for a GlcNAc attached to N45 and for two GlcNAcs attached to N162 (Fig. 3B).

Similar to previous structures of Fc:Fc $\gamma$ R11a complexes [28, 29, 31], the structure revealed an asymmetric 1:1 interaction in which the Fc $\gamma$ R11a hinge region between domain 1 (D1) and domain 2 (D2) together with the receptor D2 loops BC, C'E and FG interacted with the lower hinge region of Fc chains A and B and the C<sub>H</sub>2 domain BC, C'E and FG loops (Fig. 2A). The sites of the GASDALIE substitutions (positions 236, 239, 330, and 332) were visible in ordered electron density on Fc chains A and B (Fig. 3C). On chain A, Asp239 interacted directly with the BC loop of Fc $\gamma$ R11a. Ala236, Leu330, and, Glu332 did not contact the receptor (Fig. 2B). On chain B, Fc residue Glu332 was in direct contact with the receptor FG loop. Ala236, Asp239, and Leu330 were not at the binding interface (Fig. 2C).



In detailed comparisons of the GASDALIE Fc:Fc $\gamma$ R1IIa and wtFc:Fc $\gamma$ R1IIa (PDB 3SGJ) structures, we found electrostatic interactions resulting from one of the GASDALIE substitutions, S239D, in which a positively-charged residue, Lys120, in the Fc $\gamma$ R1IIa BC loop of D2 was positioned in a pocket between Fc chain A residues Asp239 and Asp265 (Fig. 2B, left). By comparison, in the wtFc:Fc $\gamma$ R1IIa complex, residue 239, a serine, formed a hydrogen bond with Fc $\gamma$ R1IIa Lys120 (Fig. 2B, right). The introduced residues Leu330, and Glu332 (AL and IE in GASDALIE) did not play a role in binding at the interface of Fc $\gamma$ R1IIa with chain A of GASDALIE Fc. Ala236 (the GA substitution in GASDALIE Fc) also did not play a role at the binding interface (Fig. 2B, left); however Gly236 in the wtFc:Fc $\gamma$ R1IIa complex formed a hydrogen bond with His135 of the receptor (Fig. 2B, right). The difference in binding affinity between SDALIE and GASDALIE suggests that the increase in bulkiness resulting from the G236A mutation causes unfavorable binding. This may explain the enhanced binding affinity of SDALIE Fc to Fc $\gamma$ R1IIa (170-fold) when compared to GASDALIE Fc (20-fold); the G236A mutation being the only difference between SDALIE and GASDALIE [33, 35]. Conversely, the salt bridge formed by Asp239 on Fc chain A (SD substitution in GASDALIE Fc and SDALIE Fc) and Lys120 of Fc $\gamma$ R1IIa, which is not seen in wtFc:Fc $\gamma$ R1IIa complex structures, may contribute to the increased affinity of GASDALIE Fc to Fc $\gamma$ R1IIa.

On chain B of GASDALIE Fc, we found new interactions with the introduction of the GASDALIE substitutions that may contribute to the enhanced affinity for Fc $\gamma$ R1IIa of GASDALIE compared to wtFc [33, 84]. Lys161 of Fc $\gamma$ R1IIa

formed an electrostatic interaction with residue Glu332, the IE substitution in GASDALIE Fc, an interaction not seen in wtFc:Fc $\gamma$ R111a complex structures (Fig. 2C, left); Ile332 of wtFc did not interact with Fc $\gamma$ R111a Lys161 (Fig. 2C, right). Ala236, the GA substitution in GASDALIE Fc, does not play a role at the binding interface; however Gly236 in the wtFc:Fc $\gamma$ R111a complex formed a hydrogen bond with Lys161 of the receptor (Fig. 2C, right). The decrease in hydrogen bonds in the region containing the G236A mutation may lead to unfavorable binding of GASDALIE Fc to Fc $\gamma$ R111a, similar to what was seen at the interface of at chain A.

Polymorphisms at residue 158 on Fc $\gamma$ R111A are known to affect binding to Fcs: e.g., Fc $\gamma$ R111A<sub>F158</sub> has a lower affinity for wtFc ( $K_D=2.2 \times 10^{-6}$  M) compared to with the affinity of Fc $\gamma$ R111A<sub>V158</sub> ( $K_D=4.1 \times 10^{-7}$  M) [33]. The GASDALIE Fc complex structure was solved with Fc $\gamma$ R111A<sub>F158</sub>, whereas the wtFc complex structure was solved with Fc $\gamma$ R111A<sub>V158</sub>[29]. Ala236 of GASDALIE Fc (the GA substitution in GASDALIE Fc) was near Fc $\gamma$ R111a residue Phe158 (7.3 Å between the C $\alpha$  atoms of Ala236 and Phe158 compared with 4.9 Å between the C $\alpha$  atoms of Ala236 and Val158 in the wtFc:Fc $\gamma$ R111a structure) (Fig. 4b). This difference in affinity between these two polymorphic forms of Fc $\gamma$ R111a suggests that an increase in bulkiness of residue 158 side chain (valine to phenylalanine) results in less favorable binding to Fcs. Similarly, the increase in bulkiness resulting from the G236A substitution in GASDALIE Fc may lead to unfavorable binding to Fc $\gamma$ R111a in the region containing Phe158.

### ***Modeling of interaction of GASDALIE Fc with Fc $\gamma$ R11b***

To gain understanding of the selectivity of GASDALIE Fc for the activating receptor Fc $\gamma$ R11a over the inhibitory receptor Fc $\gamma$ R11b, we used homology modeling [80] to create a models of GASDALIE Fc:Fc $\gamma$ R11b and wtFc:Fc $\gamma$ R11b complexes based on high-resolution structures of Fc $\gamma$ R11b (PDB 2FCB), the wtFc:Fc $\gamma$ R11a complex (PDB 3SGJ) and the GASDALIE Fc:Fc $\gamma$ R11a complex described in this study. The D2 domains of Fc $\gamma$ R11b and Fc $\gamma$ R11a share structural homology (root mean square deviations, rmsds, ranging from 0.5-0.7 Å for pairwise combinations) and bind to Fcs with similar orientations, as demonstrated by crystal structures and site-directed mutagenesis [11, 86-90] (Fig. 4).

To validate the modeling methods, we first constructed a homology model of the GASDALIE Fc:Fc $\gamma$ R11a using the wtFc:Fc $\gamma$ R11a complex structure (PDB 3SGJ) as a starting reference. The modeled GASDALIE Fc:Fc $\gamma$ R11a exhibited a 1.2 Å rmsd compared with the GASDALIE Fc:Fc $\gamma$ R11a crystal structure (calculated for all C $\alpha$  atoms) and reproduced the interactions of the GASDALIE substitutions with Fc $\gamma$ R11a.

To generate GASDALIE Fc:Fc $\gamma$ R11b homology model, the D2 domain of Fc $\gamma$ R11b was aligned with D2 of Fc $\gamma$ R11a in the GASDALIE Fc:Fc $\gamma$ R11a complex structure. A similar method was used to generate the wtFc:Fc $\gamma$ R11a homology model. There were several interactions predicted by GASDALIE Fc:Fc $\gamma$ R11b and wtFc:Fc $\gamma$ R11b homology models that gave insight on the difference in affinity of GASDALIE Fc vs. wtFc. As described above, the asymmetric binding of Fc $\gamma$ Rs to

two-fold symmetric Fc regions results in different effects of the Fc substitutions on the two chains of the Fc homodimer. On chain A, the Ala236, Asp239, Leu330 and Glu332 substitutions were not predicted to play a role in binding at the interface of Fc $\gamma$ R11b with GASDALIE Fc chain A; in the wtFc:Fc $\gamma$ R11b homology model Gly236 is predicted to form a hydrogen bond with Arg131 of the receptor (Fig. 5B).

On chain B of the GASDALIE Fc, Asp239 in GASDALIE Fc, the substitution in the SD portion of GASDALIE, was predicted to hydrogen bond with Thr158 in Fc $\gamma$ R11b (Fig.5C, left). By contrast, there was a serine at site 239 in wtFc predicted not to interact with the receptor (Fig.5C, right). Ala236 (the GA substitution in GASDALIE) was predicted not to form any interactions with the receptor however; if there is a glycine instead of an alanine at this position, as in wtFc, a hydrogen bond is predicted to form between Tyr160 of the receptor and Gly236. The G236A substitution in the GASDALIE Fc:Fc $\gamma$ R11b complex may decrease the number of hydrogen bonds at the interface similar to what is seen in the GASDALIE Fc:Fc $\gamma$ R11a complex thereby lowering affinity of GASDALIE Fc to both activating and inhibitory receptors when compared to SDALIE Fc (missing GA substitution) [33, 35, 84].

### ***Conformations of free and receptor-bound GASDALIE Fc***

In order to determine if unbound GASDALIE Fc exhibits conformational changes associated with its increased affinity for Fc $\gamma$ R11a compared with wtFc, we solved the crystal structure of GASDALIE Fc alone by molecular replacement to 2.4 Å ( $R_{\text{cryst}} = 0.24$ ;  $R_{\text{free}} = 0.26$ ). The structure revealed a typical Fc homodimer with *N*-

glycans attached to C<sub>H</sub>2 domain residue Asn297 (Fig. 6A). Ordered electron density was observed up to a terminal galactose on the 6-arm and up to a terminal *N*-acetyl glucosamine on the 3-arm of the *N*-linked glycan, similar to wtFc structures and to SDALIE Fc (Fig. 6B). The GASDALIE substitutions were located in ordered electron density; however, the region containing Ala236 was disordered on both chains A and B (Fig. 6C).

In order to assess potential differences between GASDALIE Fc and wtFc structures, the C<sub>H</sub>3 domains of each Fc were aligned and the positions of the C<sub>H</sub>2 domains were compared. We monitored C<sub>H</sub>2 domain separations in the various Fc structures by measuring distances between the C $\alpha$  atoms at C<sub>H</sub>2 positions 238, 241, 301, and 329 as described [54, 69]. As previously noted, wtFc structures exhibit relatively small structural differences, showing similar C<sub>H</sub>2 domain separations despite differences in crystal packing [54]. The separation between the C<sub>H</sub>2 domains of the GASDALIE Fc structure fell within range of the C<sub>H</sub>2 domain separations in wtFc (PDB 3DO3, 2DTS, 3AVE, 1HZH, and 4Q7D);, therefore the GASDALIE mutations did not greatly influence the overall C<sub>H</sub>2-C<sub>H</sub>2 domain arrangement in the unbound structure (Fig. 7). We also aligned the C<sub>H</sub>3 domains of the unbound GASDALIE Fc structure with the C<sub>H</sub>3 domains of the 2.5 Å SDALIE Fc structure (PDB 2QL1) [38]. SDALIE Fc was in a more open conformation than GASDALIE with a root mean square deviation (rmsd) of 5.8 Å calculated for the 201 C<sub>H</sub>2 domain C $\alpha$  atoms (Fig. 7).

We next compared the free GASDALIE Fc structure to the structure of GASDALIE solved in complex with Fc $\gamma$ R111a. No notable differences were seen in

side chain conformations at the sites of the GASDALIE mutations; however, the C<sub>H2</sub> domains of the bound GASDALIE Fc were in a more open conformation compared with the unbound form (Fig. 8) (rmsd of 2.3 Å calculated for the 202 C $\alpha$  atoms of the C<sub>H2</sub> domains of one Fc after alignment of the C<sub>H3</sub> domains in each structure). However, the Fc $\gamma$ R11a-bound GASDALIE Fc fell within the range of C<sub>H2</sub> domain separations for receptor-bound Fc structures (Fig. 8). This result was expected since previously-solved complexes of afucosylated and wtFc bound to Fc $\gamma$ R11a did not show major changes in overall Fc conformation [29, 91].

## DISCUSSION

IgG is a dynamic glycoprotein whose activities can be modulated with glycan and protein modifications to its Fc region. With introduction of the G236A/S239D/A330L/I332E substitutions in the Fc C<sub>H2</sub> domain, binding to activating Fc $\gamma$ R receptors is increased by 13-20-fold [33, 85]. Increased binding to activating Fc $\gamma$ Rs results in enhanced ADCC, of importance for developing therapeutic antibodies against cancer and infectious diseases [28, 29, 31, 35, 36]. Although a closely-related Fc mutant, SDALIE Fc, showed enhanced binding by ~100-fold to the activating Fc receptor Fc $\gamma$ R11a, it also enhanced binding to the inhibitory Fc $\gamma$ R11b receptor [35, 38]. By contrast, the GASDALIE Fc mutant selectively engages activating Fc $\gamma$ Rs with little to no enhanced binding to the inhibitory receptor [33, 85].

Here we present structures of GASDALIE Fc in its unbound state and in complex with the activating receptor Fc $\gamma$ R11a. Although the SDALIE Fc structure

was in a more open conformation than wtFc structures with respect to the degree of separation of its C<sub>H2</sub> domains [38], the unbound GASDALIE Fc fell within the range of C<sub>H2</sub> domain separations in wtFc structures [38]. The more open conformation of SDALIE Fc compared with GASDALIE Fc may be important for its higher binding affinity for both activating and inhibitory Fc $\gamma$ R<sub>s</sub> since notable changes in the side chain conformations of the of SDALIE substitutions were not observed when compared to GASDALIE Fc.

The binding interface between GASDALIE Fc and Fc $\gamma$ R<sub>IIIa</sub> reveals key lysines in the receptor that interact with specific side chains of the Fc important for binding. Fc $\gamma$ R<sub>IIIa</sub> Lys120 sits in a pocket containing Fc chain A residues Asp265 and Asp239. Asp265, although not one of the GASDALIE substitutions in Fc, is important for interactions with Fc $\gamma$ R<sub>s</sub> to mediate ADCC — when this residue is mutated (D265A), binding to both activating and inhibitory Fc $\gamma$ R<sub>s</sub> is abrogated [92]. The introduction of Asp239 (the SD portion of the GASDALIE substitutions) may further stabilize the Asp265 (Fc)/Lys120 (Fc $\gamma$ R) interaction, contributing to tighter binding of GASDALIE Fc than wtFc to Fc $\gamma$ R<sub>IIIa</sub>. There is also an electrostatic interaction of Fc chain B residue Glu332 (the IE portion of the GASDALIE substitutions) with receptor residue Lys161 that is not observed in the wtFc:Fc $\gamma$ R<sub>IIIa</sub> complex. Electrostatic interactions with this receptor lysine may also contribute to the increased affinity for GASDALIE Fc compared with wtFc.

Modeling of GASDALIE Fc bound Fc $\gamma$ R<sub>IIb</sub>, along with the GASDALIE Fc:Fc $\gamma$ R<sub>IIIa</sub> structure described in this work suggests the site of the G236A mutation in Fc (the GA portion of the GASDALIE substitutions) is located at the

Fc $\gamma$ R binding site, slightly disrupting binding to activating, as well as inhibitory, receptors. Additionally, analysis of these structures gave insight on how each GADALIE substitution affected binding to each receptor. Introduction of Asp239 (SD of GASDALIE Fc) in both chains A and B of GASDALIE Fc results in increased electrostatic interactions or hydrogen bonding with residues in Fc $\gamma$ RIIb and Fc $\gamma$ RIIIa. Although Leu330 (AL of GASDALIE Fc) did not play a role in the binding interface of GASDALIE Fc with any of the Fc $\gamma$ Rs, it is important in selecting for ADCC over complement-dependent cytotoxicity (CDC). This preference may result from the Leu330 substitution being close to the C1q binding site, disrupting binding of this protein to IgGs [35, 37, 93]. Substitution of Ile332 for Glu332 (IE substitution in GASDALIE Fc) results in increased electrostatic interactions with Fc $\gamma$ RIIIa, but not with the other Fc $\gamma$ Rs. Comparison of Fc $\gamma$ R affinities for the SDALIE mutant Fc compared with the GASDALIE Fc showed that substitution of Gly236 for Ala236, that distinguishes SDALIE from GASDALIE Fc, decreased binding to both activating and inhibitory Fc $\gamma$ Rs [33, 35]. The GASDALIE Fc:Fc $\gamma$ RIIIa structure and homology models of GASDALIE Fc and wtFc bound to Fc $\gamma$ RIIb show that the decrease resulting from the introduction of the G236A substitution may result from disruption of hydrogen bonds at the interface between Fc $\gamma$ RIIIa and Fc $\gamma$ RIIb.

The study presented gives structural insight on how the GASDALIE mutations enhance binding to Fc $\gamma$ RIIIa. Further co-crystallization experiments with both Fc $\gamma$ RIIIa and Fc $\gamma$ RIIb will be essential in further understanding how these mutations allow selection for activating Fc receptors.



## FIGURE LEGENDS

Figure 1. Reducing SDS-PAGE gel of Fc $\gamma$ R1IIa ectodomains expressed in HEK-293 cells (A) Unmodified Fc $\gamma$ R1IIa. (B) Fc $\gamma$ R1IIa with glycosylation sites at N38, N74, and N169 removed (Fc $\gamma$ R1IIa-N45N162). (C) Fc $\gamma$ R1IIa-N45N162 expressed in cells treated with 2.5 $\mu$ M kifunensine.

Figure 2. Front view of the GASDALIE Fc:Fc $\gamma$ R1IIa complex and interfaces at chain A and B of Fc:Fc $\gamma$ R complex structures. (A) The D1 and D2 domains of Fc $\gamma$ R1IIa are pink; the Fc C<sub>H</sub>2 domains are blue shown as cartoon ribbon diagrams; glycans (blue) are shown as sticks and G236/S239D/A330L/I332E mutations (red) are shown as spheres (left). Comparison of interfaces in the GASDALIE Fc–Fc $\gamma$ R1IIa and fucosylated Fc–Fc $\gamma$ R1IIa structures. (B) Chain A of wtFc (PDB 3SGJ) (right) and GASDALIE Fc (left) bound to Fc $\gamma$ R1IIa. (C) Chain B of wtFc (right) GASDALIE Fc (left) bound to Fc $\gamma$ R1IIa. Electrostatic interactions (red) and hydrogen bonds (yellow) are shown as dashes. Residues that do not participate in hydrogen bonds or electrostatic interactions are shown in gray.

Figure 3. 2F<sub>o</sub>-F<sub>c</sub> electron density (contoured at 0.7 $\sigma$ ) from an annealed omit map calculated in the regions of: (A) Asn297-linked glycans on Fc $\gamma$ R1IIa-bound GASDALIE Fc, (B) Asn45 and Asn162-linked glycans on Fc $\gamma$ R1IIa, and (C) the G236/S239D/A330L/I332E mutations.

Figure 4. Comparison of GASDALIE Fc complexes with Fc $\gamma$ RIIb and Fc $\gamma$ RIIIa. (A,B) alignment of the D2 domains of Fc $\gamma$ RIIb (PDB 1FCB, yellow) and Fc $\gamma$ RIIIa (magenta) in the GASDALIE Fc:Fc $\gamma$ RIIIa complex structure. The position of Fc $\gamma$ RIIb was generated using homology modeling as described in the text. (C) Sequence alignment of the three Fc $\gamma$ R receptors (ClustalW2).

Figure 5. Comparison of the interfaces of GASDALIE Fc with Fc $\gamma$ RIIb and Fc $\gamma$ RIIIa. (A) Front view of the GASDALIE Fc:Fc $\gamma$ RIIb homology model. The D1 and D2 domains of Fc $\gamma$ RIIb are yellow; the Fc C<sub>H</sub>2 domains are blue shown as cartoon ribbon diagrams; glycans and G236/S239D/A330L/I332E mutations (red) are shown as spheres (B) Chain A of wtFc (PDB 3SGJ) (right) and GASDALIE Fc (left) bound to Fc $\gamma$ RIIb. (C) Chain B of wtFc (right) GASDALIE Fc (left) bound to Fc $\gamma$ RIIb. Electrostatic interactions (red) and hydrogen bonds (yellow) are shown as dashes. Residues that do not participate in hydrogen bonds or electrostatic interactions are shown in gray.

Figure 6. 2.4 Å crystal structure of unbound GASDALIE Fc. (A) C<sub>H</sub>2 and C<sub>H</sub>3 domains shown as a ribbon diagram and glycans shown as sticks. (B-C) 2F<sub>o</sub>-F<sub>c</sub> electron density (contoured at 0.7 $\sigma$ ) from an annealed omit map calculated in the regions of: (B) Asn297-linked glycans on chains A and B of GASDALIE Fc, and (C) the G236/S239D/A330L/I332E mutations.

Figure 7. Alignment of wtFc structures (PDB IDs: 3DO3, 2DTS, 3AVE, 4Q7D, 1HZH, gray) with SDALIE Fc (PDB 2QL1, blue) and the GASDALIE Fc (this study, cyan). \*SDALIE Fc crystallized with one Fc chain in the asymmetric unit, therefore chain B of the Fc homodimer was generated by two-fold symmetry.

Figure 8. Comparison of C<sub>H</sub>2 domain separations in free Fc and complexed Fc structures. Left: location of C<sub>α</sub> atoms for Pro238, Phe241, Arg301, and Pro329 (red spheres) and Asn297 (blue spheres) indicated on the C<sub>H</sub>2 domains of wtFc (PDB 3AVE). C<sub>H</sub>2 domain separation in individual Fc structures was evaluated by measuring distances (dotted lines) between the corresponding red spheres on each chain. Right: Alignment of the C<sub>H</sub>3 domains of GASDALIE Fc, SDALIE Fc (PDB 2QL1), the Fc in the GASDALIE Fc:Fc<sub>γ</sub>R111A complex (this study), and the Fc regions in Fc:Fc<sub>γ</sub>R111a complex structures (PDB IDs: 3SGJ, 3SGK, 3AY4, 1E4K, 1T89, and 1T83).

## METHODS

### ***Protein Expression and Purification***

The S239D/A330L/I332E (SDALIE), G236A/S239D/A330L/I332E (GASDALIE) and G236R/ L328R (GRLR) mutations were introduced by site-directed mutagenesis in a pcDNA3.1 vector containing the IgG1 Fc gene (Agilent Technologies). Additionally the GASDALIE mutation was introduced into anti-HIV1 antibody, 3BNC117. IgG, Fc, and Fc $\gamma$ R proteins were expressed in transiently-transfected HEK 293-6E suspensions as described previously [63, 72]. IgG and Fc proteins were then isolated from harvested supernatants using protein A chromatography (GE Healthcare) followed by size exclusion chromatography in 25 mM Tris-Cl pH 7.5, 100 mM NaCl on a Superdex 200 10/300 gel-filtration column (GE Healthcare). Fc $\gamma$ R proteins were isolated from supernatants using affinity chromatography (HisTrap, GE Healthcare) followed by size exclusion chromatography using the buffer described above. Fractions to the corresponding proteins were pooled and used for surface plasmon resonance (SPR) and crystallographic studies. 3BNC117 IgG was papain digested to isolate the Fc region containing the GASDALIE mutation (G236A/S239D/A330L/I332E) and was used to crystallize GASDALIE Fc alone.

Site directed mutagenesis was used to remove three of five potential *N*-linked glycosylation sites on Fc $\gamma$ R11a (N38, N74, N169) by changing asparagines to glutamines to make N38Q, N74Q, N169Q substitutions, as described for

previous structural studies of Fc $\gamma$ R1IIa [29]. Potential *N*-linked glycosylation sites at sites 45 and 162 were retained due to their effects on protein expression and binding affinity, respectively [29, 30]. C-terminally 6x-His tagged Fc $\gamma$ R ectodomains Fc $\gamma$ R1IIa (residues 1-113) and Fc $\gamma$ R1IIIa (residues 1-113) were expressed in transiently-transfected HEK293 cells as described for Fc proteins and isolated from supernatants using a HisTrap HP affinity column (GE Healthcare) followed by size exclusion chromatography in 25 mM Tris-Cl pH 7.5, 100 mM NaCl on a Superdex 200 16/ 60 gel-filtration column (GE Healthcare). To reduce carbohydrate heterogeneity that might impede crystallization, 2.5  $\mu$ M kifunensine was added immediately before transfection of cells to inhibit processing of high-mannose *N*-linked glycans to their complex forms [94].

### ***Crystallization and data collection***

Crystals of GASDALIE Fc (space group P2<sub>1</sub>2<sub>1</sub>2<sub>1</sub>;  $a = 49.32$  Å,  $b = 79.13$  Å,  $c = 137.62$  Å; one Fc dimer per asymmetric unit) were grown in sitting drop vapor diffusion by mixing equal volumes of GASDALIE Fc (7.36 mg/ml) with a solution containing 0.2 M ammonium formate and 20% (w/v) PEG 3350 at 20°C. Crystals were cryopreserved in well solution supplemented with 30% glycerol. Data were collected to 2.4 Å resolution at beamline 8.2.1 of the Advanced Light Source (ALS) at Lawrence Berkeley National Laboratory (LBNL).

Crystals of GASDALIE Fc:Fc $\gamma$ R1IIIa (space group P2<sub>1</sub>2<sub>1</sub>2<sub>1</sub>;  $a = 74.38$  Å,  $b = 94.50$  Å,  $c = 108.67$  Å; one complex per asymmetric unit) were grown in sitting drop vapor diffusion by mixing equal volumes of protein (10 mg/ml) with a solution

containing 0.04 M potassium dihydrogen phosphate and 16% (w/v) PEG 8000 at 20°C. The complex crystals were cryopreserved in well solution. Data were collected for GASDALIE Fc alone and GASDALIE Fc:Fc $\gamma$ RIIIa complex to 3.1 Å resolution at beamline 8.2.1 of the Advanced Light Source (ALS).

### ***Data Processing and Structure Determination***

Diffraction data were processed, indexed, integrated and scaled using iMosflm [73] POINTLESS and SCALA, respectively [74, 75]. We used  $I/\sigma$  ratios and completeness of the highest resolution shell in addition to the criterion that the  $CC_{1/2}$  statistic (correlation coefficient between two random halves of the data set) should be greater than 10% [76] to determine the high-resolution cutoff for datasets. We used Phenix [77] to compute  $CC_{1/2}$  values. Structures were solved by molecular replacement using PHASER [78] and published Fc and Fc:Fc $\gamma$ RIIIa structures as search models (PDB codes 4BYH for determining the GASDALIE Fc structure and 3SGK for determining the GASDALIE Fc:Fc $\gamma$ RIIIa complex structure). Modeling was done using COOT [79]. Crystallographic refinement was done using the Phenix crystallography package [77] by refining individual B factors for GASDALIE Fc and group B factors for the lower-resolution GASDALIE Fc:Fc $\gamma$ RIIIa structure. We used PyMol [80] for superposition calculations and molecular representations.

The GASDALIE Fc model ( $R_{\text{free}} = 25.6\%$ ;  $R_{\text{work}} = 23.5\%$ ) included 416 protein residues in the GASDALIE Fc dimer (Leu235 – Ser444 on chain A and Gly237 – Ser444 on chain B), 18 glycan residues (GlcNAc1-Gal6, Fuc12 on chain

A and GlcNAc1-GlcNAc8, Fuc12 on Chain B), and 105 water molecules. No electron density was observed for residues Thr225 and Cys226 of the Fc hinge or for Man7-NeuNAc10 or Gal9-NeuNAc11 in the *N*-linked glycans of chain A or B, respectively.

The GASDALIE Fc:Fc $\gamma$ RIIIa complex ( $R_{\text{free}} = 29.2\%$ ;  $R_{\text{work}} = 27.4\%$ ) included 421 protein residues in the GASDALIE Fc dimer (Leu234-Ser444 on chain A and Pro232-Leu443 on chain B), 17 glycan residues on Fc (GlcNAc1-Gal6 on chain A and GlcNAc1-GlcNAc8, Fuc12 on Chain B), 169 protein residues in the Fc $\gamma$ RIIIa ectodomain, GlcNAc1 and GlcNAc2 attached to Asn162, and GlcNAc1 attached to Asn45.

## **ACKNOWLEDGEMENTS**

We thank John Desjarlies for helpful discussions, Jost Vielmetter and the Caltech Protein Expression Center for protein production and members of the Bjorkman lab for critical reading of the manuscript, Marta Murphy for help making figures, and Jens Kaiser and members of the staff at the Advanced Light Source (ALS) for help with data collection and processing. The Advanced Light Source is supported by the Director, Office of Science, Office of Basic Energy Sciences, of the U.S. Department of Energy under Contract No. DE-AC02-05CH11231. This research was supported by the National Institute Of Allergy And Infectious Diseases of the National Institutes of Health Grant HIVRAD P01 AI100148 (P.J.B.); (the content is solely the responsibility of the authors and does not necessarily represent the official views of the National Institutes of Health), and the Molecular Observatory at

Caltech supported by the Gordon and Betty Moore Foundation. P.J.B. is a Howard Hughes Medical Institute investigator.



## FIGURES AND TABLES

**Table 1. Data collection and refinement statistics**

	<b>GASDALIE Fc:FcgRIIA</b>	<b>GASDALIE Fc</b>
<b>Resolution range (Å)</b>	71.31 - 3.10 (2.98 - 2.88)	46.43 - 2.39 (2.48 - 2.39)
<b>Space group</b>	P 2 <sub>1</sub> 2 <sub>1</sub> 2 <sub>1</sub>	P 2 <sub>1</sub> 2 <sub>1</sub> 2 <sub>1</sub>
<b>Unit cell (a,b,c; Å)</b>	74.38, 94.50, 108.67	49.32, 79.13, 137.62
<b>Total reflections</b>	275073 (21164)	751679 (75586)
<b>Unique reflections</b>	17985 (1754)	22054 (2176)
<b>Multiplicity</b>	15.3 (12.1)	34.1 (34.7)
<b>Completeness (%)</b>	100.00 (100.00)	100.00 (100.00)
<b>Mean I/sigma(I)</b>	7.95 (0.25)	30.00 (3.70)
<b>Wilson B-factor</b>	78.79	45.6
<b>R-merge</b>	1.091 (12.02)	0.8385 (1.926)
<b>R-meas</b>	1.128	0.8516
<b>CC1/2</b>	0.813 (0.213)	0.759 (0.767)
<b>CC*</b>	0.947 (0.593)	0.929 (0.932)
<b>R-work</b>	0.2738 (0.4865)	0.2346 (0.3129)
<b>R-free</b>	0.2915 (0.4927)	0.2557 (0.3142)
<b>Number of non-hydrogen atoms</b>	4864	3631
<b>macromolecules</b>	4612	3306
<b>ligands</b>	252	220
<b>water</b>	0	105
<b>Protein residues</b>	600	418
<b>RMS(bonds)</b>	0.016	0.026
<b>RMS(angles)</b>	1.42	1.61
<b>Ramachandran favored (%)</b>	95	98
<b>Ramachandran outliers (%)</b>	0.17	0.24
<b>Clashscore</b>	26.52	19.99
<b>Average B-factor</b>	40.4	57.9
<b>macromolecules</b>	38.3	56.1
<b>ligands</b>	79.5	49.7

Statistics for the highest-resolution shell are shown in parentheses.

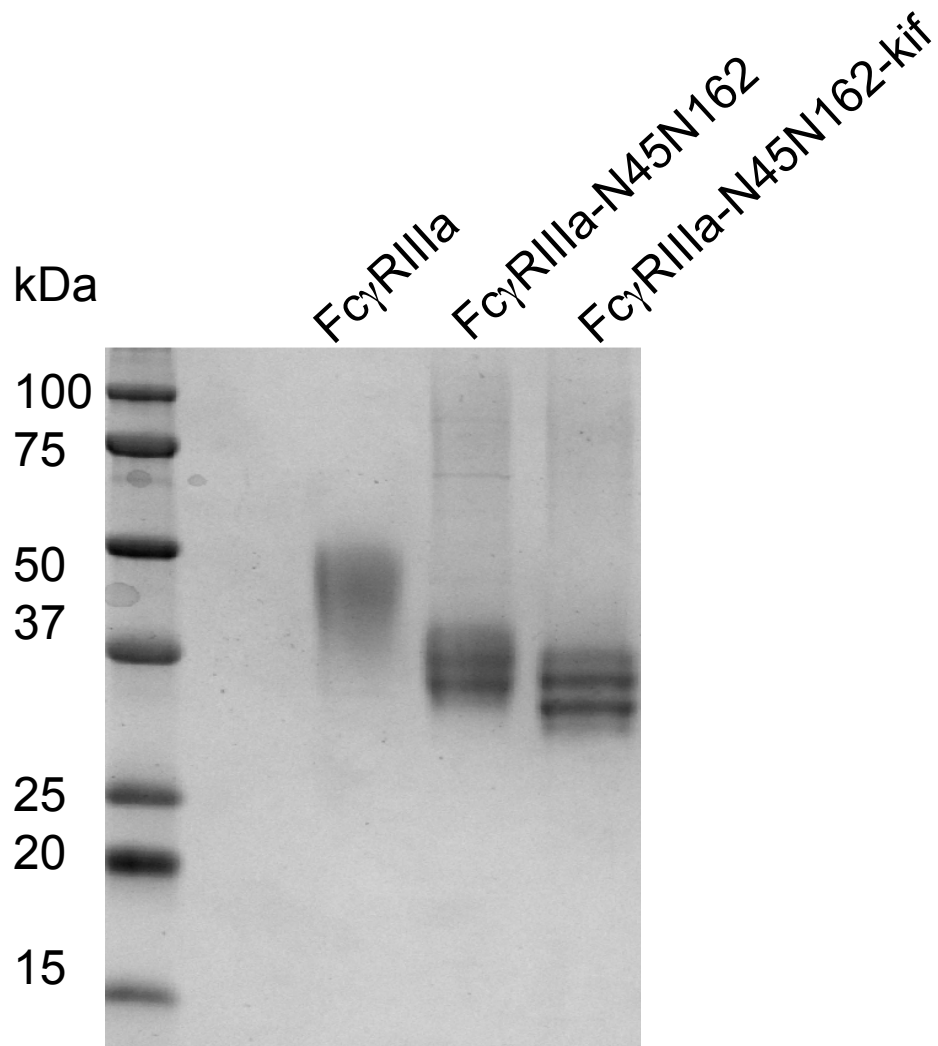


Figure 1. Reducing SDS-PAGE gel of Fc $\gamma$ RIIIa ectodomains expressed in HEK-293 cells.

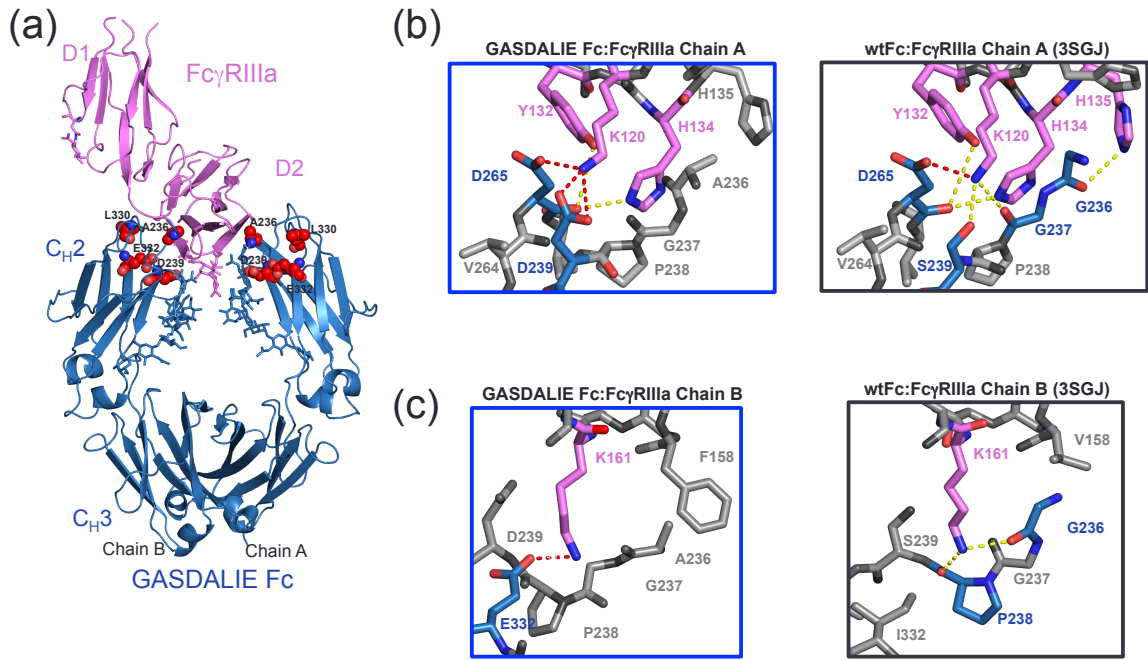


Figure 2. Comparison of interfaces in the GASDALIE Fc:Fc $\gamma$ RIIIa and wtFc:Fc $\gamma$ RIIIa (PDB 3SGJ) structures

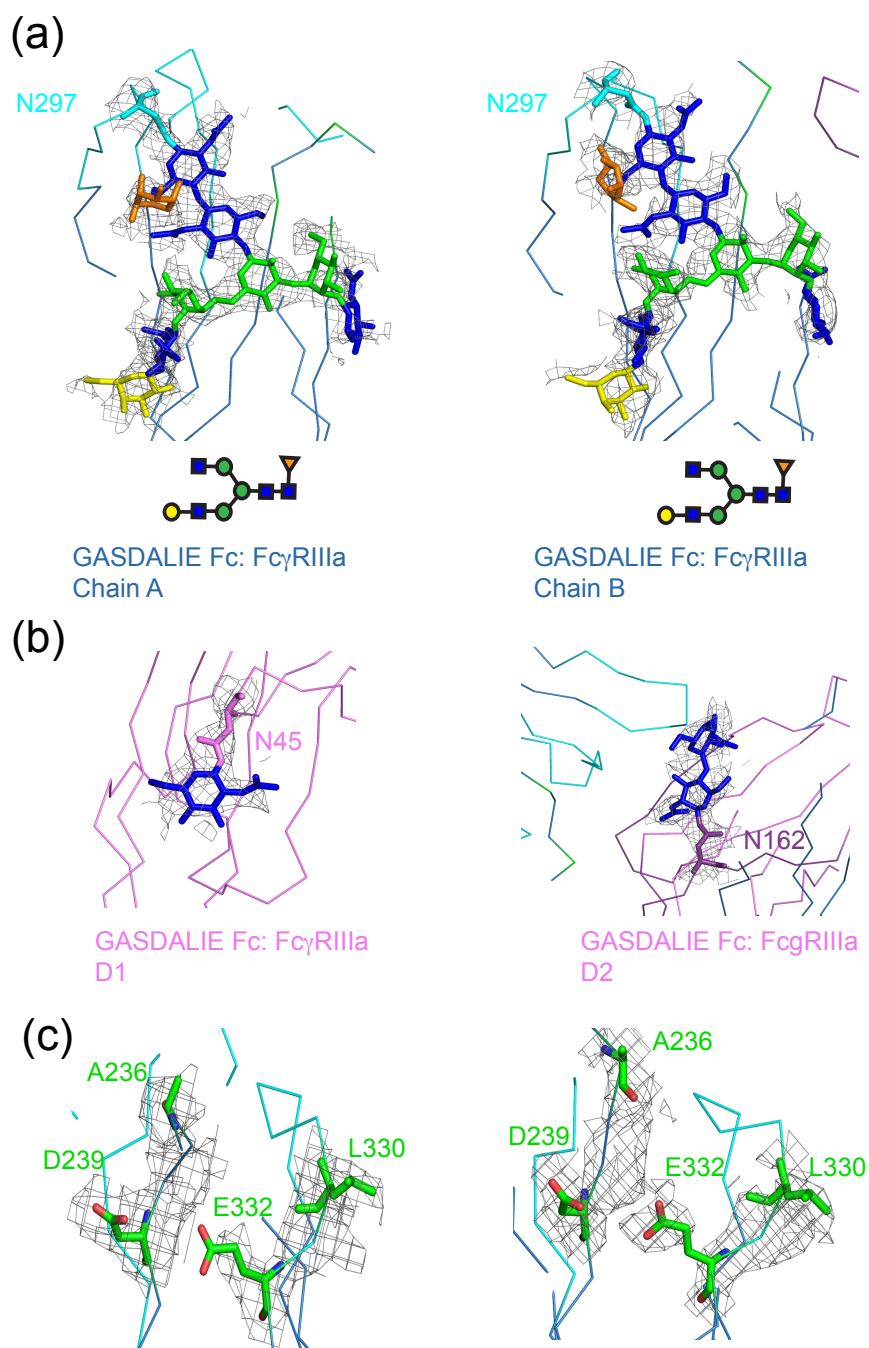


Figure 3.  $2F_o - F_c$  electron density (contoured at  $0.7\sigma$ ) from annealed omit maps calculated in the vicinity of (A) the Asn297-linked glycans on Fc $\gamma$ RIIIa-bound GASDALIE Fc, (B) the Asn45- and Asn162-linked glycans on Fc $\gamma$ RIIIa, and (C) the G236/S239D/A330L/I332E substitutions.

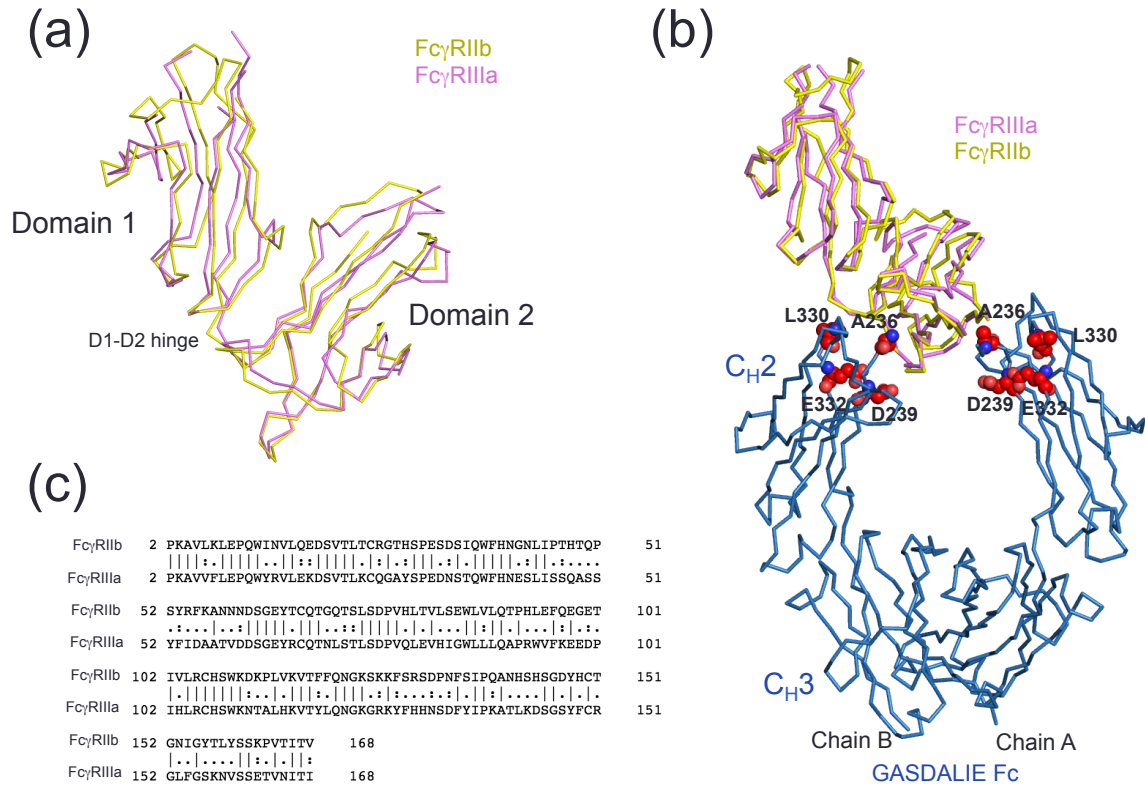


Figure 4. Comparison of Fc $\gamma$ RIIb and Fc $\gamma$ RIIIa structures bound to GASDALIE Fc

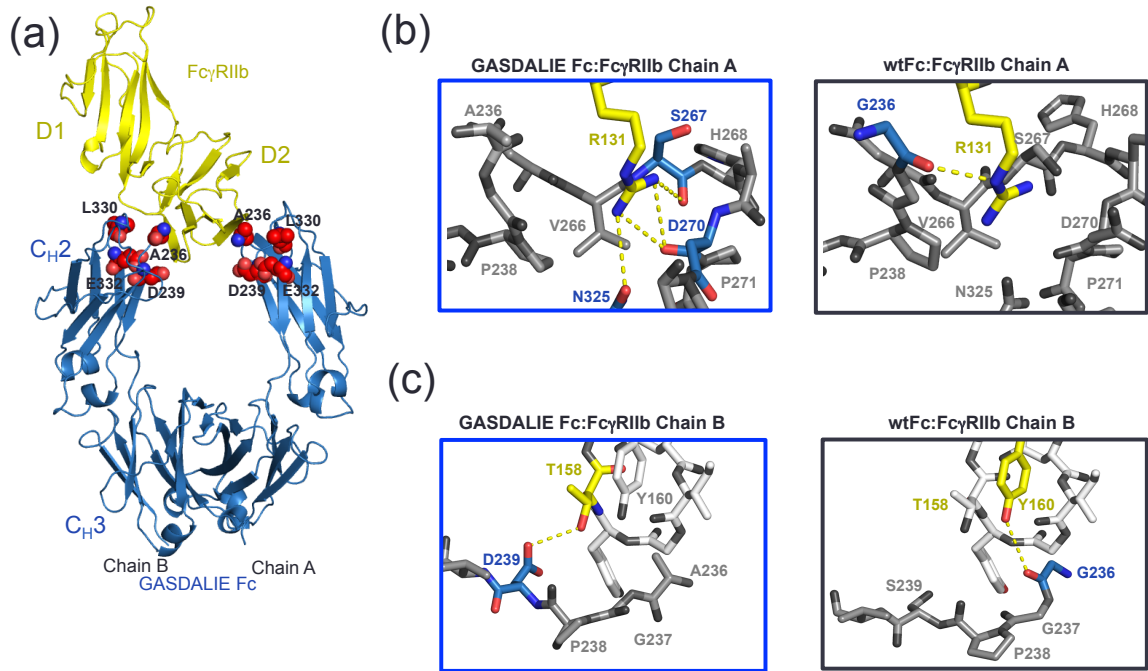


Figure 5. Comparison of the interface of FcγRIIb and FcγRIIIa bound to GASDALIE Fc

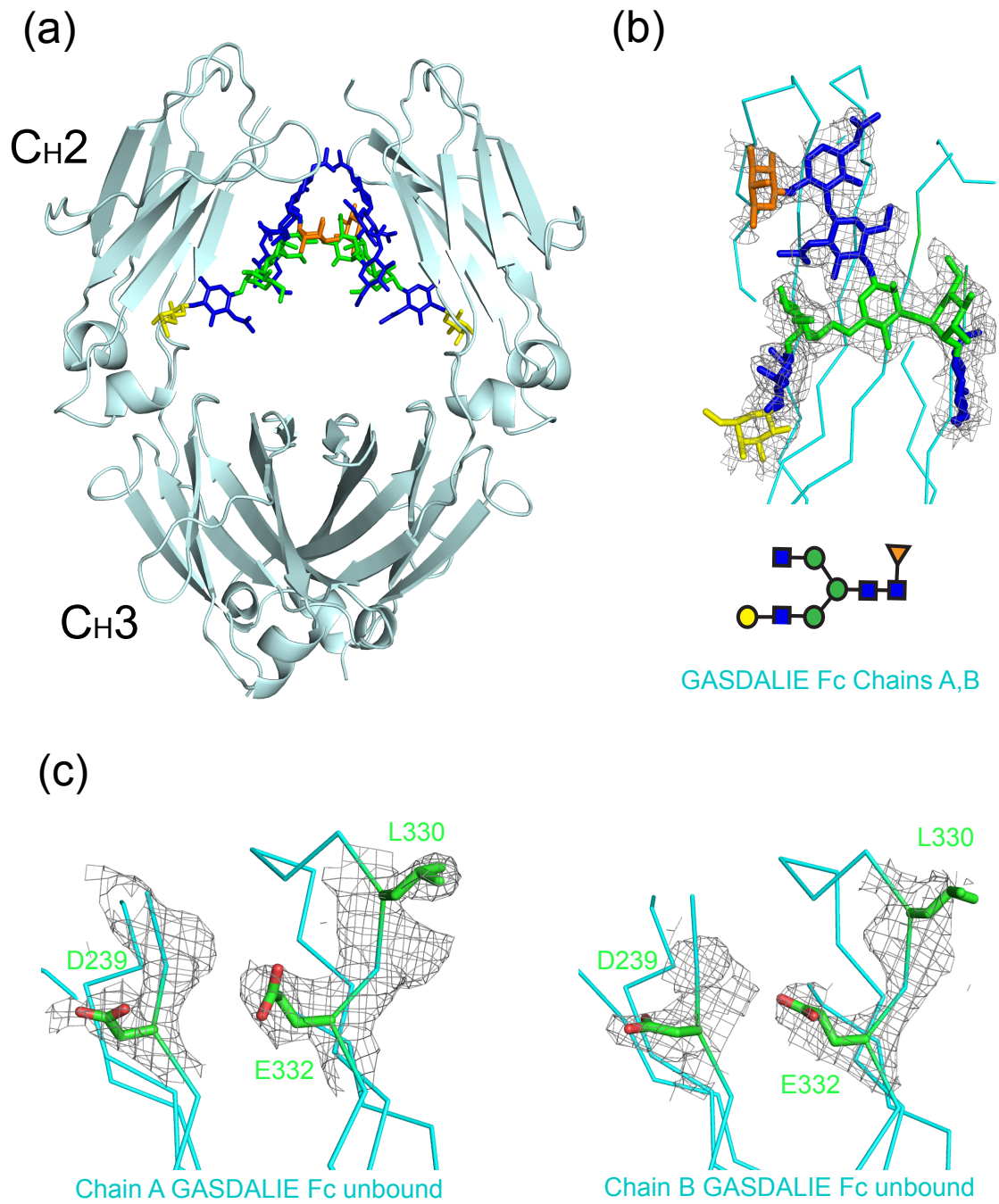


Figure 6. (a) 2.4Å crystal structure of unbound GASDALIE Fc

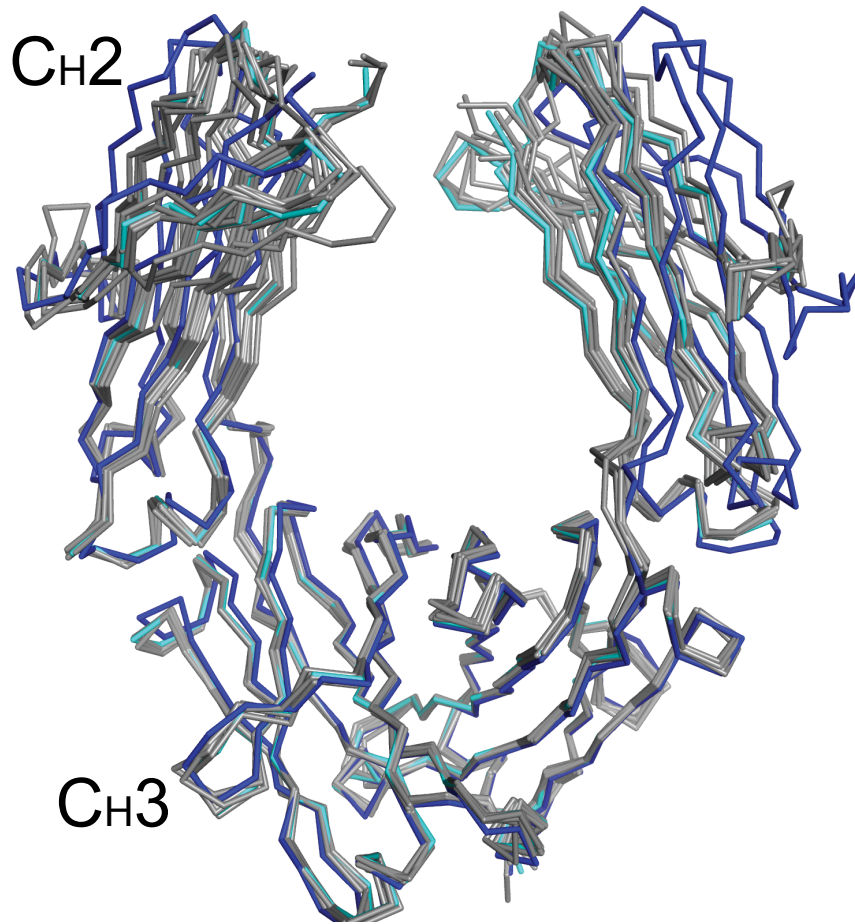
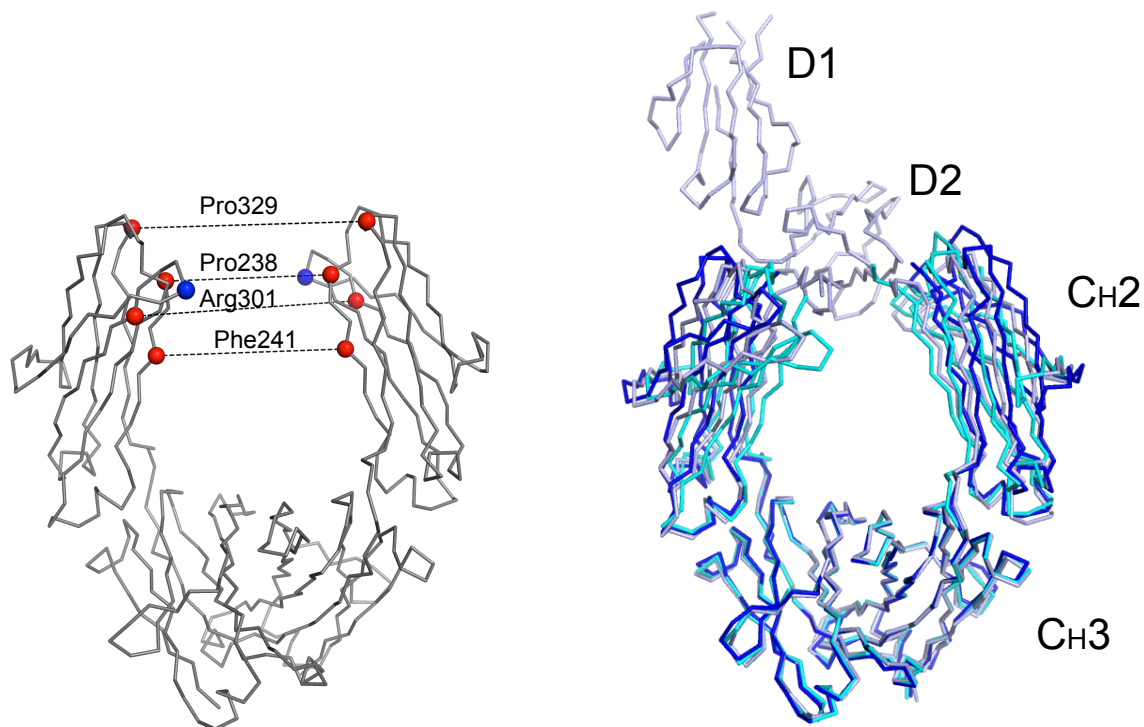


Figure 7. Carbon- $\alpha$  alignment of wild type Fc structures (3DO3, 2DTS, 3AVE, 4Q7D, 1HZH) with SDALIE Fc (2QL1) and GASDALIE Fc





PDB	Protein	Resolution (Å)	SG	Unit cell (a, b, c)	Pro238(Å)	Phe241(Å)	Arg301(Å)	Pro329(Å)
N/A	GASDALIE Fc	2.4	P2 <sub>1</sub> 2 <sub>1</sub> 2 <sub>1</sub>	49, 79, 138	19	22	33	24
2QL1	SDALIE Fc	2.5	C222 <sub>1</sub>	50, 149, 76	28	29	37	39
N/A	GASDALIE Fc: FcγRIIIA	3.1	P2 <sub>1</sub> 2 <sub>1</sub> 2 <sub>1</sub>	74, 95, 108	25	26	38	31
3SGJ	fucosylated Fc: FcγRIIIA	2.2	P2 <sub>1</sub> 2 <sub>1</sub> 2 <sub>1</sub>	67, 89, 140	26	26	37	32
3SGK	afucosylated Fc: FcγRIIIA	2.4	P2 <sub>1</sub> 2 <sub>1</sub> 2 <sub>1</sub>	67, 88, 141	26	27	37	33
3AY4	afucosylated Fc: FcγRIIIA	2.2	P4 <sub>1</sub> 2 <sub>1</sub> 2 <sub>1</sub>	77, 77, 350	25	26	37	31
1E4K	fucosylated Fc: FcγRIIIB	3.2	P6 <sub>5</sub> 22	115, 115, 299	25	26	37	30
1T89	fucosylated Fc: FcγRIIIB	3.5	P6522	115, 115, 301	25	26	37	31
1T83	fucosylated Fc: FcγRIIIB	3.0	P2 <sub>1</sub> 2 <sub>1</sub> 2 <sub>1</sub>	73, 102, 123	25	26	37	31

Figure 8. Comparison of C<sub>H</sub>2 domain separations in free and complexed Fc structures

## **Chapter 4: Investigation of the Proposed Interaction of DC-SIGN with Sialylated Fc**

## INTRODUCTION

Recently there have been conflicting reports surrounding the mechanism of action of intravenous immunoglobulin G (IVIG) in the anti-inflammatory pathway. Previous studies suggested that the activity of IVIG is due to a small percentage of IgGs with terminally sialylated *N*-linked glycans [43, 46, 70]. Based on published results, sialylation resulted in an increased affinity of IgG Fcs to human receptor DC-SIGN (dendritic cell-specific intercellular adhesion molecule-3-grabbing non-integrin) and its mouse orthologue SIGN-R1 (specific intercellular adhesion molecule-3-grabbing nonintegrin-related 1) thereby initiating a cascade of events leading to release of cytokines IL-4 and IL-33 by regulatory macrophages and basophils respectively, ultimately causing an upregulation of Fc $\gamma$ R1b on effector immune cells, increasing the threshold of activation for these cells [46, 70, 95]. This leads to suppressed inflammation.

*In vivo* experiments show that DC-SIGN is important in the anti-inflammatory pathway initiated by IVIG/sialylated Fcs [9, 46, 70]. When splenic macrophages were depleted in mice and inflammation was induced using a K/BxN serum (described in Chapter 1), there was no protection against inflammation, therefore receptors known to be expressed on the surface of splenic macrophages (MARCO, CD169, and SIGN-R1) became of interest [70, 96-98]. Out of these receptors, the deletion of only SIGN-R1 disabled the anti-inflammatory effect of IVIG and  $\alpha$ 2,6-linked sialylated Fc. In addition, blocking of this receptor abrogates IVIG/sialylated Fcs anti-inflammatory effect *in vivo* [46, 70].

Binding studies were performed in order to determine if there was direct binding of  $\alpha$ 2,6-linked sialylated Fc to SIGN-R1 [61, 70, 95]. SIGN-R1<sup>+</sup> macrophages and SIGN-R1<sup>-/-</sup> macrophages from mice were pulsed with either  $\alpha$ 2,6-linked sialylated Fc or asialylated Fc. Binding was observed between sFc to SIGN-R1<sup>+</sup> cells and not SIGN-R1<sup>-/-</sup> cells [70]. Additionally, sialylated Fc had a 10-fold decrease in binding affinity to Fc $\gamma$ Rs. In a similar binding assay, asialylated Fcs bound macrophages only when Fc $\gamma$ Rs were expressed on the surface – they did not bind SIGN-R1 [70]. Similar results were obtained when using hDC-SIGN<sup>+</sup> macrophages. These results suggested glycosylation state defines the effector function of an IgG Fc. Introduction of an F241A mutation in the C<sub>H</sub>2 domain of IgG Fc also causes protection from inflammation and an increase in IgG Fc binding affinity to DC-SIGN in *in vivo* mouse arthritis models [95]. A recent study showed binding of sialylated but not asialylated Fc to DC-SIGN, however both asialylated and sialylated F241A Fc were able to bind by ELISA [61, 95]. These findings suggest that a change in conformation of the protein or oligosaccharide chain results in an introduction of a binding site for DC-SIGN.

Based on the studies presented above we attempted to determine if structural changes occur once an Fc *N*-linked glycan is sialylated or mutated (F241A), causing an increase in affinity to DC-SIGN and if these structural changes occur in the DC-SIGN, binding site, using X-ray crystallography. This would provide insight, at atomic resolution, into protein conformational changes as well as carbohydrate-protein and protein-protein interactions between sialylated Fc

or F241A Fc and DC-SIGN. We also aimed to perform equilibrium gel filtration experiments to determine the stoichiometry of the sFc: DC-SIGN interaction. Binding of both the extracellular domain (ECD) and carbohydrate recognition domain (CRD) of DC-SIGN to sialylated or F241A mutant Fc by surface plasmon resonance (SPR) were not demonstrated although HIV glycoprotein gp120 showed signs of binding to this receptor. Due to the inability to demonstrate binding between DC-SIGN and sFc or F241A Fc, co-crystallization attempts and stoichiometry experiments were not pursued. Here, we present the results of our binding experiments and a review of results related to binding studies of this receptor with sialylated Fcs (see chapter 2 for structural characterization of disialylated Fc and F241A Fc).

**Table 1.** Affinity of sialylated Fc and asialylated Fc to SIGN-R1, hDC-SIGN and hFc $\gamma$ RIIb\*

Receptor	$\alpha$ 2,6 sialylated Fc	asialylated Fc
SIGN-R1	$2.7 \times 10^{-6}$ M	n.b
hDC-SIGN	$3.6 \times 10^{-6}$ M	n.b
hFc $\gamma$ RIIb	$1.5 \times 10^{-6}$ M	$1.6 \times 10^{-6}$ M

\*Adapted from Anthony et al. *PNAS* 2008

## **METHODS/ RESULTS**

### ***Protein Expression/ Purification***

DC-SIGN ECD and CRD proteins were expressed and purified as previously described [47]. Sialylated Fc was derived from papain digested IDEC-114 monoclonal Ab. In order to isolate the Fc, the cleaved IgG was run over a size exclusion column and purified with protein G agarose beads. The Fc fragment was then galactosylated with  $\beta$ 1-4 galactosyltransferase and sialylated with  $\alpha$ 2-6 sialyltransferase *in vitro* as previously described [61, 95]. Sialylated Fc Fragments were then purified with protein G agarose beads to remove enzymes. This protein was further purified by size exclusion chromatography on a Superdex 200 10/300 column (GE Healthcare).

### ***Surface Plasmon Resonance Analysis to Detect Binding of Sialylated Fc and F241A Fc to DC-SIGN ECD and CRD***

Surface plasmon resonance experiments were performed on a Biacore T100 at 25°C with HBS-P buffer (10mM HEPES pH6.8, 150mM NaCl, 0.05% Tween20) as a running buffer. DC-SIGN CRD or ECD was immobilized on a CM5 chip at 400 RU, 900 RU, and 1300RU for DC-SIGN CRD (AA), DC-SIGN ECD (AP), and DC-SIGN ECD (AA), respectively. Sialylated Fc and F241A Fc were injected over flow cells containing either ECD or CRD at a flow rate of 10 $\mu$ l min<sup>-1</sup> for 60 seconds. A

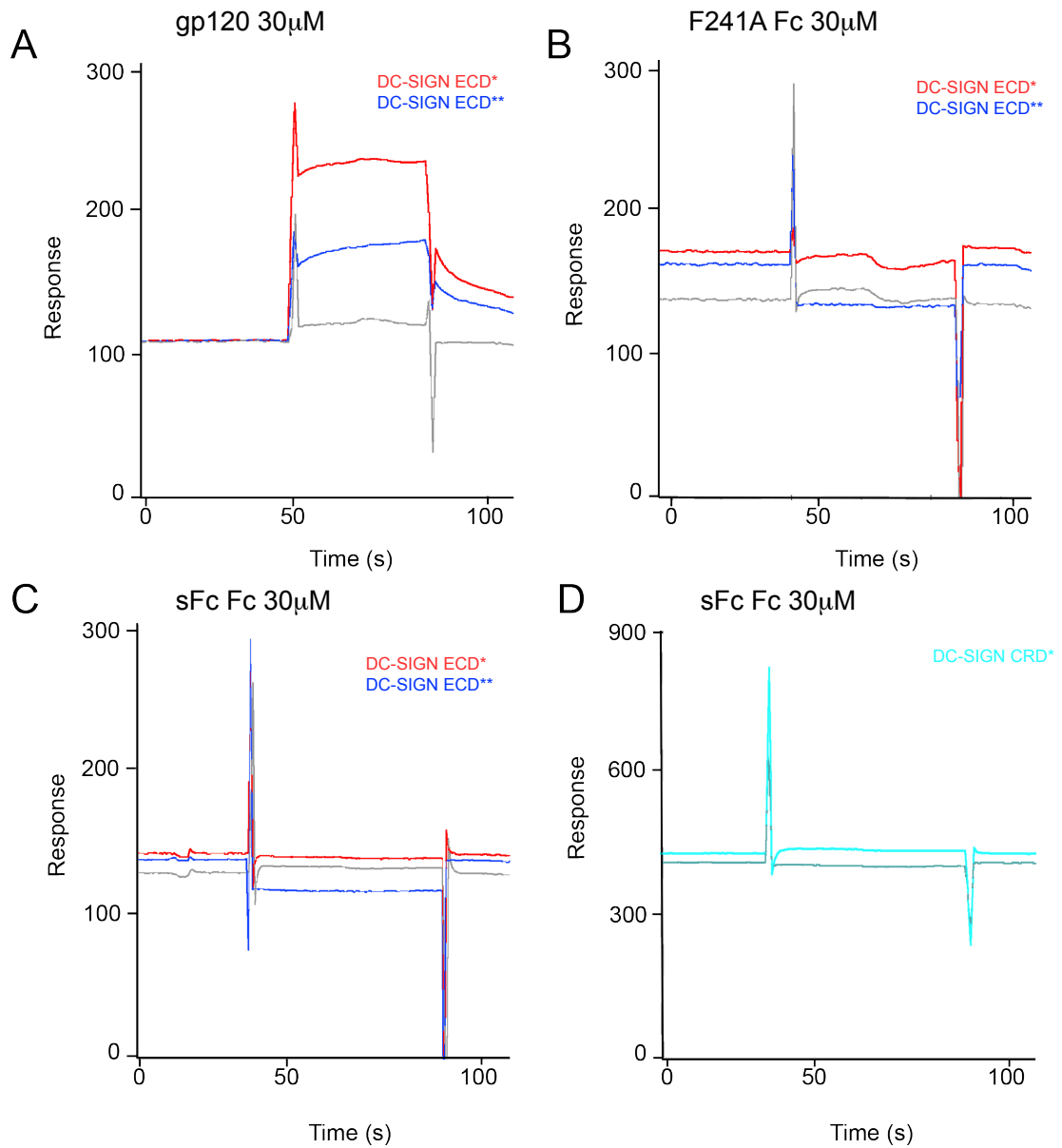


**Figure 1.** Surface plasmon resonance analysis of the interaction of DC-SIGN ECD or CRD with sialylated Fc and F241A Fc. Overlay of binding of 30 $\mu$ M of gp120 (A), F241A Fc (B), or sFc (C) to DC-SIGN ECD expressed at Caltech\* (red) or Rockefeller University\*\* (blue). (D) Binding of 30 $\mu$ M sialylated Fc to DC-SIGN CRD expressed at Caltech\* (cyan).

blank reference flow cell was used to correct bulk refractive index. Binding of sialylated Fc to DC-SIGN ECD or CRD was not detected although binding of positive control (gp120) to DC-SIGN ECD was detected. We also did not see binding of F241A Fc to DC-SIGN ECD.

## **CONCLUSION**

We could not reproduce any of the published results stating that there is direct binding of sialylated Fc to DC-SIGN ECD or CRD therefore we decided not to pursue equilibrium gel filtration experiments to determine stoichiometry or co-crystallization of the DC-SIGN:sialylated Fc complex. Our use of gp120 as a positive control showed that the protein produced at Rockefeller University and the protein expressed here at Caltech were indeed functional. These results were surprising since our collaborators showed direct binding of sialylated Fc to DC-SIGN using cell binding assays and ELISA experiments [61, 70, 95].

A recent publication showed that IVIGs interaction with DC-SIGN is independent of Fc glycoform — sialylated Fc does not bind DC-SIGN [99]. Similar to our results, the authors were able to see binding of heavily mannosylated gp120 to DC-SIGN. Hypersialylated, desialylated (neuraminidase treated), and deglycosylated serum IgG bound with similar affinity to DC-SIGN as unmodified serum IgG by ELISA. In addition, wtFc expressed recombinantly and hypersialylated Fc showed no binding to DC-SIGN, contradicting previously published results. Affinity to activating receptor Fc $\gamma$ R11a was also not affected by sialylation. Serum IgG also did not outcompete gp120 in a competition-binding



assay to DC-SIGN CRD.

Although the key players involved in the anti-inflammatory pathway have been identified, their exact role remains unclear. Contradicting reports in recent publications are an indicator that further studies are needed to characterize these receptors and signaling proteins. In addition to studies showing that binding of sialylated Fc to DC-SIGN does not occur, recent *in vivo* studies show that protection from inflammation in Collagen-antibody and K/BxN serum-induced arthritis mouse models is independent of sialylation of the Fc; however IVIG Fc is able to show a protective effect [99, 100]. Also, there have been recent studies showing that IL-4 producing basophils are not required for the protective effect of IVIG in both Collagen and K/BxN serum-induced arthritis models in addition to IL-33 inability to mediate basophil expansion *in vivo* [100, 101]. These results contradict the pathway proposed by Ravetch and colleagues based on their *in vivo* studies: sialylated Fc binds DC-SIGN on the surface of regulatory macrophages causing a release of cytokine IL-33. IL-33 binds to its receptor IL-33R $\alpha$  located on the surface of basophils causing these cells to expand and release IL-4. IL-4 binds its receptor, IL-4 $\alpha$ , on the surface of effector macrophages, causing an upregulation of the inhibitory receptor Fc $\gamma$ RIIb and an increase in the threshold of activation of these cells. Most of the results in publications from the Ravetch group could not be reproduced by any of these groups. Due to the discrepancies in the research concerning the role of IVIG and proteins involved the anti-inflammatory pathway, further investigation is essential prior to structural characterization.

## **Chapter 5: Conclusion**

Immunoglobulin G (IgG) antibodies are involved in both pro-inflammatory and anti-inflammatory activities. For my thesis work, I have studied the structural mechanisms by which IgG Fc can mediate both pro- and anti-inflammatory immune pathways. A well-known anti-inflammatory activity of IgG is mediated by intravenous immunoglobulin (IVIg), which is effective in treating a wide range of autoimmune and inflammatory disorders although its mechanism of action is poorly understood. *In vivo* studies showed that the activating factor in IVIg therapy are IgG Fcs with terminally sialylated glycans [8, 9, 43, 44, 46, 55, 70]. Additionally, introduction of an F241A substitution in the Fc C<sub>H2</sub> domain demonstrated anti-inflammatory effects similar to sialylated Fc [95]. Our structural studies gave insight on how sialylation or an F241A mutation influences conformation of the Fc protein leading to the switch from pro- to anti-inflammatory activity.

We showed that sialylated Fc could adopt both “open” and “closed” states in the same crystal. This has not been seen in the many asialylated Fc structures in the PDB suggesting an increase in conformational flexibility of sialylated Fc that may facilitate its anti-inflammatory properties [54]. Introduction of the F241A substitution may result in sialylated Fc properties since this amino acid substitution resulted in an increase of sialylated products, which may lead to increased flexibility [54]. Thus, our results suggest that increased flexibility correlates with sialylation of Fc, whether by enzymatic sialylation of Fc glycans or by the F241A substitution.

It was previously proposed that sialylation results in a conformational change allowing Fcs to bind to DC-SIGN, a lectin that exists as a tetramer on the surface of splenic macrophages [46, 47, 70]. The proposed sialylated Fc initiated anti-inflammatory pathway is as follows: binding between sialylated Fc and DC-SIGN leads to the release of cytokine IL-33 from DC-SIGN<sup>+</sup> splenic macrophages. Released IL-33 binds its receptor, IL-33R $\alpha$ , on the surface of basophils leading to activation of these cells, triggering the release of cytokine IL-4. IL-4 binds its receptor, IL-4R $\alpha$ , located on the surface of effector macrophages leading to an upregulation of the inhibitory receptor Fc $\gamma$ RIIb thereby increasing the threshold of activation of these effector cells [46]. To support the hypothesized interaction between sFc and DC-SIGN, cell-based experiments were performed that showed selective binding of sialylated Fc over asialylated Fc to DC-SIGN<sup>+</sup> or SIGN-R1<sup>+</sup> cells [61, 70]. These experiments could be interpreted to show that sFc binds to DC-SIGN and SIGN-R1 at the surface of cells either through a direct interaction or through an interaction with an unidentified cell-surface protein. However, the DC-SIGN<sup>+</sup>/SIGN-R1<sup>+</sup> cells used in these binding experiments were pulsed with sialylated or asialylated Fc at 37°C for one hour, a specific change from most/all cell binding experiments in which the cells are incubated with a potential ligand at 4°C in order to prevent endocytosis and therefore measure only cell surface binding events [50, 61, 70]. Indeed, previous SIGN-R1 binding studies were conducted using cells at 4°C [50]. Thus it is not possible to interpret these results as evidence for a specific interaction, whether direct or indirect, between sFc and DC-SIGN/SIGN-R1 [61, 70]. Other experiments using purified proteins were

conducted to investigate whether DC-SIGN/SIGN-R1 could bind directly to sFc. ELISA experiments reported selective binding of purified sialylated and asialylated F241A Fc over desialylated Fc to DC-SIGN and its mouse orthologue SIGN-R1 [95]. However, we were unable to detect binding of the DC-SIGN carbohydrate recognition domain (CRD) or the DC-SIGN tetrameric extracellular domain (ECD) to sialylated Fc or to the F241A mutant Fc by surface plasmon resonance (SPR) experiments or ELISAs using the same proteins that were used in the experiments reporting a direct binding interaction [61, 95]. Our results are in agreement with recent published studies that also contradict binding studies in Fiebiger *et al.* by showing that sialylated Fc and wtFc did not bind DC-SIGN [95, 99].

Although we have shown that neither sialylated nor F241A Fc interacts directly with DC-SIGN, previous studies have shown that deletion of this receptor abrogates the IVIG initiated anti-inflammatory pathway [46, 70]. While these findings show that this receptor is essential to IVIG activity, our results and published results indicated that direct binding of Fcs to DC-SIGN does not occur [99]. The increase in conformational flexibility may be important for binding another receptor in this pathway, perhaps Fc $\gamma$ RIIb. Fc $\gamma$ RIIb is the inhibitory receptor located on surface of B cells, macrophages, neutrophils, dendritic cells, and basophils [2]. Previous studies have shown that deletion of this receptor abrogates IVIG activity, which may suggest direct binding of sialylated Fc or F241A Fc to Fc $\gamma$ RIIb [46]. The increase in flexibility resulting from sialylation or the F241A mutation may lead to

an increase in an abundance of a specific conformation of Fcs highly selective for Fc $\gamma$ RIIb.

The IVIG pathway is poorly understood, and contradictory studies of its mechanism of action are continually reported [99-101]. Further investigations to identify the key players in this pathway are necessary to elucidate the mechanism of action of this therapy. Additionally, further studies to investigate flexibility of sialylated Fc and F241A Fc using a methods such as electron paramagnetic resonance (EPR) spectroscopy could provide insight into the flexibility of Fcs and the minimum and maximum distances between the C<sub>H</sub>2 domains of the Fc in solution. Methods to increase the flexibility of the Fc using both glycan and protein modifications need to be explored to understand the importance in destabilizing the Fc to produce anti-inflammatory effects and may be used to produce therapeutic antibodies to treat autoimmune and inflammatory disorders. Once the binding partners of sialylated Fc and F241A Fc are identified, screening of Fc mutants to enhance affinity to that receptor should be performed and correlated to the anti-inflammatory effects *in vivo*.

My thesis studies also focused on understanding the role of Fc modifications that affect the pro-inflammatory activities of IgGs. Many efforts were made to modify IgG Fc to enhance antibody dependent cell-mediated cytotoxicity (ADCC), which has been important for development and optimization of therapeutic antibodies against various cancers [11, 28, 33, 35, 36, 38, 88].

Previous studies showed that glycan modifications (e.g., afucosylation) or amino acid substitutions in the C<sub>H</sub>2 domain of IgG Fcs could enhance binding to activating FcγRs (both FcγRIIa and FcγRIIIa) that are located on the surface of immune cells – resulting in enhanced ADCC [27, 29, 33, 35]. Two promising candidates were Fcs with the set of mutations S339D/A330L/I332E (SDALIE) or G236A/S239D/A330L/I332E (GASDALIE) [33, 35]. SDALIE Fc enhanced binding to activating receptor FcγRIIIa by 170-fold and to the inhibitory receptor, FcγRIIb, by 40-fold, whereas GASDALIE Fc had a 20-fold enhancement to FcγRIIIa and little to no increase in binding to FcγRIIb [33, 35]. Introduction of the G236A substitution that distinguishes SDALIE from GASDALIE did not increase binding to the inhibitory receptor compared with wtFc, but GASDALIE Fc still exhibited enhanced binding to activating receptors making it a desirable candidate for enhancement of ADCC without increasing inhibitory FcγRIIb-related pathways [33, 35].

We solved a structure of GASDALIE Fc bound to the ectodomain of the activating receptor FcγRIIIa, which provided insight on how these mutations influenced binding to FcγRs. We found increased electrostatic interactions and hydrogen bonding at the interface between GASDALIE Fc and FcγRIIIa not seen in a wtFc:FcγRIIIa complex structures. This structure can aid in designing better mutants to selectively bind activating receptors thereby optimizing therapeutic antibodies against cancer. There are antibodies used today that recognize specific tumor antigens for the treatment of various cancers. Rituximab, Trastuzumab and Cetuximab are among the antibody-based immunotherapies used today to treat

non-Hodgkin lymphoma, breast cancer, and colorectal cancer, respectively [2]. Introducing the GASDALIE mutations in the C<sub>H</sub>2 domains of these therapeutic antibodies may be used to increase the clearance of the associated tumor cells resulting from an enhancement of ADCC. Consequently, this may result in a lower dose of antibody needed in addition to decreased amount of treatment time.



## BIBLIOGRAPHY

1. Woof, J.M. and D.R. Burton, *Human antibody-Fc receptor interactions illuminated by crystal structures*. Nat Rev Immunol, 2004. **4**(2): p. 89-99.
2. Ackerman, M.E. and F. Nimmerjahn, *Antibody Fc linking adaptive and innate immunity*. 2014, Elsevier Science,,: Amsterdam ; Burlington. p. 1 online resource (xii, 363 pages).
3. Edelman, G.M., et al., *The covalent structure of an entire gammaG immunoglobulin molecule*. Proc Natl Acad Sci U S A, 1969. **63**(1): p. 78-85.
4. Amzel, L.M. and R.J. Poljak, *Three-dimensional structure of immunoglobulins*. Annu Rev Biochem, 1979. **48**: p. 961-97.
5. Krapp, S., et al., *Structural analysis of human IgG-Fc glycoforms reveals a correlation between glycosylation and structural integrity*. J Mol Biol, 2003. **325**(5): p. 979-89.
6. Salmon, J.E. and L. Pricop, *Human receptors for immunoglobulin G: key elements in the pathogenesis of rheumatic disease*. Arthritis Rheum, 2001. **44**(4): p. 739-50.
7. Arnold, J.N., et al., *The impact of glycosylation on the biological function and structure of human immunoglobulins*. Annu Rev Immunol, 2007. **25**: p. 21-50.
8. Nimmerjahn, F. and J.V. Ravetch, *The antiinflammatory activity of IgG: the intravenous IgG paradox*. J Exp Med, 2007. **204**(1): p. 11-5.

9. Anthony, R.M. and J.V. Ravetch, *A novel role for the IgG Fc glycan: the anti-inflammatory activity of sialylated IgG Fcs*. J Clin Immunol, 2010. **30 Suppl 1**: p. S9-14.
10. Butler, M., et al., *Detailed glycan analysis of serum glycoproteins of patients with congenital disorders of glycosylation indicates the specific defective glycan processing step and provides an insight into pathogenesis*. Glycobiology, 2003. **13**(9): p. 601-22.
11. Shields, R.L., et al., *High resolution mapping of the binding site on human IgG1 for Fc gamma RI, Fc gamma RII, Fc gamma RIII, and FcRn and design of IgG1 variants with improved binding to the Fc gamma R*. J Biol Chem, 2001. **276**(9): p. 6591-604.
12. Burmeister, W.P., A.H. Huber, and P.J. Bjorkman, *Crystal structure of the complex of rat neonatal Fc receptor with Fc*. Nature, 1994. **372**(6504): p. 379-83.
13. Wallace, P.K., A.L. Howell, and M.W. Fanger, *Role of Fc gamma receptors in cancer and infectious disease*. J Leukoc Biol, 1994. **55**(6): p. 816-26.
14. Tudor, D. and M. Bomsel, *The broadly neutralizing HIV-1 IgG 2F5 elicits gp41-specific antibody-dependent cell cytotoxicity in a Fc gamma RI-dependent manner*. AIDS, 2011. **25**(6): p. 751-9.
15. Ravetch, J.V. and J.P. Kinet, *Fc receptors*. Annu Rev Immunol, 1991. **9**: p. 457-92.

16. Pincetic, A., et al., *Type I and type II Fc receptors regulate innate and adaptive immunity*. Nat Immunol, 2014. **15**(8): p. 707-16.
17. Wirthmueller, U., et al., *Signal transduction by Fc gamma RIII (CD16) is mediated through the gamma chain*. J Exp Med, 1992. **175**(5): p. 1381-90.
18. Ravetch, J.V. and S. Bolland, *IgG Fc receptors*. Annu Rev Immunol, 2001. **19**: p. 275-90.
19. Wang, D., et al., *Phospholipase Cgamma2 is essential in the functions of B cell and several Fc receptors*. Immunity, 2000. **13**(1): p. 25-35.
20. Leibson, P.J., *Signal transduction during natural killer cell activation: inside the mind of a killer*. Immunity, 1997. **6**(6): p. 655-61.
21. Zompi, S. and F. Colucci, *Anatomy of a murder--signal transduction pathways leading to activation of natural killer cells*. Immunol Lett, 2005. **97**(1): p. 31-9.
22. Hulett, M.D. and P.M. Hogarth, *Molecular basis of Fc receptor function*. Adv Immunol, 1994. **57**: p. 1-127.
23. Ono, M., et al., *Role of the inositol phosphatase SHIP in negative regulation of the immune system by the receptor Fc(gamma)RIIB*. Nature, 1996. **383**(6597): p. 263-6.
24. Trapani, J.A. and M.J. Smyth, *Functional significance of the perforin/granzyme cell death pathway*. Nat Rev Immunol, 2002. **2**(10): p. 735-47.

25. Eischen, C.M., et al., *Fc receptor-induced expression of Fas ligand on activated NK cells facilitates cell-mediated cytotoxicity and subsequent autocrine NK cell apoptosis*. J Immunol, 1996. **156**(8): p. 2693-9.
26. North, S.J., et al., *Glycomics profiling of Chinese hamster ovary cell glycosylation mutants reveals N-glycans of a novel size and complexity*. J Biol Chem, 2010. **285**(8): p. 5759-75.
27. Shields, R.L., et al., *Lack of fucose on human IgG1 N-linked oligosaccharide improves binding to human FcγR3 and antibody-dependent cellular toxicity*. J Biol Chem, 2002. **277**(30): p. 26733-40.
28. Mizushima, T., et al., *Structural basis for improved efficacy of therapeutic antibodies on defucosylation of their Fc glycans*. Genes Cells, 2011. **16**(11): p. 1071-80.
29. Ferrara, C., et al., *Unique carbohydrate-carbohydrate interactions are required for high affinity binding between FcγR3 and antibodies lacking core fucose*. Proc Natl Acad Sci U S A, 2011. **108**(31): p. 12669-74.
30. Ferrara, C., et al., *The carbohydrate at FcγR3 Asn-162. An element required for high affinity binding to non-fucosylated IgG glycoforms*. J Biol Chem, 2006. **281**(8): p. 5032-6.
31. Matsumiya, S., et al., *Structural comparison of fucosylated and nonfucosylated Fc fragments of human immunoglobulin G1*. J Mol Biol, 2007. **368**(3): p. 767-79.

32. Nimmerjahn, F. and J.V. Ravetch, *Divergent immunoglobulin g subclass activity through selective Fc receptor binding*. Science, 2005. **310**(5753): p. 1510-2.
33. Bournazos, S., et al., *Broadly neutralizing anti-HIV-1 antibodies require Fc effector functions for in vivo activity*. Cell, 2014. **158**(6): p. 1243-53.
34. Zeck, A., et al., *Cell type-specific and site directed N-glycosylation pattern of FcgammaRIIIa*. J Proteome Res, 2011. **10**(7): p. 3031-9.
35. Lazar, G.A., et al., *Engineered antibody Fc variants with enhanced effector function*. Proc Natl Acad Sci U S A, 2006. **103**(11): p. 4005-10.
36. Richards, J.O., et al., *Optimization of antibody binding to FcgammaRIIIa enhances macrophage phagocytosis of tumor cells*. Mol Cancer Ther, 2008. **7**(8): p. 2517-27.
37. Idusogie, E.E., et al., *Mapping of the C1q binding site on rituxan, a chimeric antibody with a human IgG1 Fc*. J Immunol, 2000. **164**(8): p. 4178-84.
38. Oganessian, V., et al., *Structural characterization of a mutated, ADCC-enhanced human Fc fragment*. Mol Immunol, 2008. **45**(7): p. 1872-82.
39. Parekh, R., et al., *Age-related galactosylation of the N-linked oligosaccharides of human serum IgG*. J Exp Med, 1988. **167**(5): p. 1731-6.
40. Parekh, R.B., et al., *Association of rheumatoid arthritis and primary osteoarthritis with changes in the glycosylation pattern of total serum IgG*. Nature, 1985. **316**(6027): p. 452-7.

41. Monach, P.A., D. Mathis, and C. Benoist, *The K/BxN arthritis model*. Curr Protoc Immunol, 2008. **Chapter 15**: p. Unit 15 22.
42. Ditzel, H.J., *The K/BxN mouse: a model of human inflammatory arthritis*. Trends Mol Med, 2004. **10**(1): p. 40-5.
43. Kaneko, Y., F. Nimmerjahn, and J.V. Ravetch, *Anti-inflammatory activity of immunoglobulin G resulting from Fc sialylation*. Science, 2006. **313**(5787): p. 670-3.
44. Anthony, R.M., et al., *Recapitulation of IVIG anti-inflammatory activity with a recombinant IgG Fc*. Science, 2008. **320**(5874): p. 373-6.
45. Shibuya, N., et al., *The elderberry (Sambucus nigra L.) bark lectin recognizes the Neu5Ac(alpha 2-6)Gal/GalNAc sequence*. J Biol Chem, 1987. **262**(4): p. 1596-601.
46. Anthony, R.M., et al., *Intravenous gammaglobulin suppresses inflammation through a novel T(H)2 pathway*. Nature, 2011. **475**(7354): p. 110-3.
47. Mitchell, D.A., A.J. Fadden, and K. Drickamer, *A novel mechanism of carbohydrate recognition by the C-type lectins DC-SIGN and DC-SIGNR. Subunit organization and binding to multivalent ligands*. J Biol Chem, 2001. **276**(31): p. 28939-45.
48. Geijtenbeek, T.B., et al., *DC-SIGN, a dendritic cell-specific HIV-1-binding protein that enhances trans-infection of T cells*. Cell, 2000. **100**(5): p. 587-97.

49. Tabarani, G., et al., *DC-SIGN neck domain is a pH-sensor controlling oligomerization: SAXS and hydrodynamic studies of extracellular domain.* J Biol Chem, 2009. **284**(32): p. 21229-40.
50. Galustian, C., et al., *High and low affinity carbohydrate ligands revealed for murine SIGN-R1 by carbohydrate array and cell binding approaches, and differing specificities for SIGN-R3 and langerin.* Int Immunol, 2004. **16**(6): p. 853-66.
51. Pricop, L., et al., *Differential modulation of stimulatory and inhibitory Fc gamma receptors on human monocytes by Th1 and Th2 cytokines.* J Immunol, 2001. **166**(1): p. 531-7.
52. Barb, A.W., et al., *NMR characterization of immunoglobulin G Fc glycan motion on enzymatic sialylation.* Biochemistry, 2012. **51**(22): p. 4618-26.
53. Crispin, M., X. Yu, and T.A. Bowden, *Crystal structure of sialylated IgG Fc: implications for the mechanism of intravenous immunoglobulin therapy.* Proc Natl Acad Sci U S A, 2013. **110**(38): p. E3544-6.
54. Ahmed, A.A., et al., *Structural characterization of anti-inflammatory immunoglobulin G Fc proteins.* J Mol Biol, 2014. **426**(18): p. 3166-79.
55. Nimmerjahn, F. and J.V. Ravetch, *Anti-inflammatory actions of intravenous immunoglobulin.* Annu Rev Immunol, 2008. **26**: p. 513-33.
56. Nimmerjahn, F. and J.V. Ravetch, *Fc gamma Rs in health and disease.* Curr Top Microbiol Immunol, 2011. **350**: p. 105-25.

57. Samuelsson, A., T.L. Towers, and J.V. Ravetch, *Anti-inflammatory activity of IVIG mediated through the inhibitory Fc receptor*. *Science*, 2001. **291**(5503): p. 484-6.
58. Tackenberg, B., et al., *Impaired inhibitory Fcγ receptor IIB expression on B cells in chronic inflammatory demyelinating polyneuropathy*. *Proc Natl Acad Sci U S A*, 2009. **106**(12): p. 4788-92.
59. Gelfand, E.W., *Differences between IGIV products: impact on clinical outcome*. *Int Immunopharmacol*, 2006. **6**(4): p. 592-9.
60. Schwab, I., et al., *Broad requirement for terminal sialic acid residues and FcγRIIB for the preventive and therapeutic activity of intravenous immunoglobulins in vivo*. *Eur J Immunol*, 2014.
61. Sondermann, P., et al., *General mechanism for modulating immunoglobulin effector function*. *Proc Natl Acad Sci U S A*, 2013. **110**(24): p. 9868-72.
62. Feige, M.J., et al., *Structure of the murine unglycosylated IgG1 Fc fragment*. *J Mol Biol*, 2009. **391**(3): p. 599-608.
63. Sprague, E.R., W.L. Martin, and P.J. Bjorkman, *pH dependence and stoichiometry of binding to the Fc region of IgG by the herpes simplex virus Fc receptor gE-gI*. *J Biol Chem*, 2004. **279**(14): p. 14184-93.
64. Huang, W., et al., *Chemoenzymatic glycoengineering of intact IgG antibodies for gain of functions*. *J Am Chem Soc*, 2012. **134**(29): p. 12308-18.



65. Yu, X., et al., *Engineering hydrophobic protein-carbohydrate interactions to fine-tune monoclonal antibodies*. J Am Chem Soc, 2013. **135**(26): p. 9723-32.
66. Lund, J., et al., *Multiple interactions of IgG with its core oligosaccharide can modulate recognition by complement and human Fc gamma receptor I and influence the synthesis of its oligosaccharide chains*. J Immunol, 1996. **157**(11): p. 4963-9.
67. Crispin, M., et al., *Carbohydrate and domain architecture of an immature antibody glycoform exhibiting enhanced effector functions*. J Mol Biol, 2009. **387**(5): p. 1061-6.
68. Oganesyanyan, V., et al., *Structural characterization of a human Fc fragment engineered for extended serum half-life*. Mol Immunol, 2009. **46**(8-9): p. 1750-5.
69. Teplyakov, A., et al., *IgG2 Fc structure and the dynamic features of the IgG CH2-CH3 interface*. Mol Immunol, 2013. **56**(1-2): p. 131-9.
70. Anthony, R.M., et al., *Identification of a receptor required for the anti-inflammatory activity of IVIG*. Proc Natl Acad Sci U S A, 2008. **105**(50): p. 19571-8.
71. Frank, M., et al., *Immunoglobulin G1 Fc Domain Motions: Implications for Fc Engineering*. J Mol Biol, 2014.
72. Diskin, R., P.M. Marcovecchio, and P.J. Bjorkman, *Structure of a clade C HIV-1 gp120 bound to CD4 and CD4-induced antibody reveals anti-CD4 polyreactivity*. Nat Struct Mol Biol, 2010. **17**(5): p. 608-13.

73. Leslie, A.G.W. and H.R. Powell, *Processing Diffraction Data with Mosfilm*, in *Evolving Methods for Macromolecular Crystallography*. 2007. p. 41-51.
74. Evans, P.R., *An introduction to data reduction: space-group determination, scaling and intensity statistics*. Acta Crystallogr D Biol Crystallogr, 2011. **67**(Pt 4): p. 282-92.
75. Evans, P., *Scaling and assessment of data quality*. Acta Crystallogr D Biol Crystallogr, 2006. **62**(Pt 1): p. 72-82.
76. Karplus, P.A. and K. Diederichs, *Linking crystallographic model and data quality*. Science, 2012. **336**(6084): p. 1030-3.
77. Adams, P.D., et al., *PHENIX: a comprehensive Python-based system for macromolecular structure solution*. Acta Crystallogr D Biol Crystallogr, 2010. **66**(Pt 2): p. 213-21.
78. McCoy, A.J., et al., *Phaser crystallographic software*. J Appl Crystallogr, 2007. **40**(Pt 4): p. 658-674.
79. Emsley, P., et al., *Features and development of Coot*. Acta Crystallogr D Biol Crystallogr, 2010. **66**(Pt 4): p. 486-501.
80. Schrödinger, L., *The PyMOL Molecular Graphics System*. 2011, The PyMOL Molecular Graphics System.
81. Gessner, J.E., et al., *The IgG Fc receptor family*. Ann Hematol, 1998. **76**(6): p. 231-48.
82. Oganessian, V., et al., *Structural characterization of a human Fc fragment engineered for lack of effector functions*. Acta Crystallogr D Biol Crystallogr, 2008. **64**(Pt 6): p. 700-4.

83. Duncan, A.R., et al., *Localization of the binding site for the human high-affinity Fc receptor on IgG*. Nature, 1988. **332**(6164): p. 563-4.
84. Smith, P., et al., *Mouse model recapitulating human Fcγ receptor structural and functional diversity*. Proc Natl Acad Sci U S A, 2012. **109**(16): p. 6181-6.
85. Bournazos, S., et al., *Human IgG Fc domain engineering enhances antitoxin neutralizing antibody activity*. J Clin Invest, 2014. **124**(2): p. 725-9.
86. Sonderrmann, P., R. Huber, and U. Jacob, *Crystal structure of the soluble form of the human fcγ receptor IIb: a new member of the immunoglobulin superfamily at 1.7 Å resolution*. EMBO J, 1999. **18**(5): p. 1095-103.
87. Maxwell, K.F., et al., *Crystal structure of the human leukocyte Fc receptor, FcγRIIa*. Nat Struct Biol, 1999. **6**(5): p. 437-42.
88. Mimoto, F., et al., *Engineered antibody Fc variant with selectively enhanced FcγRIIb binding over both FcγRIIa(R131) and FcγRIIa(H131)*. Protein Eng Des Sel, 2013. **26**(10): p. 589-98.
89. Ramsland, P.A., et al., *Structural basis for FcγRIIa recognition of human IgG and formation of inflammatory signaling complexes*. J Immunol, 2011. **187**(6): p. 3208-17.
90. Sonderrmann, P., J. Kaiser, and U. Jacob, *Molecular basis for immune complex recognition: a comparison of Fc-receptor structures*. J Mol Biol, 2001. **309**(3): p. 737-49.

91. Sondermann, P., et al., *The 3.2-A crystal structure of the human IgG1 Fc fragment-Fc gammaRIII complex*. Nature, 2000. **406**(6793): p. 267-73.
92. DiLillo, D.J., et al., *Broadly neutralizing hemagglutinin stalk-specific antibodies require Fc gamma R interactions for protection against influenza virus in vivo*. Nat Med, 2014. **20**(2): p. 143-51.
93. Thommesen, J.E., et al., *Lysine 322 in the human IgG3 C(H)2 domain is crucial for antibody dependent complement activation*. Mol Immunol, 2000. **37**(16): p. 995-1004.
94. Edberg, J.C. and R.P. Kimberly, *Cell type-specific glycoforms of Fc gamma RIIIa (CD16): differential ligand binding*. J Immunol, 1997. **159**(8): p. 3849-57.
95. Fiebiger, B.M., et al., *Protection in antibody- and T cell-mediated autoimmune diseases by antiinflammatory IgG Fcs requires type II FcRs*. Proc Natl Acad Sci U S A, 2015.
96. Crocker, P.R., et al., *Purification and properties of sialoadhesin, a sialic acid-binding receptor of murine tissue macrophages*. EMBO J, 1991. **10**(7): p. 1661-9.
97. Elomaa, O., et al., *Cloning of a novel bacteria-binding receptor structurally related to scavenger receptors and expressed in a subset of macrophages*. Cell, 1995. **80**(4): p. 603-9.
98. Park, C.G., et al., *Five mouse homologues of the human dendritic cell C-type lectin, DC-SIGN*. Int Immunol, 2001. **13**(10): p. 1283-90.

99. Yu, X., et al., *Dissecting the molecular mechanism of IVIg therapy: the interaction between serum IgG and DC-SIGN is independent of antibody glycoform or Fc domain*. J Mol Biol, 2013. **425**(8): p. 1253-8.
100. Campbell, I.K., et al., *Therapeutic effect of IVIG on inflammatory arthritis in mice is dependent on the Fc portion and independent of sialylation or basophils*. J Immunol, 2014. **192**(11): p. 5031-8.
101. Sharma, M., et al., *Intravenous immunoglobulin-induced IL-33 is insufficient to mediate basophil expansion in autoimmune patients*. Sci Rep, 2014. **4**: p. 5672.